Generation of heralded multi-photon parallel state for realizing a large-scale photonic quantum circuit

Takayuki Kiyohara

2020

Abstract

The authors study the efficient generation of multi-photon parallel states from heralded single-photon sources for realizing large-scale photonic quantum circuits. Photonic quantum circuits can be implemented with a multi-photon multi-port interferometer, and will contribute to research on quantum computation, quantum communication, and quantum metrology. The multi-photon multi-mode interferometer can also serve as a platform for Boson sampling for showing quantum supremacy.

To further scale up quantum circuits, it is essential to efficiently generate a multi-photon parallel state consisting of highly indistinguishable single photons. To date, multiple heralded single-photon sources (HSPS) via nonlinear processes have been widely used because they can generate highly indistinguishable photons at room temperature. However, a problem with HSPS is that occasionally more than two photons are generated, which may cause errors in the operation of quantum circuits. This is a critical problem for multi-photon interference experiments when there are many input photons.

To solve the problem of unwanted multi-photon generation from an HSPS, we propose combining two methods: multiplexing of multiple HSPSs (multiplexed-HSPS) and photon pair number discrimination. In Chapter 3, we report the realization of multiplexed heralded single photon sources using photon number resolving detectors. For this, we adopt a photon number resolving detector (PND) using cascaded detectors. We also develop a theory to describe multiplexed-HSPS with PNDs considering a limited number of cascaded detectors. We find that even a small number of detector cascades are very effective in reducing excess photon emission in certain circumstances. With the realized multiplexed-HSPS with a PND equipped with two SPDC sources and a PND consisting of two on–off detectors, we found that the two-photon components are reduced to $44.2 \pm 0.7\%$ compared to a normal HSPS.

Next, we studied more efficient and compact preparation of the multi-photon parallel state. For this, serial–parallel conversion is a strong candidate since the converter can route a stream of N photons at successive intervals from one source to N different spatial modes. However, the previously used method of applying a serial–parallel convertor is not efficient with an increasing number of photons. In Chapter 4, we theoretically demonstrate that serial–parallel conversion for HSPS can be more efficient than for the unheralded photon source. The authors report the experimental realization of a serial–parallel conversion system for two photons with heralding signals. In the experiments, we achieved a conversion efficiency of 0.533 ± 0.003, which exceeds the maximum achievable efficiency of 0.5 for serial–parallel conversion using unheralded photons, and is double the efficiency of 0.25 for that using beamsplitters.

Developing on the previous investigations, we studied the efficient generation of a multi-photon parallel state in which the probability of having more than two photons in

one mode is suppressed. We propose a new method to produce a multi-photon parallel state by using active spatial routing. In Chapter 5, we demonstrate a method to efficiently generate a multi-photon parallel state by active spatial networking (ASN) and compare the procedure to the simple method using N single-photon sources. First, we consider how the proposed method allows us to exponentially increase the efficiency in preparing an N-photon parallel state when compared with the simple method of N HSPSs. Second, we present a proof-of-principle demonstration of ASN using two HSPSs for generating a two-photon parallel state. With the realization of an active spatial 2×2 network and a fixed delay, we achieved an enhancement factor of 1.59 ± 0.14, compared with a source using two HSPSs.

The multi-photon interferometer with a linear optical circuit will become a key tool for producing entanglement in multi-mode and multi-photon systems. The entangled state between two optical systems is a useful resource for various quantum technologies. Usually, entanglement is experimentally evaluated by quantum state full tomography. However, the required resources exponentially increase as the number of photons or modes increases. To solve this problem, our collaborator has recently proposed a novel method to verify the generation of entanglement between two multi-mode and multi-photon optical systems using mode discrete Fourier transform (DFT) circuits. This method exponentially decreases the number of resources required for tomography. In Chapter 6, the authors report the first demonstration of three-photon entanglement between two three-mode optical systems. For this experiment, we implemented a pair of super-stabilized optical DFT circuits by using displaced-Sagnac architecture and hybrid polarizing beamsplitters. We successfully achieved correlation of the photon number statistics between the two systems with and without DFT circuits, and the sum of the fidelities $F_{\boldsymbol{n}} + F_K = 1.555 \pm 0.018$ exceeded the lower bound $4/3$ for verifying the generation of entanglement with 12.3 standard deviations.

In Chapter 7, this dissertation is summarized.

Mathematical Variables

$\hat{a}_j^\dagger$	Creation operator of the j-th (input) field
$\hat{a}_j$	Annihilation operator of the j-th (input) field
$\alpha(\omega_{\mathrm{p}})$	Pump envelope function
$\hat{b}_j^\dagger$	Creation operator of the j-th (output) field
$\hat{b}_j$	Annihilation operator of the j-th (output) field
C_j	Count rate of detected photons at mode j
$C(n)$	Rate of events where n photons are successfully detected when the series of heralding signals are generated
$C_{\mathrm{h}}(n)$	Rate of events where a series of n heralding signals is generated
$C_{\mathrm{m}}(N)$	Generation rate of N-photon parallel state
χ_{j}	Overall quantum efficiency of mode j
$\chi^{(x)}$	Nonlinear susceptibility tensor
$d_{\boldsymbol{p}}$	Cardinality of the pattern class $\boldsymbol{p}$
D	Cascading level
D_{Aj}	j-th detector at system A
D_{Bj}	j-th detector at system B
$\hat{E}_j$	Quantised field operator of j field
$\hat{E}_j^{(+)}$	Positive frequency component of the quantised field of j field
$\hat{E}_j^{(-)}$	Negative frequency component of the quantised field of j field
η_{D}	Over all detection efficiency of the detector
η_{SW}	Switching efficiency defined as the average probability
η_{n}	Loss in $N \times N$ network
η	Loss in 2×2 network
η_{f}	Loss of the delay fiber in $N \times N$ network
η_{h}	Trigger-mode system detection efficiency including the detection efficiency of a detector, coupling efficiency of photons into a fiber, and losses of optical components
$f(\omega_{\mathrm{s}}, \omega_{\mathrm{i}})$	Joint spectral amplitude
$\lvert f(\omega_{\mathrm{s}}, \omega_{\mathrm{i}})\rvert^2$	Joint spectral intensity
$f(\omega_j)$	Spectral distribution function of the j-th field
$F(\tau)$	HOM dip function
F_{state}	Quantum state fidelity
$F_{\mathrm{s}j}(\omega)$	Function of a band pass filter of j- signal photon with the frequency of ω

F_n	Fidelity given by the probability of the observed distribution, and summing over the probability of all correctly correlated combinations of photon number distributions without DFTs
F_K	Fidelity given by the probability of the observed distribution, and summing over the probability of all correctly correlated combinations of photon number distributions with DFTs
$g(x)$	Photon pair creation rate at x in the crystal
Γ_{12}	Difference of the effect of GVD between two mediums
$\hat{H}_l(t)$	Hamiltonian of spontaneous parametric down conversion
I	Intensity of the pump laser
K_A	k-value of photon number distribution at system A
K_B	k-value of photon number distribution at system B
$\boldsymbol{k}_j$	Wave vector of j-photon
$K(\boldsymbol{n})$	k-value of photon number distribution of $\boldsymbol{n}$
$k^{(2)}$	Effect of group velocity dispersion
L	Length of the crystal
λ	Wavelength of photon
$\Delta\lambda$	Bandwidth of ban pass filter
L_j	Length of i-th dispersion medium
M	Total number of photons for entanglement between two systems
n_i	Number of photons of the mode i
$\|n_1, n_2, \cdots\rangle$	Fock state of photon number distribution of n_j photons at mode j
n	Number of photons
$\bar{N}$	Mean number of photon pairs
$n_{\mathrm{o}}(\lambda)$	Ordinary refractive index of wavelength λ
$n_{\mathrm{e}}(\lambda)$	Extraordinary refractive index of wavelength λ
N	Number of photons containing multi-photon parallel state
$\nu_{go}(\lambda)$	Group velocity of ordinary ray
$\nu_{ge}(\lambda)$	Group velocity of extraordinary ray
$N_{\max}$	Maximum parameter of the interference signal
$N_{\min}$	Minimum parameter of the interference signal
$\boldsymbol{n}_A$	Multi-dimensional vectors describing the photon number distribution of the local multi modes at system A with DFTs
$\boldsymbol{n}_B$	Multi-dimensional vectors describing the photon number distribution of the local multi modes at system B with DFTs
N	Number of photons in multi-photon parallel state
$\overline{\boldsymbol{n}}$	Multi-dimensional vectors describing the photon number distribution of the local multi modes without DFTs
ω_i	Frequency of photon j
ω_{j0}	Central frequency of j-photon
$P_{\mathrm{Po}}(k)$	Poisson distribution
$P_{\mathrm{th}}(k)$	Thermal distribution
$P_{\mathrm{D}}(n\|m)$	Conditional probability to detect n photons from m photons at the input

$P_{\mathrm{h}}(n)$	Conditional probability of heralded single photon with n photons
P_{h}	Experimental heralding probability
$P_C(n)$	n photons detection probability at the output when heralding signals is emitted
$P(n)$	General photon pair number distribution
$P_{\mathrm{herald}}(N)$	Heralding probability for N-photon parallel state
$P_{\mathrm{T}}(N)$	N-photon output probability
$\|\phi_{N,M-N}\rangle$	Bipertite entanglement state between two optical multi-photon multi-mode systems
$P_{\mathrm{exp.}}(p_A, p_B)$	Pattern probability represented by the photon number distribution p_A in A and p_B inl B
$P_{4C}(\tau)$	Four-fold coincidence events of HOM dip function
p	Heralding probability for one photon
$\hat{\Pi}_{4\mathrm{C}}$	Detection operator that four photons are detected
$\phi(\omega_{\mathrm{s}}, \omega_{\mathrm{i}})$	Phasematching function
ϕ	Phase difference between optical paths of Mach-Zehnder interferometer
Ψ	Angle of the optical axis with respect to the direction of the pump laser
$\|\Psi_4\rangle$	Initial four photon state from two photon pair sources
$\|\Psi(t)\rangle$	Two photon state at time t
$\|\psi_M\rangle$	Photon number state with M photons and M beam splitters without post-selecting
$R(N)$	Enhancement ratio for n photons
R	Reflection amplitude coefficient of beam splitter
R_{rep}	Repetition rate of pump pulsed laser
R_{sup}	Suppression ratio
$\hat{\rho}_{\mathrm{exp.}}$	Experimental generated state of entanglement
$S(n)$	Conversion efficiency for a stream of n single photons of routing a single photon into the desired modes
S	Number of SPDC sources per Multiplexed HSPS
$\hat{S}^{\dagger}$	Cyclic mode shift operator
σ_{p}	Full width at half maximum bandwidth of the pump laser
σ_j	Full width at half maximum bandwidth of photon j
t_k	Time bin information (detection time) of k-th photon
T	Transmission amplitude coefficient of beam splitter
t	Optical transmittance between a SPDC source and a fiber
t_{wait}	Waiting time for firing multi photons simultaneously
$\theta_{\mathrm{i}j}(\omega)$	Group velocity dispersion of j- signal photon with the frequency of ω
τ	Relative time delay between input photons for HOM interference
U_{ij}	Unitary matrix of linear circuit
$\hat{U}_{\mathrm{F}}$	Unitary matrix of mode discrete fourier transform
V	Visibility of the interference signal
V_{vol}	Amplitude of voltage
$\xi_j(\omega)$	Gaussian frequency distribution of j-mode with the effect of GVD

Contents

Chapter 1

Introduction

1.1 Quantum technology with single photons

Quantum technology is an emerging field of physics and engineering that uses novel and powerful applications, such as quantum computing [1], quantum sensing [2], quantum cryptography [3], quantum simulation [4, 5], quantum metrology [6], and quantum imaging [7]. These technologies are based on quantum mechanical properties, especially quantum entanglement and quantum superposition. Quantum technology offers fundamental improvements over classical information processing and measurement. One of the most celebrated quantum technologies is quantum computers, which can solve given problems much faster than classical computers and will assist research, such as solving integer factorization problems [8], searching a database for a single target address [9] and calculating the ground state energy of molecules [10]. Quantum sensing, which uses a quantum system, quantum properties, or quantum phenomena to measure a physical quantity, is another technology that offers great advances for research. While the advances that quantum technology offer will help address global problems for the next generation, the advent of quantum technology also provides an opportunity to revisit existing applications. For example, quantum computers will lead to breakthroughs in the field of cryptography by means of the method of key exchange known as RSA using factoring integers, which is difficult for classical computers. In this way, various kinds of cryptographic protocols become vulnerable to quantum computers.

Quantum technology is currently in an emerging stage, but is developing steadily. Quantum devices of physical systems are constructed using various kinds of quantum architectures, such as atoms [11, 12], trapped ions [13, 14], nuclear magnetic resonance [15], and superconducting circuits [16], as well as single photons [17]. Among these various approaches, photons have advantages for realizing photonic quantum applications, such as low-loss light-speed transmission and easy manipulation with high precision by simple optical components at room temperature. One feature of photons is that they do not readily interact with the environment, and hence photonic systems are decoherence free. These features are also attractive for the realization of quantum key distribution, providing security based on the laws of quantum mechanics [18, 19, 20, 21, 22]. However, the lack of interaction with the environment limits the development of quantum information processing with protons because the interactions between quantum states encoded with single photons are too weak. While quantum gates using the nonlinear effect have been developed for interacting photons, it is difficult to achieve a sufficient success rate.

As an alternative approach, in 2001 Knill, Laflamme and Milburn (KLM) demonstrated an implementation of photonic universal quantum computers achieved using linear optical elements, single-photon sources, and photon detectors [23]. The KLM protocol exploits the photon bunching that occurs in quantum interference between indistinguishable single photons, and the post-detection event. Multi-photon quantum interference with a multi-port interferometer is a key to the operation of a universal set of quantum gates implemented with the KLM scheme. Furthermore, a photonic circuit using multi-photon quantum interference can be a platform not only for quantum computation [24], but also for quantum metrology [25, 26, 27, 28, 29] and communication [30, 31, 32].

In the last twenty years, we have studied multi-photon interference using single photons and a linear optical quantum circuit for realizing quantum technologies. We have demonstrated the realization of several unique photonic quantum devices. In the field of quantum information processing, we have demonstrated quantum gates implemented using the KLM scheme [33, 34]. There are several kinds of quantum gates between two quantum states, such as the C-NOT gate and C-SWAP gate. The development of quantum gates is important since a universal quantum computer can be realized by combining quantum gates. In the field of quantum metrology, we reported beating the standard quantum limit by a phase super-sensitive interferometer in the NOON state [25, 26]. In this paper, we show that quantum entanglement enables higher precision than would otherwise be possible. This research opens the way for high-precision measurement applications using quantum entanglement.

To scale up quantum information processing with single photons, it is essential to increase the number of photons in the quantum interference. This is because the dimension of Hilbert space which describes the multi-photon parallel state exponentially increases as the number of photons increases [35]. Numerous studies have been conducted to develop quantum technologies with many photons [34]. Furthermore, the efforts to prepare multi-photon parallel states is also useful for Boson sampling for quantum supremacy [36]. If a multi-photon parallel state can be prepared with 70–80 photons [37], quantum supremacy can be shown by a multi-mode interferometer [38, 39, 40] and single-photon detectors [41]. Thus, to scale up the multi-photon interference experiments it is important to prepare a multi-photon parallel state.

Increasing the number of photons used in multi-photon quantum interference makes it possible to perform large-scale experiments with a huge Hilbert space. Few studies have focused on the coherence information of the output state of multi-photon quantum interference. Boson sampling only focuses on the output photon number distribution, not the coherence information. If the coherence of a quantum state with many photons can be controlled by a multi-mode interferometer, it is expected that unknown high-dimensional quantum entanglement or more efficient evaluation of complex quantum state can be generated.

For the experimental realization of a source producing a multi-photon parallel state, high visibility in the interference between photons from multiple independent sources is crucial, which means that precise control of generated indistinguishable photons is required. To date, spontaneous parametric down-conversion (SPDC) was considered a convenient source of pairs of photons for testing quantum information [42, 43, 44, 45, 46]. However, a problem with SPDC in a source is that events are occasionally generated with more than a two-photon pair, which can cause errors in the operation of quantum circuits. This is a serious problem for multi-photon interference experiments with many photons included in the input state of the interference, multi-photon parallel state. In this research, we aim to realize a source to generate a multi-photon parallel state in which the probability of having more than two photons in one mode is suppressed.

1.2 Research purpose and outline of this thesis

In this thesis, we study the efficient generation of a multi-photon parallel state from heralded single-photon sources for realizing a large-scale photonic quantum circuit. A photonic quantum circuit can be implemented with a multi-photon multi-port interferometer that can be used for quantum computation, quantum communication, and quantum metrology. It is also an attractive platform for Boson sampling for showing quantum supremacy. Furthermore, a multi-mode interferometer with a complex unitary matrix may be able to evaluate the quantum state more efficiently than quantum full state tomography, as shown in the theoretical paper [47]. Based on this background, we focus on two topics. In the first, we develop experimentally a method to efficiently generate a multi-photon parallel state as the input state of a photonic quantum circuit. Secondly, we demonstrate a novel method [47] to verify the generation of entanglement using mode discrete Fourier transform circuits consisting of linear optical components.

In Chapter 1, we present a brief introduction to the research background and the purpose of this study.

In Chapter 2, we introduce the basic theory of a heralded single-photon source (HSPS) and multi-photon interference between indistinguishable single photons.

In Chapter 3, we report the development of the HSPS employing suppression of the probability of having more than two photons input as a pulse. Unwanted multi-photon generation is a critical problem for scaling up photonic quantum circuits. In this research, we combine two methods to decrease the multi-photon probability: multiplexing of multiple HSPSs and photon pair number discrimination. In this chapter, we report the realization of multiplexed HSPSs using photon number resolving detectors. Then, we adopt photon number resolving detectors using cascaded detectors.

In Chapter 4, we detail the efficient preparation of a multi-photon parallel state from an HSPS. Serial–parallel conversion is an appropriate method to generate the state. The converter can route a stream of N photons at successive intervals from one source to N different spatial modes. We report the experimental realization of a serial–parallel conversion system for two photons with heralding signals. We also theoretically show that serial–parallel conversion for an HSPS can be more efficient than for an unheralded photon source.

In Chapter 5, we present a study of the efficient preparation of a multi-photon parallel state from multiple HSPSs. We propose a new method to convert randomly generated multiple heralded single photons into the desired multi-photon parallel state by active spatial networking (ASN). Compared with the results in Chapters 3 and 4, our new method can reduce the effect of unavoidable losses in the active router because of the optimized routing rules. First, we consider how the proposed method allows us to exponentially increase the efficiency of preparing N-photon parallel states compared with the simple method of N HSPSs. Second, we present a proof-of-principle demonstration of ASN using two HSPSs for generating a two-photon parallel state.

In Chapter 6, we report the first demonstration of the novel method to generate entanglement between two multi-photon and multi-mode local systems using mode discrete Fourier transform (DFT) circuits. This method exponentially decreases the number of resources required for tomography compared with quantum full state tomography. We verify generated three-photon entanglement between two three-mode optical systems. For this experiment, we implement a pair of super-stabilized optical DFT circuits using displaced-Sagnac architecture and hybrid polarizing beamsplitters.

In Chapter 7, this dissertation is summarized.

Chapter 2

Heralded single photon source and multi-photon interference

2.1 Generation of single photons and multi-photon parallel state

It is essential for the large-scale quantum interference experiments to prepare the state of multi-photon in parallel (Multi-photon parallel state) with large number of photons. Therefore, the quality of single photon sources to emit single photons one by one is required to be high. In the field of photonic quantum information processing, an ideal single photon source would have such characteristics; a single photon can be emitted deterministically, the probability of emitting a single photon in a pulse is 100%, the probability of emitting multiple photons is 0%, the emitted photons are indistinguishable, and the generation rate is fast. In this section, firstly, we introduce the brief background and principal of modern techniques for realizing such an ideal single photon source, by use of single photon emitters consisting of one source of emission such as a quantum dots, and heralded single photon source via the nonlinear process. Secondly, we also express the method and current problems about the generation of multiple single photons in parallel for photonic quantum interference experiments.

2.1.1 Single photon emitters

There are various kinds of optical systems that have been investigated for use as on-demand sources of single photons. Until now, a lot of efforts to build single emitter have been performed using color centers [48], quantum dots [49, 50], single atoms [11, 12], single ions [51], single molecules [52]. Although the approaches of these emitter depend on the material system, most of them utilize the same principle to generating a single photon. In general, external driving field is used to put the two-level system into an excited state, and a single photon will be emitted upon relaxation to ground state.

In the optical experiments, the coupling a material with an optical cavity is used to operate the emission characteristic (direction, frequency, and so on) of a photon emitter. By coupling the single emitter to the cavity, the photons is collected into only the field modes of the cavity. As the results, the emission of photons is close to being deterministic. However, for realizing an ideal single photon source, the current single photon emitters have still some challenges to overcome; high-efficiency collection of emitted photons into a single spatial mode, indistinguishable output photons from different sources, cryogenic cooling, and their limited wavelength and bandwidth. Here, we will introduce the some current development of the single emitter.

Semiconductor quantum dots with the artificial atomic system are well developed to produce high brightness and indistinguishable single photons [49, 50]. QDs emit single photons by recombining the electrons and holes when the QD is excited. Until now, various efforts have been made to control the emission from QDs by use of cavities; a photonic-crystal cavity [53], micropillar cavity [54], elliptical micropillars [55], a bragg grating taper fiber [56]. When the emission field of photons is matched to the cavity, the spontaneous emission rate of QDs can be increased due to the Purcell effect. As the recent dramatic development, it is reported that optical systems of QDs in electrically controlled cavities can generate highly indistinguishable single photons efficiently because the electrical bias on the structure reduces charge noise [57]. Furthermore, Wang reported the near-unity single photon emitter with single-photon efficiency of more than 0.5 since they optimized the coupling emitted photons into a fiber [55]. However, it is still challenging to achieve the spectral indistinguishability of photons between two independent QDs, and this way is required cryogenic temperature.

A nitrogen vacancy (NV) color center is formed by an atom and a vacancy at an adjacent lattice position in diamond [58]. NV centers have some advantages. It can be worked at room temperature although some atoms are operated at cryogenic temperature. The spin coherence of NV center is long. NV centers apply to optically detected magnetic resonance [59]. Recently, a silicon vacancy center have developed to overcome some disadvantage of NV center for utilizing a single photon source because of narrower bandwidth of spectrum [60].

2.1.2 Heralded single photon source (HSPS)

As the alternative method, a heralded single photon source (HSPS) based on the process of spontaneous parametric down conversion (SPDC) [61, 62] or four wave mixing (FWM)[63, 64], has been especially widely used. The photons are created in pairs (called signal and idler photon), and one photon (the heralding photon) can be used to herald the creation of the other photon (the heralded single photon). For the case of SPDC, when the pump laser ($\omega_{\mathrm{p}}, \boldsymbol{k}_{\mathrm{p}}$) passes through a nonlinear crystal, the photon pairs ($\omega_{\mathrm{s,i}}, \boldsymbol{k}_{\mathrm{s,i}}$) are generated

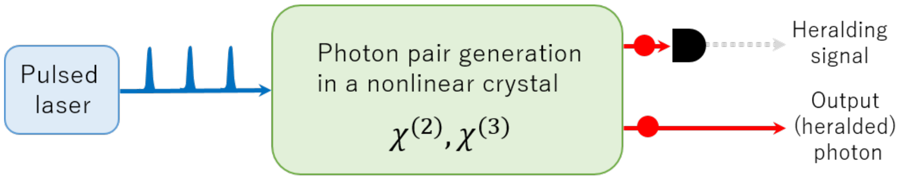

Figure 2.1: Heralded single photon source.

under the energy conservation and phase match condition,

$$\omega_\mathrm{p} = \omega_\mathrm{s} + \omega_\mathrm{i}, \tag{2.1}$$

$$\boldsymbol{k}_\mathrm{p} = \boldsymbol{k}_\mathrm{s} + \boldsymbol{k}_\mathrm{i}, \tag{2.2}$$

where ω_j, $\boldsymbol{k}_\mathrm{j}$ $(j = \mathrm{p}, \mathrm{s}, \mathrm{i})$ is the frequency and wave vector of pump, signal or idler photon. The photon pairs via the process of SPDC are generated from a non-linear crystal, for example, KDP (potassium dihydrogen phosphate), BBO (beta barium borate), $LiNbO_3$ (lithium niobate). Furthermore, periodic poling is promising as the way to engineer the desired phase matching condition and wavelength of photon pairs. This technique benefits the optimization of the state produced, such as no spectral correlation [65, 66] or broadband spectral correlation between signal and idler photons [67]. Until now, quantum optics experiments have typically used this nonlinear optical parametric source due to experimental convenience and their stable performances at room temperature and high indistinguishability of generated photons.

The process of SPDC is inherently probabilistic, and so there is no knowledge of when the events of heralding will occur. For utilizing a HSPS as single photon source, by use of a ultra-short pulsed laser, photon pairs can be produced only within the certain duration time of the pulsed laser. However, because of the nature of SPDC, in addition to the generation of only one pair, there are the finite probability of generating more than one pair, which decreases the purity of heralded photons. This probability of generating unwanted photon pairs increases non-linearity with the interaction strength of the pump laser and the nonlinear crystal. To limit the generation of unwanted multi-photon generation, a HSPS has to be operated with a low probability to generate a single photon pair.

To date there have been various kinds of heralded single photon sources using SPDC or FWM, which can generate high indistinguishable photons [68, 69]. Furthermore, it is reported that a HSPS can be implemented with the integrated optical platforms [70]. For realizing an ideal single photon source, however, the conventional HSPS have still some challenges to overcome; probabilistic generation of photons, unwanted multi-photon generation. In this thesis, we report some demonstrations for solving these problems.

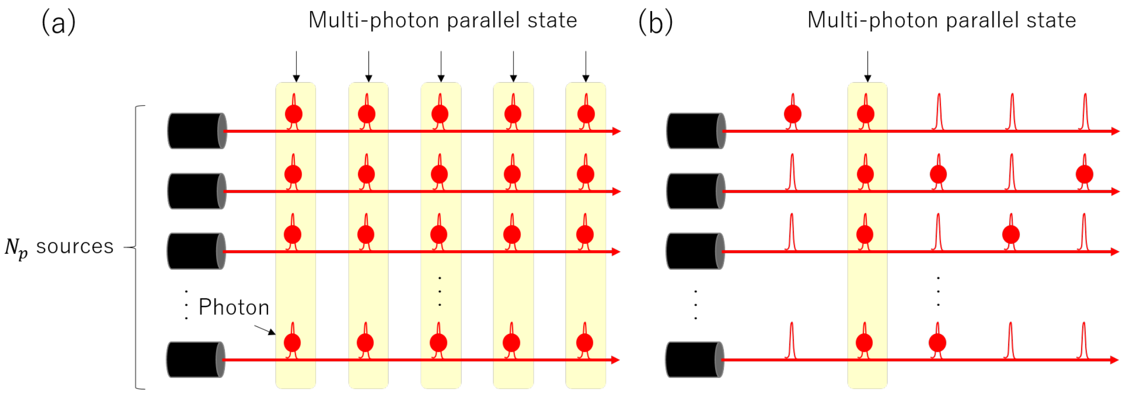

Figure 2.2: (a)Multi-photon generation from multiple independent deterministic single photon sources. (b) Multi-photon generation from multiple independent non-deterministic single photon sources.

2.1.3 Generation of multi-photon parallel state from independent HSPSs

In this section, we would like to talk about the method and current problems about the generation of multiple single photons in parallel.

For multi-photon interference experiments, it is important to realize the source to generate indistinguishable multiple single photons in parallel (Multi-photon parallel state). Figure 2.2(a) shows the multi-photon emitter with independent deterministic single photon sources, where requiring all sources to fire simultaneously. Multi-photon parallel state is existed in the yellow box. Therefore, the probability of having a single photon per pulse of the laser is unity to be one. The rate generating the multi-photon parallel state is also one at the same time. As the results, when the repetition rate of the laser is R_{rep}, we can obtain the results R_{rep} times per a second. Note that the required number of generating multi-photon state per a second depends on the quantum algorithm to calculate faster than the current supercomputer when the interference is optimized perfectly. See the following paper and book for details [23, 71, 72].

However, as discussed, the single photon sources based on SPDC and FWM have the fundamental limitations of spontaneous emission of photons. Therefore, the probability of having a single photon per pulse of the laser is not unity to be p ($0 \leq p \leq 1$). Figure 2.2(b) shows the multi-photon emitter with independent non-deterministic single photon sources. To decrease the unwanted multi photon pair emitted from the source, p is typically limited to low. As the results, even if the HSPS produces perfectly indistinguishable photons, the rate of generating the multi-photon with N sources is p^N. And the waiting time t_{wait} for firing N photons simultaneously is,

$$t_{\text{wait}} = \frac{1}{p^N R_{\text{rep}}}. \tag{2.3}$$

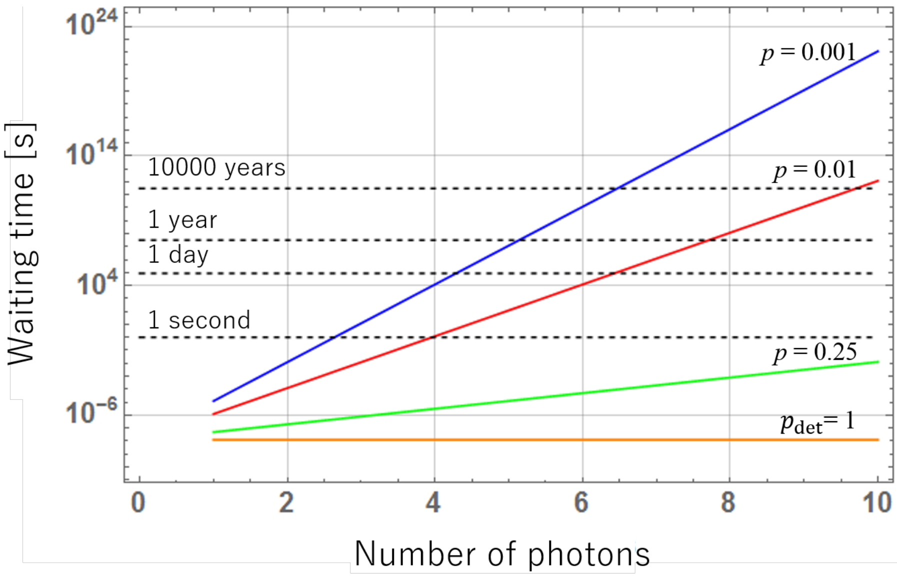

Figure 2.3: Approximate waiting time to produce N_p photons from N_p independent sources. The repetition rate of the pump laser is 82MHz. Blue, Red, Green lines are the time for $p = 0.001, 0.01, 0.25$. The current experiments usually use multiple HSPSs with low p (=0.001,0.01). The maximum p of a HSPS via the nonlinear process is 0.25. Orange line corresponds to the deterministic multi-photon emitter p_{det}=1.

where $R_{\mathrm{rep}} = 82 \times 10^6$ that is the same with the repitition rate of our fs pulsed laser.

Figure 2.3 shows t_{wait} with varying p. As the probability to emit one photon in a pulse p decreases, t_{wait} is exponentially increased with the number of photons. When a HSPS via the SPDC process is used, the maximum heralding probability which corresponds to p is 0.25. However, as we mentioned before, the generation of unwanted multi photons in a pulse can not be ignored if p is large. This is a crucial problem for multi-photon interference experiments when there are many input photons. Therefore, p is usually limited up to 0.1 for performing multi-photon interference experiment. Furthermore, when the experiments is quite sensitive to the generation of unwanted multi photons such as high-fidelity quantum gate operation, p is much less than 0.01. If p is 0.01, the waiting time for producing the ten-photon parallel state (N=10) is the order of 10000 years. This results shows that the development of single photon sources a essential key to increase the number of photons. Especially, it is necessary to overcome the upper-bound of p of 0.25 while suppressing the unwanted multi-photon generation for the multi-photon interference experiments utilizing a HSPS via SPDC or FWM.

2.2 Spectral property of indistinguishable single photons from HSPS

Here, we introduce the spectral property of generated photon pairs via spontaneous parametric down conversion (SPDC), for emitting high indistinguishable heralded single photons. The process of SPDC can be given as the spontaneous annihilation of one pump photons and the creation of two photons (signal photon and idler photon). The frequency of generated photons is correlated due to the energy conservation. However, it is known that the visibility of two-photon interference between independent HSPS to have such a spectral correlation is decreased. Thus, it is necessary to remove the spectral correlation for achieving high indistinguishable heralded photons. In this section, we introduce the meaning of indistinguishable single photons, and the way to generate the indistinguishable single photons from a HSPS using a nonlinear crystal.

2.2.1 Indistinguishable single photon

In the multi-photon interference toward quantum information processing or metrology, we need to know well about experimental grasp of an essential phenomenon called "indistinguishable photons". This is because the quantum state encoded by single photons are usually assumed indistinguishable each other for the interaction between photons. Here, we introduce the indistinguishability of single photons.

A single photon can be described as the single excitation of the electromagnetic field, and can be written in terms of the creation and annihilation operators of the j-th field [73],

$$|1\rangle = \hat{a}_j^\dagger|0\rangle, \tag{2.4}$$

$$|0\rangle = \hat{a}_j|1\rangle, \tag{2.5}$$

where $|1\rangle$ is the state to describe a mode containing one photon, and $|0\rangle$ is the vacuum state. If the independent single photon sources can produce the indistinguishable photons each other, the relations between the creation operators become $\hat{a}_i^\dagger = \hat{a}_j^\dagger$ $(i \neq j)$. And it is also necessary for a single photon source to generate a stream of indisitinguishable single photons. However, for single photon state, this description is incomplete because any information requiring for single photons is not be contained such as frequency, polarization, and so on. Furthermore, since the photon is also wave, it is necessary to have the property of wave function such as infinite spectral bandwidth. For example, the photon with the spectral property can be written as,

$$|\phi(\omega_j)\rangle = \int d\omega_j f(\omega_j)\hat{a}_j^\dagger(\omega_j)|0\rangle, \tag{2.6}$$

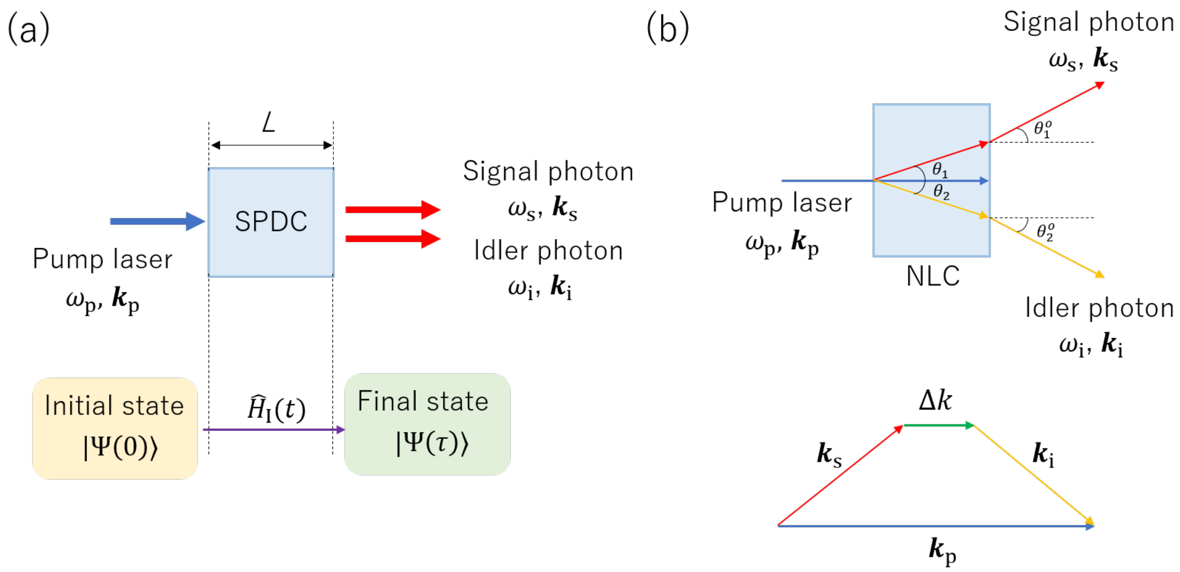

Figure 2.4: (a) The process of spontaneous parametric down conversion. (b) Schematic illustration of a noncollinear photon pair source

where $f(\omega)$ is the spectral distribution. This is not enough to describe the indistinguishable single photons since it still only define the spectral degrees of freedom for a single photon. A highly "indistinguishability" requires almost complete wave-packet overlap, or perfect photon matching, of energy, space, time and polarization. For this, we have to control absolutely over the all degree of freedoms in order to utilize single photons for quantum information processing. In the next sections, we express the method to generate frequency-correlated photon pairs, and indistinguishable single photons from a heralded single photon source via the nonlinear process.

2.2.2 Photon pair generation from a nonlinear crystal

Here, we express the way to generate frequency-correlated photon pairs from a nonlinear crystal. We focus on the generation of photon pairs from a bulk crystal (Type-I and non–colinear) which is used in our experiment. As shown in Fig. 2.4(a), the state of the generated two-photon via SPDC can be given by calculating the time evolution of the initial state $|\Psi(0)\rangle$ into the final state $|\Psi(\tau)\rangle$ under the SPDC Hamiltonian $\hat{H}_I(t)$ [74],

$$|\Psi(t)\rangle = \exp\left(\frac{1}{i\hbar}\int_0^\tau dt\hat{H}_I(t)\right)|\Psi(0)\rangle, \tag{2.7}$$

This two-photon state can also be expressed approximately as,

$$|\Psi(t)\rangle \approx \left(1 + \frac{1}{i\hbar}\int_0^\infty dt\hat{H}_I(t)\right)|\Psi(0)\rangle. \tag{2.8}$$

In the process of interaction, the effective Hamiltonian of SPDC $\hat{H}_l(t)$ can be given as,

$$\hat{H}_l(t) = \epsilon_0 \int \chi^{(2)} d^3\boldsymbol{r} \hat{E}_{\mathrm{p}}(\boldsymbol{r}, t) \hat{E}_{\mathrm{s}}(\boldsymbol{r}, t) \hat{E}_{\mathrm{i}}(\boldsymbol{r}, t), \tag{2.9}$$

where $\hat{E}_j$ are the quantised field operators for the pump (p), signal (s) and idler (i) respectively. $\boldsymbol{r} = (x, y, z)$ is the position vector in the crystal. $\chi^{(2)}$ is the non-linear susceptibility tensor. After decomposing the operators into positive and negative components, $\hat{E}_j(\boldsymbol{r}, t) = \hat{E}_j^{(+)}(\boldsymbol{r}, t) + \hat{E}_j^{(-)}(\boldsymbol{r}, t)$, the SPDC Hamiltonian is expressed as,

$$\hat{H}_l(t) = \epsilon_0 \int \chi^{(2)} d^3\boldsymbol{r} \hat{E}_{\mathrm{p}}^{(+)}(\boldsymbol{r}, t) \hat{E}_{\mathrm{s}}^{(-)}(\boldsymbol{r}, t) \hat{E}_{\mathrm{i}}^{(-)}(\boldsymbol{r}, t) + \mathrm{H.c.}, \tag{2.10}$$

The each components of the field operators using annihilation and creation operators are,

$$\begin{aligned} \hat{E}_j^{(+)}(\boldsymbol{r}, t) &= (\hat{E}_j^{(-)}(\boldsymbol{r}, t)))^\dagger \\ &= \int_0^\infty d\omega_j A_j(\omega_j) \hat{a}_j(\omega_j) \mathrm{exp}[i(\boldsymbol{k}(\omega_j)\boldsymbol{r} - \omega_j t)], \end{aligned} \tag{2.11}$$

where we simplified $A_j(\omega_j) = i\sqrt{\hbar\omega_j / 2\epsilon_0 n^2(\omega_j) V_Q}$ and V_Q is the quantization volume. $\boldsymbol{k}(\omega_j)$ is the wavevector in the bulk crystal. As the field of the pump has to be strong, it allows the electric field operator treated classically. The positive frequency component of the pump is replaced with,

$$\hat{E}_p^{(+)}(\boldsymbol{r}, t) = E_p^{(+)}(\boldsymbol{r}, t) = A_{\mathrm{p}} \int_0^\infty d\omega_{\mathrm{p}} \alpha(\omega_{\mathrm{p}}) \mathrm{exp}[i(\boldsymbol{k}(\omega_j)\boldsymbol{r} - \omega_j t)], \tag{2.12}$$

where A_{p} is the amplitude of the pump and $\alpha(\omega_{\mathrm{p}})$ is the spectral property of the pump laser (called pump envelope function). Substituting Eqs.2.10,2.11,2.12 into Eq.2.8, the two photon wave function of signal and idler photons after the SPDC interaction can be described as,

$$|\Psi(\omega_{\mathrm{s}}, \omega_{\mathrm{i}})\rangle = \eta \iint d\omega_{\mathrm{s}} d\omega_{\mathrm{i}} \alpha(\omega_{\mathrm{s}} + \omega_{\mathrm{i}}) \phi(\omega_{\mathrm{s}}, \omega_{\mathrm{i}}) \hat{a}_{\mathrm{s}}(\omega_{\mathrm{s}}) \hat{a}_{\mathrm{i}}(\omega_{\mathrm{i}}) |0\rangle, \tag{2.13}$$

where $\eta = \epsilon_0 \chi^{(2)} A_{\mathrm{s}}(\omega_{\mathrm{s}}) A_{\mathrm{i}}(\omega_{\mathrm{i}}) A_{\mathrm{p}} L$ is the integrated parameter related to the length of the crystal L. The zero photon state is removed because of the coincidence measurement. The phasematching function $\phi(\omega_{\mathrm{s}}, \omega_{\mathrm{i}})$ is given by,

$$\phi(\omega_{\mathrm{s}}, \omega_{\mathrm{i}}) = \mathrm{exp}\left[\frac{i\Delta k L}{2}\right] \mathrm{sinc}\left[\frac{\Delta k L}{2}\right], \tag{2.14}$$

where Δk is the phase mismatch between the fields. The correlated frequency amplitude of the two-photon state is found by calculating the product of the pump envelope function $\alpha(\omega_{\mathrm{s}} + \omega_{\mathrm{i}})$ with the phasematching function $\phi(\omega_{\mathrm{s}}, \omega_{\mathrm{i}})$. The function is called the joint spectral amplitude $f(\omega_{\mathrm{s}}, \omega_{\mathrm{i}})$, and $|f(\omega_{\mathrm{s}}, \omega_{\mathrm{i}})|^2$ is the joint spectral intensity (JSI).

For the case of a Type - I SPDC (Fig. 2.4(b)), the pump photon (extraordinary ray) is converted to signal and idler photons (ordinary ray). This nonlinear process have to satisfy the phase match conditions and the energy conservation,

$$\boldsymbol{k}_{\rm s} + \boldsymbol{k}_{\rm i} = \boldsymbol{k}_{\rm p}, \tag{2.15}$$

$$\omega_{\rm s} + \omega_{\rm i} = \omega_{\rm p}, \tag{2.16}$$

where $\boldsymbol{k}_j (j = {\rm p, s, i})$ is the vector of pump, signal and idler photon. However, the phase match condition can not always be satisfied perfectly due to the some experimental problems. The term is called phase mismatch Δk. For the Type-I noncolinear condition, Δk is calculated to be [75],

$$\Delta k = k_{\rm p}(\lambda_{\rm p}, \Psi) - k_{\rm s}(\lambda_{\rm s})\sqrt{1 - \left(\frac{\sin\theta_{\rm s}^0}{n_{\rm o}(\lambda_{\rm s})}\right)} - k_{\rm i}(\lambda_{\rm i})\sqrt{1 - \left(\frac{\lambda_{\rm i}}{\lambda_{\rm s}}\right)^2 \left(\frac{\sin\theta_{\rm i}^0}{n_{\rm o}(\lambda_{\rm i})}\right)}, \tag{2.17}$$

where $k_{\rm p}(\lambda_{\rm p}, \Psi)$ is simplified from $2\pi n_{\rm e}(\omega_{\rm p}, \Psi)/\lambda_{\rm p}$. $n_{\rm o}, n_{\rm e}$ is the ordinary and extraordinary refractive index of the bulk crystal. Ψ is the angle of the optic axis with respect to the direction of the pump laser. From the energy conservation, the pump envelope function can be expressed as follows,

$$\alpha(\omega_{\rm s} + \omega_{\rm i}) = \exp\left[-\left(\frac{\omega_{\rm s} + \omega_{\rm i} - 2\omega_{\rm p0}}{\sigma_{\rm p}}\right)^2\right], \tag{2.18}$$

where $\sigma_{\rm p}(= 2\pi {\rm c}\delta_{\rm p}\lambda/\lambda_{\rm p0}\sqrt{2\ln 2})$ is the full width at half maximum bandwidth of the pump laser. c is speed of light.

2.2.3 Spectral property of heralded single photons

Photon pairs without spectral correlation are required for a heralded single photon source. Even if most of the current photon detectors can not discriminate the frequency of generated photons, the state of two-photon state is projected into a mixture of spectral state after one of the photon pairs are detected for heralding. This mixed state reduces the visibility of the two-photon interference because of low indistinguishability of photons. Thus, it is necessary to eliminate the frequency correlation of signal and idler photons. Also, the frequency correlation decreases the visibility of the two photon interference due to the group velocity mismatch of the photons [68, 69].

In general, there are a simple way to generate the frequency non-correlated photon pairs. That is to use narrow band spectral filtering to reshape the JSI. For the filtered JSI, the spectra of signal and idler photons is Gaussian frequency profile,

$$f(\omega) = \frac{1}{\sqrt{2\pi}\sigma_0}\exp\left(\frac{-(\omega - \omega_0)^2}{2\sigma_0^2}\right). \tag{2.19}$$

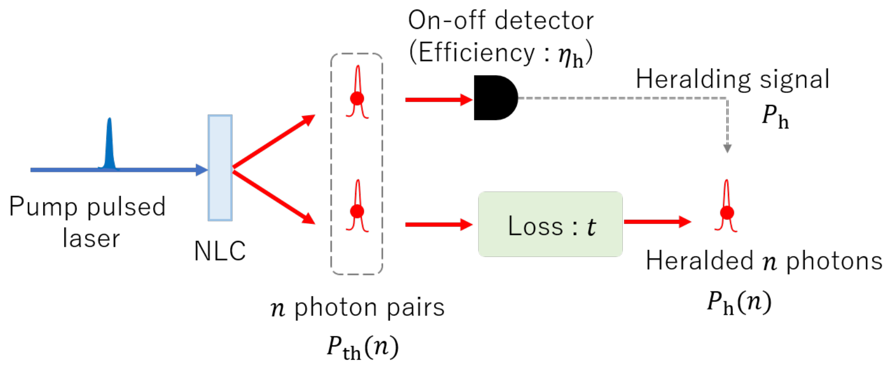

Figure 2.5: Schematic illustration of a heralded single photon source.

where ω_0 is the central of the frequency. The state of heralded single photons of high purity is,

$$|\phi\rangle = \int d\omega f(\omega)\hat{a}^\dagger(\omega)|0\rangle. \tag{2.20}$$

This spectral profile improves the high pure heralded single photon state. Note that the effect of group velocity mismatch is reduced as the narrower filter [68, 69]. Note also that the spectral correlation can be eliminated by controlling the quasi-phase matching condition of the "periodic poling" crystal [65, 66].

2.3 Photon number distribution of generated heralded photons

Photon number distribution of generated single photons from a HSPS is one of the most important characteristics for a single photon source. This is because the measurement time depends on the probability to produce single photons in a pulse, and the error in photonic quantum operation is caused by the unwanted multi-photon generation. This section consists of two topics; theory of photon number distribution of a HSPS and the way to obtain absolute experimental parameters for estimating the distribution.

2.3.1 Theory of photon number distribution

The output photon number distribution from a conventional HSPS can be described by use of some parameters. In this section, the general method of the photon number distribution is introduced.

Figure 2.5 shows a conventional HSPS. A nonlinear crystal (NLC) is pumped by a pulsed laser and generates a photon pair via an SPDC process. One of the photons in a pair is detected by an on–off detector, which generates a heralding signal upon detection. In this paper, we call the photon detected to generate heralding signals 'idler photon' and the photon to be selected and emitted 'signal photon'. We can calculate the output photon number distribution from a heralded single photon source $P_{\mathrm{h}}(n)$, where n is the number of output photons. The photon number distribution produced by a photon pair source is,

$$|\Psi\rangle = \sum_{n=0}^{\infty} a_n |n_{\mathrm{s}}, n_{\mathrm{i}}\rangle, \tag{2.21}$$

where $|a_n|^2 = P(n)$ is the probability to generate n photon pairs simultaneously. For spectrally correlated photon pairs, $P(n)$ is given by Poisson distribution $P_{\mathrm{Po}}(n)$,

$$P(n) = P_{\mathrm{Po}}(n) \equiv \frac{\bar{N}^n e^{-\bar{N}}}{n!}. \tag{2.22}$$

where $\bar{N}$ is the mean number of photon pairs in a pulse. For spectrally uncorrelated photon pairs, $P(n)$ is given by a Thermal distribution $P_{\mathrm{th}}(n)$ as discussed in next section,

$$P(n) = P_{\mathrm{th}}(n) \equiv \frac{\bar{N}^n}{(1+\bar{N})^{1+n}}. \tag{2.23}$$

When the pulse duration of the pump laser is much shorter than the measurement time of the single detector, the probability $P(n)$ of generating n photon pairs per pulse is Thermal distribution [76]. Note that the number of photons in the measurement time window of the detector is needed to be negligibly low.

One of the photon pair from the NLC is detected by a single photon detector for generating heralding signals which indicates the presence of another photons. It is assumed that the detector at the heralding arm is an on–off detector. An on–off detector generates only one detection signal, even when more than one photon hit the detector. Therefore, in some cases where multiple pairs are generated in one pulse duration time, more than two photon signals will be produced for one heralding signal because the on-off detector cannot distinguish such events. The heralding measurement performed by the detector is described by two kinds of positive operator value measure elements when m photons are inserted into the on–off detector,

$$P_{\mathrm{D}}(\text{"trigger"}|m) = 1 - (1-\eta_{\mathrm{h}})^m, \tag{2.24}$$

$$P_{\mathrm{D}}(\text{"no} - \text{trigger"}|m) = (1-\eta_{\mathrm{h}})^m, \tag{2.25}$$

where η_{h} is the over all detection efficiency of the detector which include all losses at the heralding arm.

The probability of heralded n-photons can be characterized by the coincidence probability $P_{\mathrm{C}}(n)$ that n photons are detected at the output when the heralding signal is emitted, and the heralding probability P_{h} that a heralding signal is produced. The conditional probability of heralded single photon with n photons are given as,

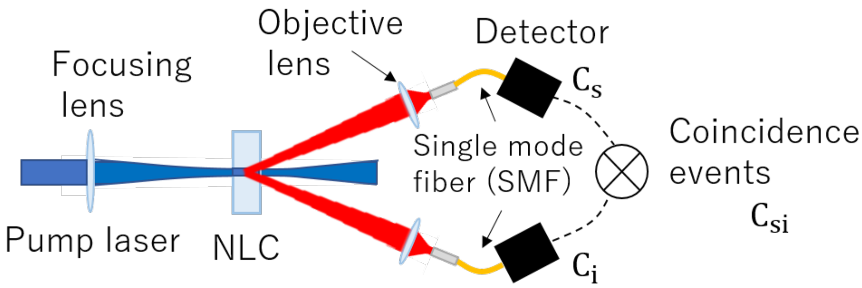

Figure 2.6: Experimental setup to couple the generated photon pairs into single mode fibers, and to measure the coincidence events between two detection signals from the two detectors.

$$P_{\mathrm{h}}(n) = \frac{P_{\mathrm{C}}(n)}{P_{\mathrm{h}}}, \tag{2.26}$$

$$P_{\mathrm{h}} = \sum_{k=0}^{\infty} P(k)\{1-(1-\eta_{\mathrm{h}})^k\}, \tag{2.27}$$

$$P_{\mathrm{C}}(n) = \sum_{m=n}^{\infty} P(m)\{1-(1-\eta_{\mathrm{h}})^k\}_m C_n t^n (1-t)^{m-n}. \tag{2.28}$$

The single-pair generation probability of $P_{\mathrm{th}}(1)$ peaks at only 25% due to the non-negligible likelihood of unwanted zero- and multiple-pair generations. The unwanted multi-photon emission is a crucial problem for multi-photon interference experiments when there are many input photons. This results that $P_{\mathrm{C}}(n)$ is also limited. Hence the performance of sources is far from the ideal single photon source.

2.3.2 Obtain the absolute experimental parameters for estimating the output photon number distribution

For estimating the photon number distribution of a HSPS, it is necessary to achieve some experimental parameters. Here, we will explain how to achieve these parameters. They are detection efficiency for heralding signals (η_{D}), optical losses (t), and mean number of photon pairs generated from a NLC ($\bar{N}$), as mentioned in the previous section. Figure 2.6 shows the experimental setup for obtaining required parameters by use of a photon pair source. For various experiments using photon pairs, the pair of photons are coupled into single mode fibers. Therefore, the losses include optical component's losses and coupling photon pairs into single mode fibers.

The efficiency of optical losses and detection efficiency is named as overall quantum efficiency χ_{j} ($j = \mathrm{s}, \mathrm{i}$). χ_{j} can be characterized by some parameters; $C_{\mathrm{s,i}}$ is the rate of detecting the number of signal or idler photons, and C_{si} is the coincidence events among the detection signals from the two detectors.

$$C_{\mathrm{s}} = \chi_{\mathrm{s}} C_0 + C_{\mathrm{dark}}, \tag{2.29}$$

$$C_{\mathrm{i}} = \chi_{\mathrm{i}} C_0 + C_{\mathrm{dark}}, \tag{2.30}$$

$$C_{\mathrm{si}} = \chi_{\mathrm{s}} \chi_{\mathrm{i}} C_0, \tag{2.31}$$

where C_{dark} is dark counts of the detector, assuming negligible small. Note that these equations can be used when the mean number of photon pairs $\bar{N}$ is very low. C_0 is the rate of generating photon pairs from a NLC without any losses. The efficiency of coupling photon pairs into single mode fibers is defined as,

$$\chi_{\mathrm{s,i}} = \frac{C_{\mathrm{si}}}{C_{\mathrm{i,s}}}. \tag{2.32}$$

If the heralded photons are idler photon, χ_{i} is the product of t and detection efficiency, and χ_{s} corresponds to η_{D}. The mean number of photon pairs ($\bar{N}$) corresponds to C_0/R_{rep}, where R_{rep} is the repetition rate of a pump pulsed laser. For utilizing such parameters, we can estimate the probability to have n photons in a pulse from a HSPS.

Finally, we would like to say that achieving the optimal coupling efficiency is significantly important way to enhance the performance of a HSPS. Now, the maximum overall detection efficiency ($\chi_{\mathrm{s,i}}$) is up to about 15% for quite narrow bandwidth of 2 nm, and up to about 25% for narrow bandwidth of 4nm. For the future large-scale experiments, the optimization of photon pair sources ($\chi_{\mathrm{s,i}} \approx 1$) is required by referring the recipes [77, 78, 79], the reports [65, 80, 81] and the useful application *spdcalc.org*.

2.4 Multi-photon interference

For performing quantum information processing, quantum information is needed to be encoded in quantum state of given degree of freedom of photons (for example, path, time-bin, polarization), and to be interacted between the encoded quantum states. Single photons are powerful candidate of quantum information processing because quantum states of photons can be easily manipulated with high precision by use of passive linear-optical devices, including beam splitters, polarizing beam splitters, wave plates, and phase shifters. For the interaction between photons, quantum interference is important. Here, we introduce one of the famous two-photon interference (Hong-Ou-Mandel interference), and general multi-photon interference using a multi-port optical circuit.

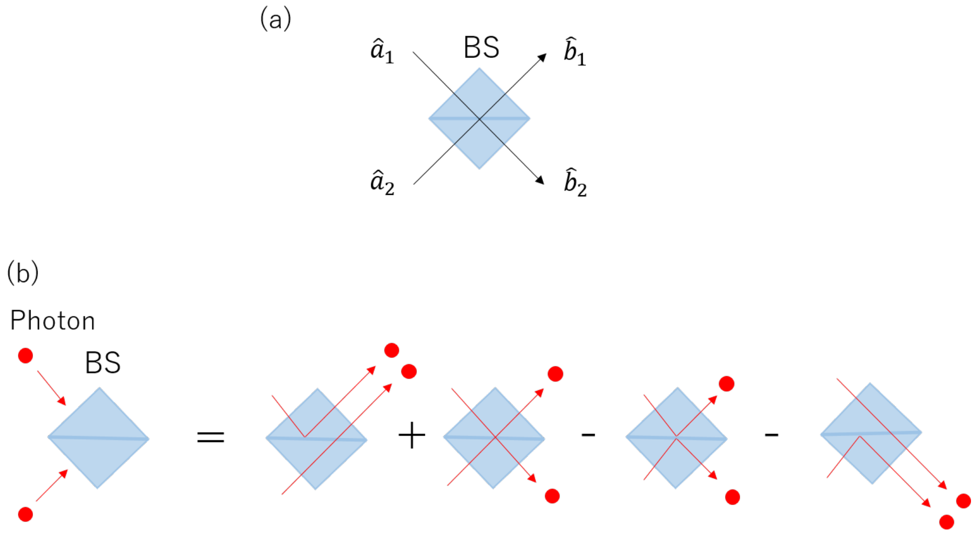

Figure 2.7: (a)Illustration of the input and output modes of a beamsplitter(BS).(b)Illustration of four patterns corresponding to the interference between two single photons at a 50:50 beamsplitter.

2.4.1 Hong-Ou-Mandel interference

Hong-Ou-Mandel (HOM) interference is an effect of qunatum interference between two single photons at a beamsplitter [82]. This effect of HOM interference is dependent on the indistinguishability of photons, and is the most elementary optical effect for the KLM scheme.

The beamsplitter is one of the most important optical elements. It has two spatial input modes and two output modes (Fig.2.7(a)). For a 50:50 beamsplitter, a photon incident into one of the input ports can be found in either output port with equal probability (50%). In general, the beamsplitter can be written by a reflection coefficient R and a transmission coefficient T. The transformation by use of the beamsplitter is given by,

$$\hat{b}_1 = R\hat{a}_1 + T\hat{a}_2, \tag{2.33}$$

$$\hat{b}_2 = T\hat{a}_1 - R\hat{a}_2, \tag{2.34}$$

where $\hat{a}_i$ $(i = 1, 2)$ is the annihilation operator for the i'th input mode of the beamsplitter, and $\hat{b}_i$ $(i = 1, 2)$ is the annihilation operator for the i'th output mode of the beamsplitter. As the energy conservation $(R^2 + T^2 = 1)$ and π phase shift on reflection, the relation can be converted to that described by creation operators,

$$\hat{a}_1^\dagger = R\hat{b}_1^\dagger + T\hat{b}_2^\dagger. \tag{2.35}$$

$$\hat{a}_2^\dagger = T\hat{b}_1^\dagger - R\hat{b}_2^\dagger. \tag{2.36}$$

When two single photons are input to the beamsplitter, the input state and output state can be described by Fock state,

$$
\begin{aligned}
|\psi\rangle &= \hat{a}_1^\dagger \hat{a}_2^\dagger |0\rangle \\
&= (R\hat{b}_1^\dagger + T\hat{b}_2^\dagger)(T\hat{b}_1^\dagger - R\hat{b}_2^\dagger)|0\rangle \\
&= (RT\hat{b}_1^\dagger\hat{b}_1^\dagger + T^2\hat{b}_2^\dagger\hat{b}_1^\dagger - R^2\hat{b}_1^\dagger\hat{b}_2^\dagger - TR\hat{b}_2^\dagger\hat{b}_2^\dagger)|0\rangle,
\end{aligned}
\tag{2.37}
$$

where $|0\rangle$ is the vacuum state that no photons are existed. Now, as the beamsplitter is balanced ($R = T = 1/\sqrt{2}$), and $\hat{b}_1^\dagger$ and $\hat{b}_2^\dagger$ commute ($[\hat{b}_1^\dagger, \hat{b}_2^\dagger]$=0), the above equation is,

$$
|\psi\rangle = \frac{1}{\sqrt{2}}(\hat{b}_1^\dagger\hat{b}_1^\dagger - \hat{b}_2^\dagger\hat{b}_2^\dagger)|0\rangle. \tag{2.38}
$$

Therefore, when two photons enter a 50:50 beamsplitter, they will always exit the beamsplitter in the same output mode. This results also shows that HOM interference will only occur if the two photons are pure and indistinguishable.

Figure 2.7(b) shows the two photons in the output modes in a superposition of four patterns from a beamsplitter. The effect of HOM interference arise as the phase shift that occurs on reflection at the face of the beamsplitter. The term corresponding to both photons reflected changes π phase relative to the transmitted term. When the input photons are indistinguishable, the terms corresponding to photons transmitted and reflected destructively interfere and cancel out. Finally, only two terms, which both photons in either output mode, are left.

The Hong-Ou-Mandel interference provides a powerful tool to estimate the degree of indistinguishability of two separately emitted photons [83]. The visibility of the HOM interference dip signal is degraded mainly due to the distinguishability of the two photons, for example in the spatial or temporal domain. Only if one photon is perfectly the same with another photon, both photons always output in the same mode. This HOM interference is the unique technique to confirm the indistinguishability of generated single photons.

2.4.2 Multi-photon interference using a multi-port optical circuit

Multi-photon interference using a multi-port optical circuits is essential to realize an universal quantum computer [23] or generate high-dimensional entanglement [35]. Then, the multi-photon interferometer can be realized by a linear optical circuit which describes an unitary operator [38]. Arbitrary unitary operators can be implemented mathematically on optical modes [84, 85, 86, 87]. Figure 2.8 shows the schematic illustration of photonic quantum circuits. In general, a multi-port interferometer conserves energy, which the

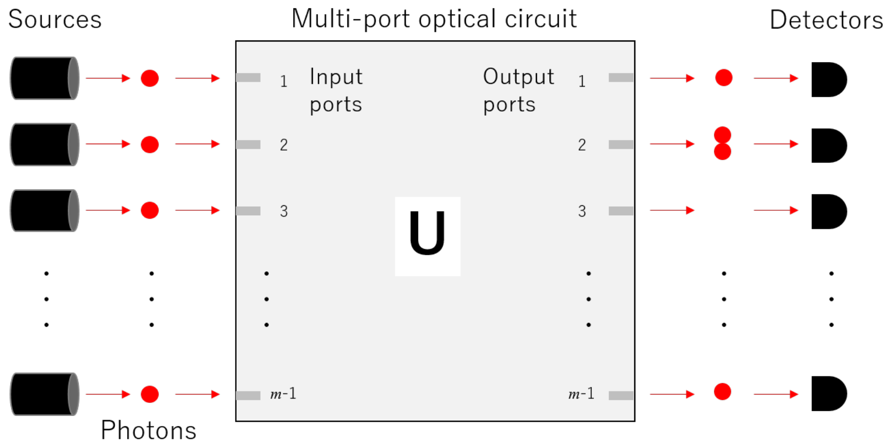

Figure 2.8: Schematic illustration of a multi-photon interference using a multi-port optical circuit. The input state is $|1, 1, \cdots\rangle$.

total input energy equals the total output energy. The circuits consists of multiple single photons,a linear optical multi-port interferometer, and single photon detectors.

The unitary operation in the circuit is described by unitary transformation of input Fock state. The general quantum state of multiple indistinguishable single photons in the Fock space can be defined as [88],

$$|n_1, n_2, \cdots\rangle = \prod_{i=1} \frac{\hat{a}_i^{\dagger n_i}}{\sqrt{n_i!}}|0\rangle \tag{2.39}$$

where $\hat{a}_i^\dagger$ is the creation operators of photons in the mode i, satisfying bosonic commutation. n_i is the number of photons in the mode i. A passive linear-optical device is described by a unitary transformation of creation,

$$\hat{b}_j^\dagger = \sum_n U_{ij}\hat{a}_i^\dagger, \tag{2.40}$$

where U denotes the unitary matrix of linear circuit. An arbitrary unitary circuit with multiple inputs and outputs can be obtained with such devices, as the general theory in [84]. Finally, the output results can be obtained by post-selected detection of output photons from the circuit [23, 71].

Until now, various kinds of quantum gates with optical linear circuits and a few single photons have been demonstrated. For example, as the smallest circuits with KLM protocol, various quantum gates have been demonstrated; C-NOT gate [33], C-SWAP [34], Square root of Swap gate [89], and so on. Furthermore, some kinds of quantum algorithm with small scale photonic quantum linear circuits have also been realized; Shor's factorization [90], Grover's algorithm [91, 92], Deutsch–Jozsa algorithm [93], and so on. Integrated re-programmable and universal linear optical circuits have already realized, and quantum calculation with small scale has been already done by the integrated universal circuit [38, 94, 95]. Multi-port interference with multi single photons or multiple nonlocal photon pairs is also useful to produce specific quantum state; NOON state [25], W state [96], GHZ state [97], cluster state [91], graph state [98], or Qudit [99]. Different from an universal quantum computer, photonic quantum simulator using the method of variational quantum eigensolver is also attractive attention due to relatively practical method by use of a hybrid classical-quantum algorithm [100, 101].

Next, we introduce alternative ways to implement multi-photon interference circuits. Recently, the quantum interference between different color photons with a nonlinear interferometer is proposed and demonstrated [102]. This uses the mode mixing by frequency conversion instead of a beam splitter. Also, three photon interference using different color photons and multi-port linear optical circuits has been attractive attention [103, 104, 105, 106, 107]. This uses the mode mixing by complex linear operation. These ways are expected to be one of the practical methods because it is not necessary to prepare multiple indistinguishable single photons.

Despite the recent developing technologies, the implementation of an universal quantum computer is still challenging. Boson sampling becomes hot topic since the calculation of the photon number distribution of single photons with a given linear photonic network is believed to be classically hard task (NP-hard) and will be a promising candidate for the quantum supremacy [36]. To date, some kinds of Boson sampling experiments with 3-6 photons have been demonstrated [108, 109, 110, 111, 112].

Chapter 3

Suppressing the generation of undesired multi photons from a heralded single photon source

3.1 Introduction

As we mentioned before, heralded single photon sources (HSPS) using spontaneous parametric down conversion (SPDC) have been widely used for generating photons with negligibly small jitter, which makes it possible to achieve high visibility for quantum interference at room temperature [68]. However, for scaling up the photonic quantum circuit with multiple single photons and multiple modes, the unavoidable generation of multi photons from a HSPS is a crucial problem for multi-photon interference experiments when there are many input photons. The multi-photon generation is one of the problems for a HSPS that occasionally events that generate more than two photons occur, which may cause errors in the operation of quantum circuits.

To solve this problem, two methods have been proposed. The first method is called the multiplexed heralded single-photon source (Multiplexed-HSPS). A Multiplexed-HSPS consists of multiple SPDC sources, and upon the detection of an idler photon from one of the sources, the corresponding signal photon is selected and emitted [113, 114, 115, 116, 117, 118, 119, 120, 121, 122]. The second method uses a photon-number-resolving detector (PND) to monitor the number of generated photon pairs from a SPDC source and select cases for which only one pair is created [118, 123, 124, 125, 126]. To evaluate the performance of these methods, Shapiro and Wong conducted a theoretical analysis assuming a Poisson distribution for the generated photons from the SPDC source [115], and D. Bonneau et al. conducted an analysis assuming a thermal distribution of the generated SPDC [118]. However, in these theoretical analyses, the PNDs are assumed to be able to distinguish a number of photons up to infinity. Although the development of PNDs is under investigation, there are still limitations in the detection efficiencies and response times. Furthermore, the realization of multiplexing of heralded single photon sources using photon number resolving detectors (Multiplexed-HSPS with PND) has not yet been reported.

In this section, we report the experimental realization of Multiplexed-HSPS with PND. For this, we adopted a PND using cascaded detectors. We also developed the theory to describe such Multiplexed-HSPS with PND considering a limited number of cascaded detectors. We found that even a small number of detector cascade is very effective in reducing excess photon emission in certain circumstances. With the realized Multiplexed-HSPS with PND equipped with two SPDC sources and a PND consisting of two on–off detectors, we found that the two-photon components are reduced to $44.2 \pm 0.7\%$ compared to a normal HSPS.

3.2 Methods to suppress unwanted multi-photon emission

In this research, we focus on the methods of photon pair number discrimination and spatial multiplexing for suppressing unwanted multi-photon emission from a HSPS. We introduce them.

3.2.1 Photon pair number discrimination

Here, we introduce the method of photon pair number discrimination to suppress unwanted multi-photon emission from a HSPS. For a conventional HSPS using an on–off detector (Section 2.1.2), the multi-photon emission can not be discriminated. To prevent multiple photon signals from being produced, a HSPS using a photon number resolving detector (PND) [Fig. 3.1(a)] generates a heralding signal only when the PND detects only one photon. The excess-photon emission can thus be suppressed.

Although considerable effort has been put into realizing PNDs, the current devices are well short of being an ideal detector that can distinguish a number of incident photon up to infinity. As a more practical approach, we consider a PND using cascaded on–off detectors. As shown in Fig. 3.1(b), an incoming mode is divided equally into 2^D paths using 50:50 beam splitters (BS) and directs them into 2^D on–off detectors, where D is the number of detector cascade. Figure 3.1(b) illustrates an example of such a cascaded detector [$D = 2$]. Note that recently developed PNDs consisting of multiple superconducting nanowire single-photon detectors can be considered such a type of cascaded detector, with $D = 6$ [127]. If $D \to \infty$, an ideal cascaded detector is able to distinguish a number of photons up to infinity.

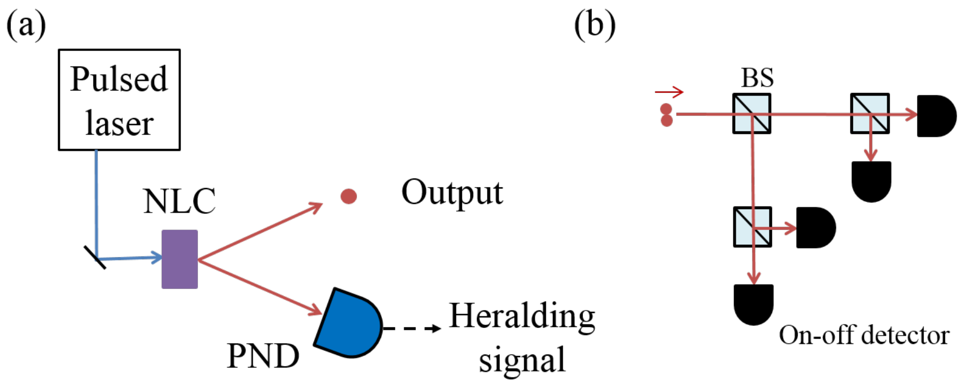

Figure 3.1: (a)Scheme of HSPS using a PND $[S = 1, D = 1]$. (b)cheme of a cascaded detector $[D = 2]$. The detector consists of 50:50 beam splitters (BS) and on–off detectors.

3.2.2 Spatial multiplexing

Here, we introduce the method of multiplexing of heralded single photon sources to suppress the unwanted multi-photon emission. Until now, spatial [113, 114, 115, 116, 117, 128], temporal[120, 122], frequency[129], and orbital momentum angular multiplexing [130] have been proposed and demonstrated. In this research, we focus on spatial multiplexing.

Spatial multiplexed-HSPS is an approach to reduce the two or more photon probability. A Multiplexed-HSPS consists of two SPDC sources. Figure 3.2 shows a schematic of a simple Multiplexed-HSPS for two SPDC sources and a 2×1 optical switch, $S = 2$, where S is the number of SPDC sources per Multiplexed-HSPS. The pump laser is split equally by a BS, and injected into each NLC. The heralding signals to detect idler photons are used to identify which source has created a photon pair. The signal photon of the generated pair is guided to an output port by an optical switch. Even if each idler photon is detected by an on–off detector, the unwanted multi photons are suppressed. By replacing the on–off detectors with PNDs, the performance of Multiplexed-HSPS with PND is improved.

The reason why the method of multiplexing can reduce only the probability of unwanted multi photons is because each photon pair sources in parallel is pumped by the pump laser with reduced intensity. Here, we compare the photon number distribution of a conventional HSPS and a multiplexed HSPS when the intensity of the pump laser is I. Approximately, the photon number distribution of a conventional HSPS is,

$$P(1) = \alpha I, \tag{3.1}$$

$$P(2) = \beta I^2. \tag{3.2}$$

$P(1)$ is proportional to I. $P(2)$ is the square of I. The photon number distribution of a

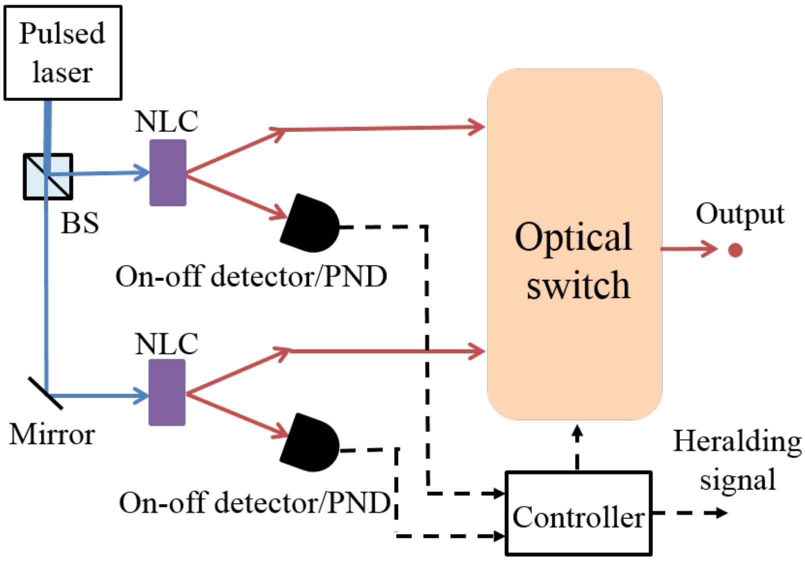

Figure 3.2: Scheme of Multiplexed-HSPS [$S = 2$] with on-off detectors/ Multiplexed-HSPS with PND [$D = 2$] with PNDs.

multiplexed HSPS consisting two photon pair sources is,

$$P(1) = \alpha\frac{I}{2} + \alpha\frac{I}{2} = \alpha I \tag{3.3}$$

$$P(2) = \beta\left(\frac{I}{2}\right)^2 + \beta,\left(\frac{I}{2}\right)^2 = \beta\frac{I^2}{2}. \tag{3.4}$$

Therefore, only $P(2)$ is decreased by half compared with that of a conventional HSPS. The strict photon number distribution and numerical analysis are introduced in the next section.

For further suppressing the probability to generate the unwanted multi-photon in a pulse, the spatial Multiplexed-HSPS can be extended to multiple number of sources by cascading them [115].

3.3 Numerical analysis of photon number statistics

Here, we express the numerical analysis of the output photon number distribution of our suggested multiplexed-HSPS using cascaded on-off detectors.

3.3.1 Theory of photon number statistics

Here, we derive the photon number distribution of a Multiplexed-HSPS using cascaded detectors $P_{\mathrm{h}}(n)$ under non-ideal experimental conditions. For such conditions, we consider that a cascaded detector has a non-unity detection efficiency (η_{h}), and optical switches exhibit losses (t).

A SPDC source is characterized by the mean number of photon pairs in a pulse ($\bar{N}$), the probability that a heralding signal is produced P_{herald} and the probability that n photons are detected at the output when the heralding signal is obtained $P_{\text{C}}(n)$. We derive P_{herald} and $P_{\text{C}}(n)$ using a cascaded detector. The output state $P(n)$ of a single-mode SPDC follows a thermal distribution $P_{\text{th}}(n)$:

$$P(n) = P_{\text{th}}(n) \equiv \frac{\bar{N}^n}{(1+\bar{N})^{1+n}}, \tag{3.5}$$

where $\bar{N}$ is the mean number of photon pairs in a pulse. For a multi-mode SPDC, $P(n)$ follows a Poisson distribution $P_{\text{Po}}(n)$:

$$P(n) = P_{\text{Po}}(n) \equiv \frac{\bar{N}^n e^{-\bar{N}}}{n!}. \tag{3.6}$$

When only one of the on–off detectors is activated, a cascaded detector produces a heralding signal with a probability of

$$P_{\text{h}} = \sum_{m=1}^{\infty} P(m) P_D(1|m), \tag{3.7}$$

where

$$P_{D=0}(1|m) = 1 - (1-\eta_{\text{h}})^m, \tag{3.8}$$

$$P_D(1|m) = \frac{1}{2^{m-1}} \sum_{a=0}^{m} {}_mC_a \{P_{D-1}(1|a)(1-\eta_{\text{h}})^{m-a}\}, \tag{3.9}$$

where$P_{D=0}(1|m)$ is a probability of one detector triggered by one or more photons and generate a detection signal when m photons are incident to the detector. Note that for Eq. 3.8, the number of detector cascade D is 0, meaning that there is only one detector. Similarly, $P_D(1|m)$ denotes the probability where only one detector in the detector cascade generates the detection signal when m photons are incident to the detector cascade. η_{h} is detection efficiency of a cascaded detector. ${}_n\text{C}_a$ is used for the combination selecting a items from n distinct elements. In the case of $D \to \infty$, the cascaded detector can distinguish a number of photons up to infinity with $P_{D=\infty}(1|m) \approx m\eta_{\text{h}}(1-\eta_{\text{h}})^{m-1}$.

The coincidence probability $P_{\text{C}}(n)$ that n photons are detected at the output when the heralding signal is obtained is given as

$$P_{\text{C}}(n) = \sum_{m=n}^{\infty} P(m) P_D(1|m)_m C_n t^n (1-t)^{m-n}, \tag{3.10}$$

where t is the transmittance between the SPDC sources and the output.

$P_{\text{h}}(n)$ is the n-photon output probability for a heralding signal for a Multiplexed-HSPS using cascaded detectors, and can be derived using Eqs. 3.7 and 3.10:

$$P_{\mathrm{h}}(n) = \frac{(P_{\mathrm{C}}^{1}(n) + (1 - P_{\mathrm{h}}^{1})(P_{\mathrm{C}}^{2}(n) + (1 - P_{\mathrm{h}}^{2})(P_{\mathrm{C}}^{3}(n) + \cdots))}{1 - (1 - P_{\mathrm{h}}^{1})(1 - P_{\mathrm{h}}^{2})(1 - P_{\mathrm{h}}^{3}) \cdots}, \tag{3.11}$$

where P_{h}^{i} is the probability that the idler photon is detected with the cascaded detector for the ith SPDC source, and $P_{\mathrm{C}}^{i}(n)$ is the coincidence probability for the cascaded detector for the ith SPDC source. Here, we used the mean number of photon pairs per one SPDC source, which is given by $\bar{N}/S$.

If $P(n)$ follows a Poisson distribution and $D \to \infty$, our model is consistent with the theory in [115]. If $P(n)$ are output follows a thermal distribution and $D \to \infty$, our model is also consistent with the theory in [118].

Depending on the experimental setup, an produced photon from an SPDC source contains just a few modes, and the produced photon is neither single nor multi-mode [76, 131]. To analyze this condition, we use the following photon number distribution consisting of the thermal and Poisson distribution connected with a parameter γ ($0 \leq \gamma \leq 1$):

$$P(n) = \gamma P_{\mathrm{th}}(n) + (1 - \gamma) P_{\mathrm{Po}}(n). \tag{3.12}$$

When the mean number of photon pairs is small ($\bar{N} \ll 1$), the two photon probability $P_{\mathrm{h}}(2)$ in Eq. 3.11 can be approximated to the following linear function of $\bar{N}$:

$$P_{\mathrm{h}}(2) \sim \frac{(1 + \gamma) t^{2} P_{D}(1|2)}{2 \eta_{\mathrm{h}} S} \times \bar{N}. \tag{3.13}$$

3.3.2 Numerical analysis of the suppression of the two-photon probability

Here, using our theory in previous section, we numerically analyze the suppression of the two-photon probability [$P_{\mathrm{h}}(2)$] for an HSPS using a cascaded detector, a Multiplexed-HSPS and a Multiplexed-HSPS with PND. For this calculation, we assumed a thermal distribution $P_{\mathrm{th}}(n)$ for $P(n)$. Note that a smaller $P_{\mathrm{h}}(2)$ indicates a higher quality single-photon source.

Figure 3.3(a) shows $P_{\mathrm{h}}(2)$ versus the mean photon pair number $\bar{N}$, which corresponds to the generation rate of the HSPS. We assumed a detection efficiency of the detector cascade of $\eta_{\mathrm{h}} = 0.5$ and an overall transmittance between the SPDC sources and the output of $t = 0.5$. The solid black lines for $S = 1$ and $D = 0$ in Fig. 3.3(a) correspond to the conventional HSPS. The solid lines colored red, blue and purple indicate $P_{\mathrm{h}}(2)$ for $S = 1$ (no source multiplexing) and $D = 1$, 2 and ∞, respectively. Note that two and four detectors are used for $D = 1$ and $D = 2$ at each SPDC sources. These lines show that $P_{\mathrm{h}}(2)$ decreases with increasing D. The results also show that $P_{\mathrm{h}}(2)$ rapidly approaches the value for $D = \infty$ when we increase D, suggesting that we can effectively decrease $P_{\mathrm{h}}(2)$ even with a relatively small D.

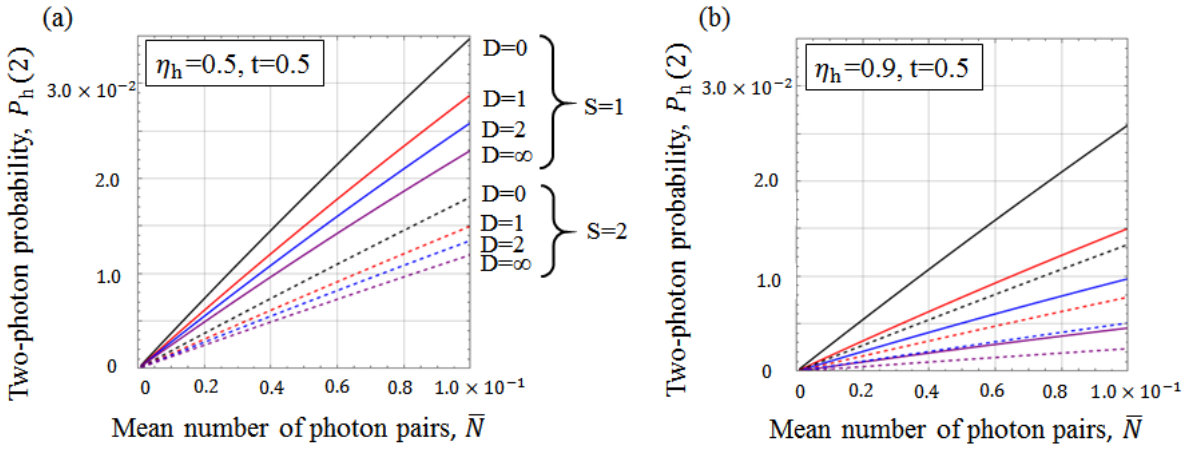

Figure 3.3: Two-photon probability from the Multiplexed-HSPS with PND versus the mean number of photons pairs for (a) η_h=0.5, t=0.5, (b) η_h=0.9, t=0.5. Black line: $S = 1$, $D = 0$; red line: $S = 1$, $D = 1$; blue line: $S = 1$, $D = 2$; purple line: $S = 1$, $D = \infty$; black dashed line: $S = 2$, $D = 0$; red dashed line: $S = 2$, $D = 1$; blue dashed line: $S = 2$, $D = 2$; purple dashed line: $S = 2$, $D = \infty$.

By multiplexing two SPDCs [$S = 2$], we could halve $P_h(2)$ for $D = 0$ (black dashed lines in Fig. 3.3(a)) compared with the conventional HSPS (solid black line). The dashed lines colored red, blue and purple indicate $P_h(2)$ for $S = 2$ and $D = 1$, 2 and ∞, respectively. These lines show $P_h(2)$ at the output of a Multiplexed-HSPS with PND. A Multiplexed-HSPS with PND suppresses $P_h(2)$ more efficiently than a Multiplexed-HSPS. However, since $P_h(2)$ for $S = 2$ and $D = 0$ is lower than that for $S = 1$ and $D = \infty$, the effect of source multiplexing is higher than that of detector cascading in the case of $\eta_h = 0.5$.

If we can achieve a higher detection efficiency, $\eta_h = 0.9$ ($t = 0.5$), the situation changes as shown in Fig. 3.3(b). The solid lines correspond to no source multiplexing (black) and detector cascade numbers of $D = 2$ (blue) and ∞ (purple). The blue and purple solid lines achieve lower $P_h(2)$ than the black dashed line, corresponding to source multiplexing [$S = 2$] and no detector cascading [$D = 0$]. Thus, the effect of the suppression using the detector cascading method increases with η_h. On the other hand, the effect of source multiplexing does not depend on η_h.

Figure 3.4 shows how the suppression ratio depends on the detection efficiency η_h, where we assume the case of $\bar{N} = 0.05$, $t = 0.5$. The suppression ratio R_{sup} is defined as the ratio of the two photon probability of a Multiplexed-HSPS with PND to that of a normal HSPS, and smaller R_{sup} indicates better performance as a heralded single photon source. R_{sup} can be derived using Eq. 3.11:

$$R_{sup} = \frac{P_h(2)[S, D]}{P_h(2)[S = 1, D = 0]}, \tag{3.14}$$

where $P_h(2)[S, D]$ is the two-photon probability of Multiplexed-HSPS with PND. The

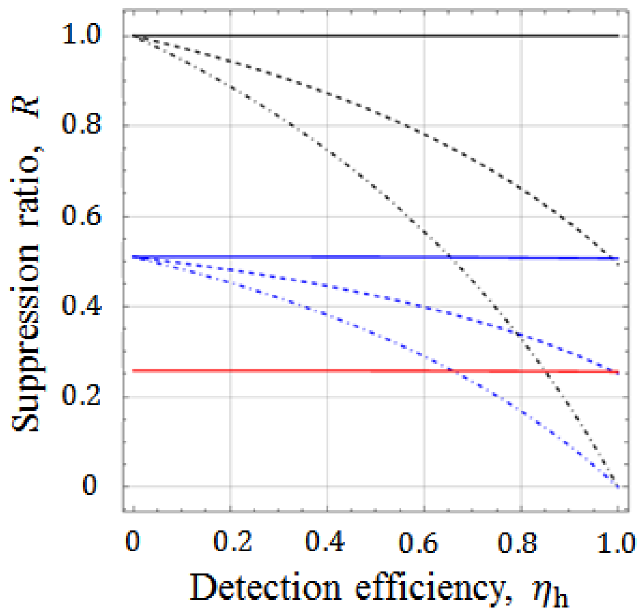

Figure 3.4: Suppression ratio versus detection efficiency. Ratio between HSPS [$S = 1, D = 0$] and Multiplexed-HSPS with PND [S, D] for $\bar{N}$= 0.05, t = 0.5. Black curve: $S = 1$, $D = 0$; blue curve: $S = 2$, $D = 0$; red curve: $S = 4$, $D = 0$; black dashed curve: $S = 1$, $D = 1$; blue dashed curve: $S = 2$, $D = 1$; black long dashed/short dashed curve: $S = 1$, $D = \infty$; blue long dashed/short dashed curve: $S = 2$, $D = \infty$.

results show that Multiplexed-HSPS [$D = 0$] gives a suppression ratio of about $1/S$ regardless of η_h. On the other hand, for HSPS using a PND [$S = 1, D = 1$], the suppression ratio decreases with increasing detection efficiency. Without source multiplexing, to reduce the two-photon probability by 0.51 (the ratio of Multiplexed-HSPS [$S = 2$]), detector cascading for $D = 1$ and ∞ requires $\eta_h = 0.99$ and 0.65, respectively. With $\eta_h = 1.0$, Multiplexed-HSPS with PND [S, D] gives a suppression ratio of about $1/(S \times 2^D)$.

In the theoretical analysis, the detection efficiency is an important parameter determining the ability of a cascaded detector. On the other hand, it is found that a source multiplexing system does not depend on the detection efficiency.

3.4 Experiment

3.4.1 Experimental setup

A schematic illustration of the experimental setup is shown in Fig. 3.5. We implemented a Multiplexed-HSPS with PND consisting of two SPDC sources (SPDC-A and SPDC-B), each of which is equipped with two cascaded detectors [$S = 2, D = 1$]. A femtosecond pulse laser (repetition rate of 82 MHz and central wavelength of 390 nm, Spectra-Physics, Tsunami) is used to pump a BBO crystal. The injected pump pulses generate photon

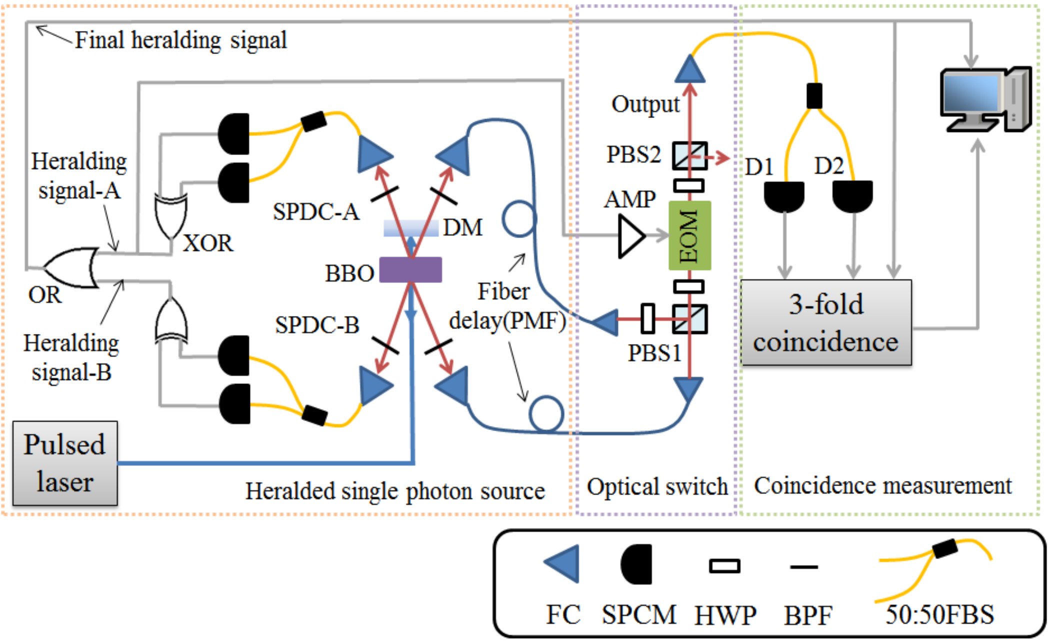

Figure 3.5: Schematic diagram of experimental set up. BBO: beta-barium-borate crystal (Type-I); DM: dichroic mirror; FC: fiber coupler; SPCM: single-photon counting module; XOR: XOR gate; AND: AND gate; EOM: electro-optic modulator; PBS: polarizing beam splitter; HWP: half wave plate; BPF: band pass filter ($\Delta\lambda = 4$ nm); PMF : polarization maintaining fiber; 50:50 FBS: 50:50 fiber beam splitter; AMP: high-voltage pulsed amplifier; fiber delay is 65 m.

pairs in the forward direction (SPDC-A). After passing through the crystal, the pump pulse is reflected back by a dichroic mirror (DM) and generates photon pairs in the backward direction (SPDC-B). For each of the sources (SPDC-A and SPDC-B), idler photons are detected by cascaded two single-photon counting modules (SPCMs, Excelitas Technologies, SPCM-AQR), and the signal photons are sent to the optical switch via long polarization maintaining fibers. A long fiber (65 m) is necessary to compensate the delay caused by the electric signal processing. A heralding signal-A or signal-B is generated when only one of the two SPCMs monitoring SPDC-A or SPDC-B, respectively, detects the idler photon. The final heralding signal is generated when either both heralding signal-A or heralding signal-B is generated.

According to whether heralding signal-A or heralding signal-B from the SPDC sources is generated, the signal photons are appropriately routed and gated by the optical switch. The optical switch consists of an EOM and two PBSs. The optical switch passes the signal photons from SPDC-A (SPDC-B) when the heralding signal-A from SPDC-A exists (non exists). Note that when signal-A and signal-B are generated, only the signal photon generated by SPDC-A is produced and the photon from SPDC-B is cut.

In the next section, we evaluate the two-photon probability at the output $P_{\mathrm{h}}(2)$ to

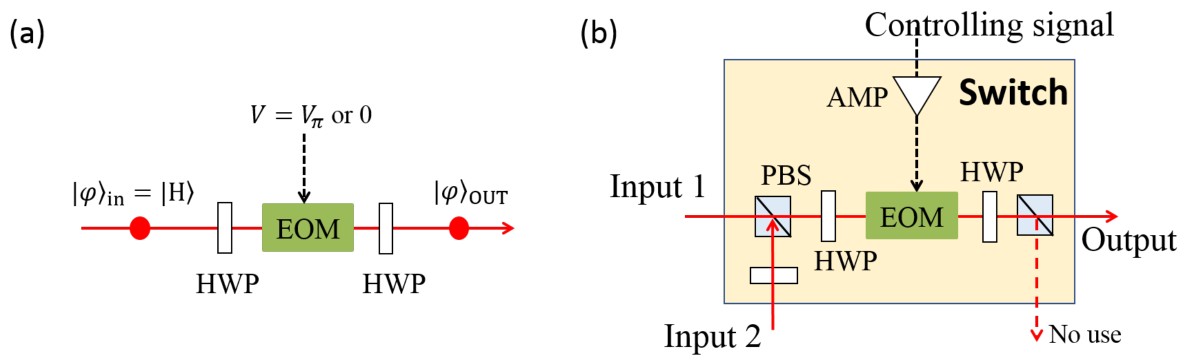

Figure 3.6: (a)Schematic illustration of a polarization rotater. (b) Active 2×1 switch. EOM : Electro-optical modulator, HWP : Half wave plate, PBS : Polarizing beam splitter.

check the performance of our single-photon source while changing the mean number of photon pairs. The conditional two-photon probability for the final heralding signal was estimated using three fold coincidence events among the detectors (D1, D2) and the final heralding signal. Note that the detection efficiencies of the detectors (D1, D2) and the effect of the 50:50 FBS are compensated, and we assumed that all of the three-fold coincidences are due to $P_{\mathrm{h}}(2)$.

3.4.2 Optical implementation of an active spatial router

We explain the method to route the photons into desired modes with heralding signals and the optical implementation. Figure 3.6(a) shows the polarization router consisting of an electro-optical modulator (EOM) and half wave plates (HWP). The arbitrary process to rotate the polarization of the input photon $|\varphi\rangle_{\mathrm{in}}$ into $|\mathrm{H}\rangle$ or $|\mathrm{V}\rangle$ is,

$$\begin{aligned} |\varphi\rangle_{\mathrm{in}} &= |\mathrm{H}\rangle \\ &\xrightarrow{HWP} \frac{1}{\sqrt{2}}(|\mathrm{H}\rangle + |\mathrm{V}\rangle) \\ &\xrightarrow{EOM} \begin{cases} \frac{1}{\sqrt{2}}(|\mathrm{H}\rangle + |\mathrm{V}\rangle), & V_{\mathrm{vol}} = 0 \\ \frac{1}{\sqrt{2}}(|\mathrm{H}\rangle - |\mathrm{V}\rangle), & V_{\mathrm{vol}} = V_\pi \end{cases} \\ &\xrightarrow{HWP} \begin{cases} |\mathrm{H}\rangle, & V_{\mathrm{vol}} = 0 \\ |\mathrm{V}\rangle, & V_{\mathrm{vol}} = V_\pi \end{cases} \\ &= |\varphi\rangle_{\mathrm{OUT}}. \end{aligned} \tag{3.15}$$

To pass the horizontal (H) polarization of the photon, the EOM is biased to zero rotation. To pass the vertical (V) polarized output, the half-wave bias voltage V_π is applied to rotate the polarization by 90 degree. Normally, the bias voltage set to zero. For the experiment of spatial multiplexing, the polarization of photons from different input (Input1,2) is changed to the same polarization. The last PBS corresponds to the filter to select H-polarized photon.

We show our way to realize such an active switch. To manipulate the polarization of heralded photons one by one, the speed of active router is required to be high. The EOM is a high speed device with high throughput efficiency. The PBS and HWP are the passive linear optical components. The active router with these components matches to the requirement of this research. Then, the transmittance, the rising time, the extinction ratio, and speed of EOM is quite important parameters for our research. The transmittance of our EOM (LM0202, LINOS) is over 96% and the extinction ratio is over 100. Compared with these values, the rising time and speed depends on the amplifier (AMP). In this experiments, We used a high speed pulse amplifier LIV-20 (LINOS) because the rising time is less than the duration time of pulses and high speed of a few MHz (this value depends on the amplified voltage.). And we use the optimized EOM with the small size of Pockels cell of 3mm because the gain of the AMP is limited. For adjusting the timing to apply voltage and the pulse of rectangle controlling signals, we used a digital pulse generator (DG645). If the pulse width of controlling signals increases, undesired events are occurred that the repetition rate of active switch is decreased with the inverse of the pulse width, and the uncontrollable time is occurred after manipulating the heralded photon. Therefore, we set the pulse width as small as possible, the inverse of the speed of the amplifier (3MHz). Note that these setup were used in our another experiments as shown in Chapter 4 and Chapter 5.

Finally, we introduce the alternative way to implement the active router. Different from our experimental setup, there are some reports to use noticeable devices. Kaneda used the Pockels cell device with quite high transmittance (99%) and low rising time (4ns) [132]. Zhang used the fiber integrated device with relatively high transmittance (2dB) [133]. And the products of AGILTON and Bergmann Messgeraete Entwicklung KG will be developed better to use as the router.

3.5 Experimental results and discussion

Figure 3.7 shows the two-photon probability $P_{\mathrm{h}}(2)$ at the output of our Multiplexed-HSPS with PND versus the coincidence rate. The horizontal axis shows the number of events where only one of the two detectors (D1, D2) detects a photon when the final heralding signal is produced. The two-photon probability was measured with various pump powers. The blue and red circles indicate HSPS $[S = 1, D = 0]$ (SPDC-A) and HSPS using a cascaded detector $[S = 1, D = 1]$ (SPDC-A), respectively. The blue and red squares indicate Multiplexed-HSPS $[S = 2, D = 0]$ and Multiplexed-HSPS with PND $[S = 2, D = 1]$, respectively. These data points show that $P_{\mathrm{h}}(2)$ increases with the coincidence

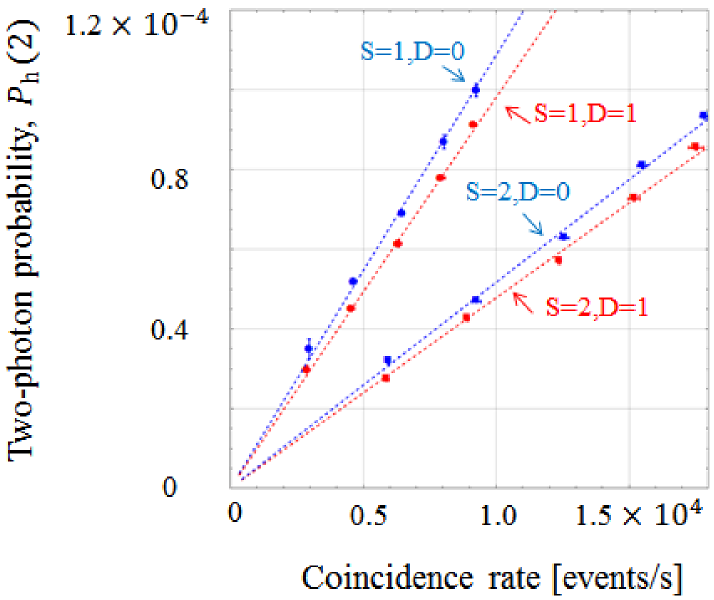

Figure 3.7: Experimental results: The vertical axis is the two photon probability at the output. The horizontal axis shows the number of events where one of the two detectors (D1, D2) detects a photon when the final heralding signal is produced. HSPS (SPDC-A) [S=1, D=0] (blue circles), HSPS (SPDC-A) using PND [S=1, D=1] (red circles), Multiplexed-HSPS [S=2, D=0] (blue squares), a Multiplexed-HSPS with PND [S=2, D=1] (red square), where all contain the optical switch. The dashed lines are based on our model.

rate. For constant coincidence rate, Multiplexed-HSPS has a two times lower two-photon probability than HSPS. We achieved further suppression with the Multiplexed-HSPS with PND.

The dashed lines in Fig. 3.7 show the theoretical curves calculated with Eq. 3.11. For η_h and transmittance t, we used the separately measured values (Table 3.1). Since we used the BPFs which have a relatively broad bandwidth of 4 nm in order to increase the detection efficiency of the cascaded detectors, the output state of the SPDC follows neither the thermal distribution nor the Poisson distribution. Thus, for the photon number distribution $P(n)$, we adopted the intermediate distribution in Eq. 3.12. The dashed lines are the theoretical curve when γ is 0.59, 0.72. The theoretical lines are in good agreement with the experimental results. Note that plotted curves are derived from Eq. 3.11, not from the approximated one shown in Eq. 3.13. Note also that we compensated a small effective loss in the optical switch which appeared when we used the multiplexing method. The effective loss was caused by the deadtime of the electrical amplifiers used for driving the EOMs.

Note also that, in our experiment, the detector darkcounts ($\sim$ 200 counts/s) does not impact the results since it is negligibly small when compared to the average count rates

Table 3.1: Separately measured parameters. $\eta_{\mathrm{h,A/B}}$: detection efficiency of the detector in SPDC-A/B. $t_{A/B}$: transmittance of the single photon between the SPDC-A/B and the output.

	$\eta_{\mathrm{h,A}}$	$\eta_{\mathrm{h,B}}$	t_{A}	t_{B}
HSPS (SPDC-A)	0.137 ± 0.002	n/a	0.0305 ± 0.0004	n/a
HSPS with PND (SPDC-A)	0.141 ± 0.001	n/a	0.0293 ± 0.0003	n/a
HSPS (SPDC-B)	n/a	0.192 ± 0.005	n/a	0.0411 ± 0.0004
HSPS with PND (SPDC-B)	n/a	0.194 ± 0.002	n/a	$0.0405 \pm 0,0005$
Multiplexed-HSPS	0.137 ± 0.002	0.192 ± 0.005	0.0275 ± 0.0004	0.0361 ± 0.0004
Multiplexed-HSPS with PND	0.141 ± 0.001	0.194 ± 0.002	0.0263 ± 0.0003	$0.0355 \pm 0,0005$

of each of the detectors in the cascade ($\sim 1.5 \times 10^5$ counts/s). Note also that the effect of the deadtime of the detectors is also negligible. In more detail, the average count rate at the heralding arm was about 1.5 $\times 10^5$ counts/s and is much smaller than 2.5 $\times 10^8$, which is the inverse of the deadtime (40 ns) of our detector.

To confirm the suppression clearly, we calculated the suppression ratio R_{sup} in Eq.3.4 defined as the two-photon probability ratio between a normal HSPS (SPDC-A) $[S = 1, D = 0]$ and the other HSPS. The suppression ratios of HSPS using PND, Multiplexed-HSPS and Multiplexed-HSPS with PND were found to be $91.1 \pm 0.7\%, 47.6 \pm 0.7\%$ and $44.2 \pm 0.6\%$, respectively. Thus, a Multiplexed-HSPS with PND exhibits a significant improvement, compared to the normal HSPS.

Due to the limited effective detection efficiencies (about 0.14 for SPDC-A, about 0.19 for SPDC-B) in our experiment, the suppressions of two photon probability with the help of cascaded detectors were not as significant as shown in Fig. 3.3 where the detection efficiencies were assumed to be 0.5 and 0.9. However, we would like to note that the experimental result is consistent with Fig. 3.4 for the given detection efficiencies. It is important to improve the effective detection efficiencies by adopting highly efficient single photon detectors [127, 134] and highly efficient coupling of down converted photons into single mode optical fibers [135, 136].

3.6 Summary

In conclusion, we realized a Multiplexed-HSPS with PND using cascaded detectors. We also developed the theory for describing such a Multiplexed-HSPS with PND considering a limited number of cascaded detectors. We found that even a small number of detector cascade is very effective in reducing the excess photon emission in certain circumstances. With the realized a source equipped with two SPDC sources and a PND consisting of two on-off detectors, we found that the two-photon components were reduced to $44.2 \pm 0.6\%$

of that of a HSPS.

Chapter 4

Efficient preparation of multi-photon parallel state from a stream of heralded single photons

4.1 Introduction

In the previous section, we studied for multiplexed heralded single photon source (HSPS) which can maintain the probability of generating one photon while suppressing the probability of having more than two photons. Many researchers also pay attention to the multiplexing of HSPSs for increasing the number of photons of multi-photon parallel state [116, 117, 120, 122, 137]. However, when this scheme is used for the multi-photon interference experiments, it is necessary to construct a lot of multiplexed HSPSs. This scheme requires considerable resource overhead in terms of multiple optical switches and heralded SPSs, since a multiplexed heralded SPS requires multiple nonlinear crystals, detectors and other elements. This is still challenging. A further alternative method comprising a single photon source using single emitters such as quantum dots (QD) has been developed recently [57, 138], although achieving multiple and identical single emitters is still a challenge.

To address this difficulties in multiple single photon sources, a serial–parallel conversion method has been proposed by us in 2015. The converter can route a stream of n photons at successive intervals from one SPS to n different spatial modes. Until now, a converter using a passive router consisting of a balanced beam splitter has been widely used [139]. Recently, Lenzini et al. [140] and Wang et al. [110] have realized active serial–parallel conversion for single photons generated from a quantum dot, where photons were produced without heralding signals.

In this section, we report the experimental realization of a serial–parallel conversion system for two photons with heralding signals. We theoretically compared the conversion efficiency for n heralded photons with that for n unheralded photons and found that

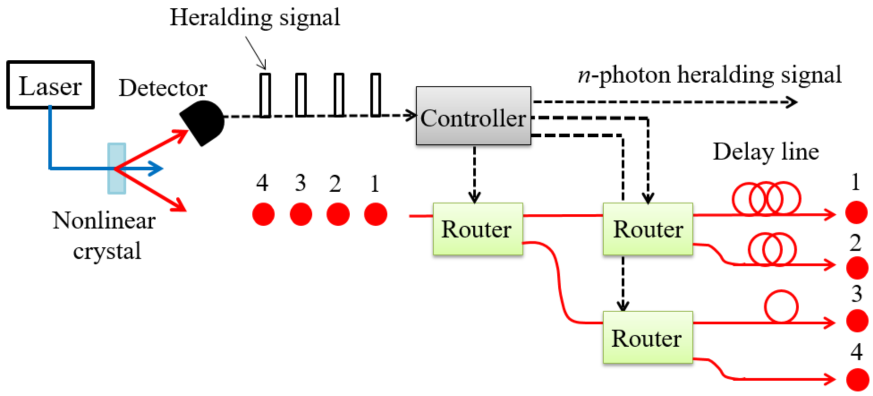

Figure 4.1: Scheme of serial–parallel conversion for four photons generated from a heralded single photon source $n = 4$. A nonlinear crystal is pumped by a pulsed laser and generates photon pairs via the SPDC process. A stream of photons (Red dots) is intendedly routed into different spatial modes by a convertor consisting of the routers and delay lines. The controller generates the n-photon heralding signal and the signal of controlling the routers when a stream of n photons is detected at the heralding arm. Red lines connecting the routers represent the path of photons. The dotted arrows from the controller to the router represent the path of electrical signal.

serial–parallel conversion for the heralded photon source could be more efficient than for the unheralded photon source. With the realized two-photon serial–parallel converter, we confirmed the efficacy of serial–parallel conversion for the case where a series of two heralding signals is detected. We achieved a conversion efficiency of 0.533 ± 0.003, which exceeds the maximum achievable efficiency of 0.5 for serial–parallel conversion using unheralded photons, and is double the efficiency of 0.25 for that using beamsplitters. The efficiency of current setup can be increased up to 0.996 ± 0.006 when the losses in the optical converter are corrected for.

4.2 Model of serial–parallel converter with heralding signals

Figure 4.1 shows an example of the scheme for a serial–parallel converter, where four photons are converted into four different spatial modes. A nonlinear crystal is pumped by a pulsed laser and generates photon pairs via the SPDC process. When one of the photons in the pair is detected, a heralding signal is generated. Using the heralding signals, the controller identifies which pulses have corresponding photons, and generates an n-photon heralding signal when a stream of n photons is detected. In this example, a series of four photons from a heralded SPS $n = 4$ is routed into the four different spatial modes by

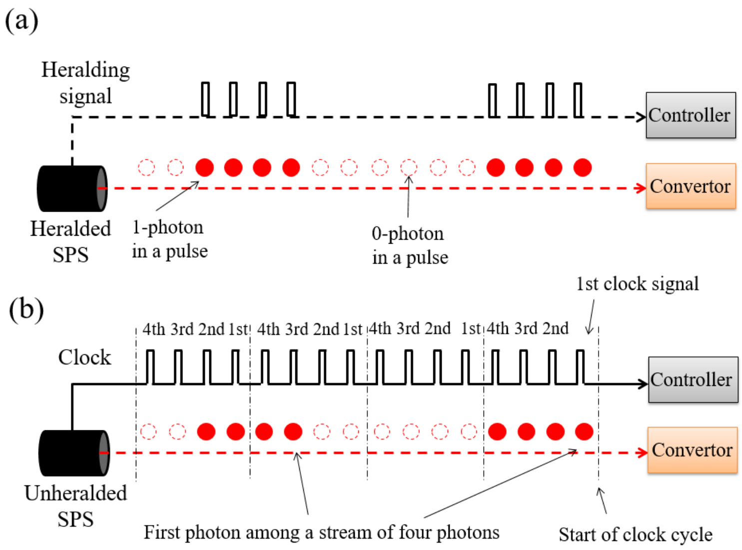

Figure 4.2: (a) Heralded SPS and serial–parallel converter. A heralded SPS emits a stream of four photons and the corresponding heralding signals. (b) Unheralded SPS and serial–parallel converter. An unheralded SPS emits a stream of four photons and the clock signal of the pump pulse laser. The clocking is derived from the pump laser. The converter operates according to the interval of a four-clock cycle. The conversion succeeds only when the first clock from the divided line corresponds to the first photon among the four photons.

the serial–parallel converter consisting of three optical routers and delay lines. Note that for n-mode output, the number of required routers is $n-1$. The converted photons are output to the four modes at the same time using optical delay lines.

4.3 Conversion efficiency of a stream of single photons

Here, we compare the conversion efficiency $S(n)$ for a heralded SPS with that for an unheralded SPS. $S(n)$ is a parameter that represents how efficiently an arbitrary n-photon stream is converted into different spatial modes using a serial–parallel converter.

In the case of heralded photons, we consider the conversion efficiency $S(n)$ for the case where a series of n photon heralding signals is detected. Then, the optical routers are driven using the heralding signals, which indicate the presence of the corresponding photons. When the heralded SPS emits a stream of n photons, the n-photon heralding signal identifies the presence of the generated n photons precisely. For example, figure 4.2(a) shows that a heralded SPS emits a stream of four photons, and the corresponding heralding signals. The ideal converter perfectly transfers a stream of heralded single photons to different optical modes. For the case where a n-photon heralding signal is

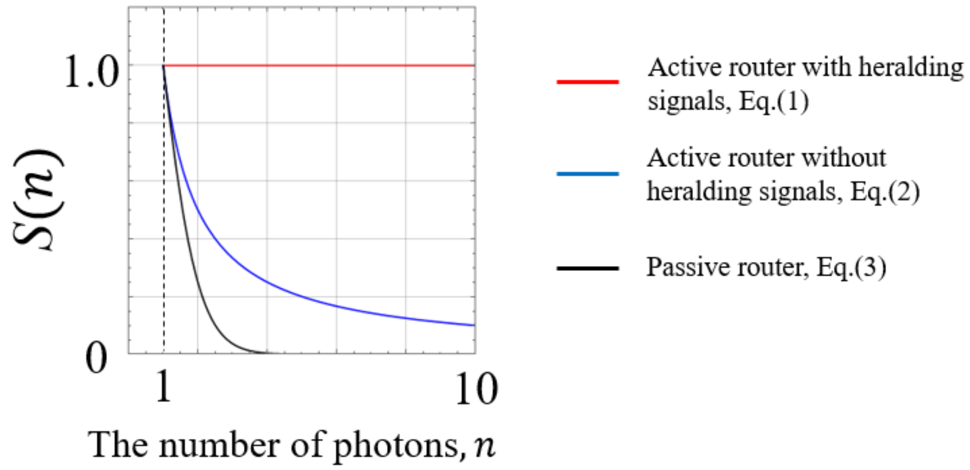

Figure 4.3: Theoretical comparison of the efficiencies of serial–parallel conversion using active routers with heralding signals (red line), active routers without heralding signals (blue line) and passive routers (black line). Here an ideal switching efficiency is assumed.

generated, the conversion efficiency for a stream of n photons is given by

$$S(n) = \eta_{\mathrm{SW}}^n, \tag{4.1}$$

where η_{SW} is the switching efficiency defined as the average probability of routing a single photon in the desired modes.

Next, let us consider the case of single photons without heralding signals [140] [Fig.4.2(b)]. In this case, the serial–parallel converter routes the photons automatically according to the clock signals provided by the source (e.g., a pumping laser) [see Fig.4.2(b)]. However, in this case, the routing of a stream of four photons is only successful when the '1st clock signal' by chance coincides with the existence of the first photon among a stream of four photons. For this case, the conversion efficiency is given by

$$S(n) = \frac{1}{n}\left[\eta_{\mathrm{SW}}^n + (n-1)\left(\frac{1-\eta_{\mathrm{SW}}}{n-1}\right)^n\right], \tag{4.2}$$

Finally, if a beam splitter is used as a passive router, [139], the efficiency for heralded photons is at most

$$S(n) = (1/n)^n, \tag{4.3}$$

which can only be attained when the loss of the beamsplitters is negligibly small.

Figure 4.3 shows the plots of eqs.(1) – (3) for an ideal switching efficiency $\eta_{\mathrm{SW}} = 1$. As n is increased, conversion efficiencies $S(n)$ of the passive router (black line) and the active router without heralding signals (blue line) degrade, while $S(n)$ of the active router with heralding signals (red line) is maintained. Comparing these conversion efficiencies shows that serial–parallel conversion using active routers with heralding signals is more efficient than those using active routers without heralding signals, or passive routers obviously.

4.4 Experimental setup of serial–parallel conversion for two photons

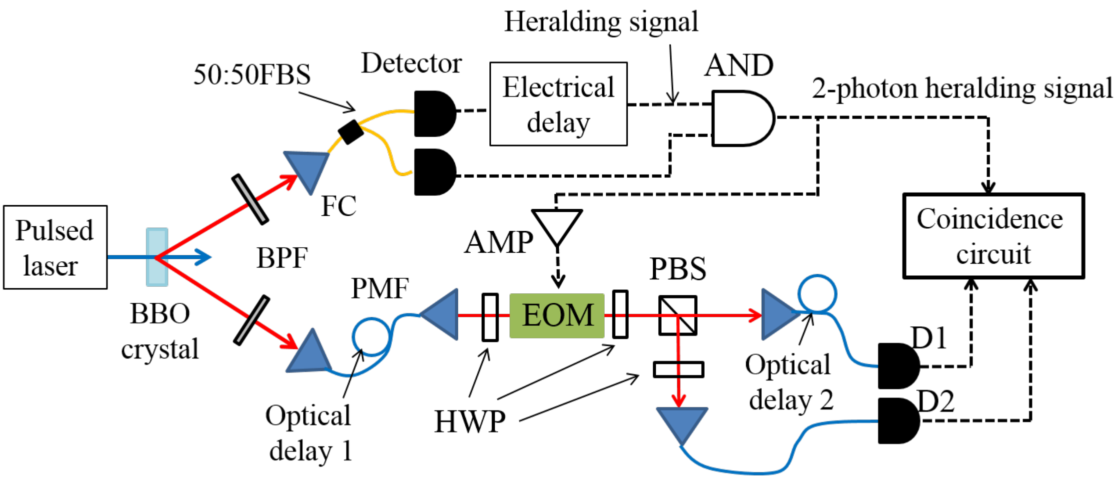

Figure 4.4: Schematic diagram of experimental setup. BPF: band pass filter, HWP: half wave plate, FC: fiber coupler, 50:50FBS: 50:50 fiber beam splitter, AND: AND gate, PMF: polarization maintaining fiber, AMP: high-voltage pulsed amplifier, PBS: polarizing beam splitter, EOM: electro optics modulator. Optical fiber delay 1 is 65 m long. Optical fiber dealy 2 is 2.5 m long.

We implemented a serial–parallel converter for two photons with heralding signals. A schematic of the experimental setup is shown in Fig. 4.4. A femtosecond pulse laser (Tsunami with second harmonic generation, Spectra Physics, repetition rate of 82 MHz and central wavelength of 390 nm) is used to pump a beta barium borate (BBO) crystal (Type-I, thickness of 1.5 mm), and generates photon pairs (signal photons and idler photons). For the SPDC source, the idler photons are detected by two detectors (SPCM-AQR, Excelitas Technologies) because the detector's deadtime (40 ns) is larger than the interval (12.5 ns) between the pump pulses. Using the electrical delay line and an AND logic gate, we select the cases where a series of two heralding signals exist. Then the electric signal (final heralding signal) is sent to the coincidence circuit (SR 400, Stanford Research Systems) and an electro optics modulator (EOM, LM0202, LINOS).

The signal photons are sent to an optical converter consisting of half wave plates (HWP) and the EOM. Optical delay 1 (65 m) is inserted to correct for the delay caused by the electric signal processing mentioned above. With an appropriate timing adjustment, the EOM rotates the polarization of the second photon just after the first signal photon passes the EOM. Then, the first and second signal photons are routed into different spatial modes after a polarizing beam splitter (PBS) and are detected by detectors D1 and D2. Optical delay 2 corresponds to the "delay line" in Fig. 4.1.

We estimate the conversion efficiency $S(n)$ of our converter based on the experimentally obtained parameters $P_{\mathrm{h}}(1)$, the probability of having one photon in a pulse when the heralding signal is generated, $C_{\mathrm{h}}(n)$, the rate of events where a series of n heralding signals is generated, and $C(n)$, the rate of events where n photons are successfully detected at the same time at each of n detectors when the series of n heralding signals are generated. The conversion efficiency is thus given by

$$S(n) = \frac{C(n)}{C_{\mathrm{h}}(n)} \frac{1}{[P_{\mathrm{h}}(1)\eta_{\mathrm{D}}]^n}, \tag{4.4}$$

where the non-unity efficiency of the source ($P_{\mathrm{h}}(1)$) and the photon detectors (η_{D}) are corrected to evaluate the performance of the serial–parallel converter.

4.5 Experimental results and discussion

Using Eq. 4.4, we evaluated the conversion efficiency $S(2)$ for the case where a series of two heralding signals is detected, to check the performance of our serial–parallel converter.

In our experiment, the rate of the measured coincidence events $C(2)$ between the final heralding signals and the two output signals from detectors D1 and D2 was 2.62 ± 0.15 cps, indicating that the photons are sent to both D1 and D2 simultaneously with this rate. Note that the coincidence rate was 0.006 ± 0.003 cps when EOM was not operated by the final heralding signal, indicating that both photons are sent to only one of the two detectors (D1) with these results. We confirmed the successful operation of the serial–parallel conversion.

The rate of the n-photon heralding signal $C_{\mathrm{h}}(2)$ is 785 ± 8 cps, and the one-photon probability from HSPS, including the detection efficiency, $P_{\mathrm{h}}(1)\eta_{\mathrm{D}}$ is 0.079 ± 0.001. For these measured parameters, we evaluated the conversion efficiency, using Eq.(4), to be

Table 4.1: Theoretical conversion efficiencies $S(n)$ for an ideal switching efficiency ($\eta_{\mathrm{SW}} = 1$), using Eqs.(1)-(3): an active router with heralding signals, an active router without heralding signals, a passive router using balanced beam splitters.

	Active router with heralding signals	Active router without heralding signals	Passive router
$S(n)$	1	$1/n$	$(1/n)^n$
$S(2)$	1	0.5	0.25

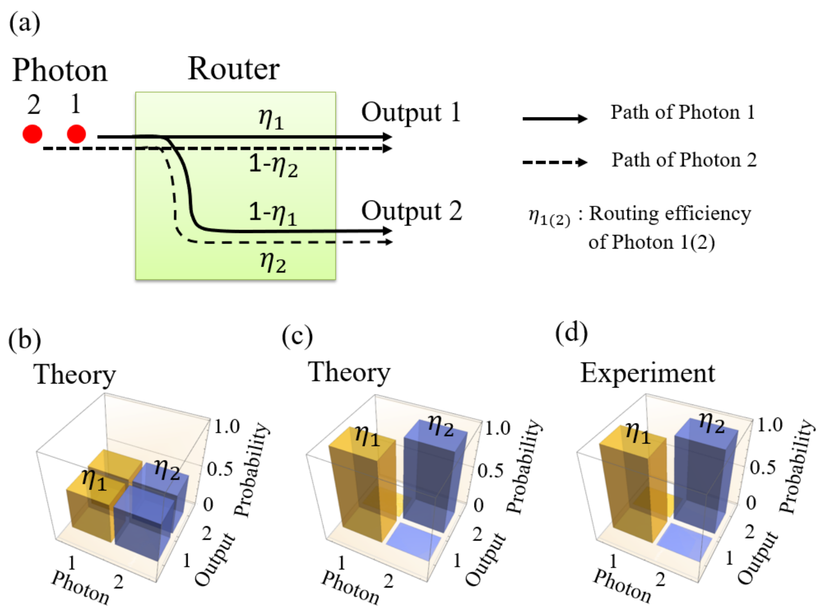

Figure 4.5: (a) Sketch of an optical router. This routes photon 1 into output 1 with routing efficiency η_1, and routes photon 2 into output 2 with efficiency η_2. (b,c,d) Routing efficiency. (b) Theoretical efficiency for a passive router using a balanced beam splitter. (c) Theoretical efficiency for an active router with heralding signals. (d) Experimental efficiency for an active router with heralding signals.

$S(2) = 0.533 \pm 0.003$. To confirm the advantage of our serial–parallel converter, we compared the conversion efficiency using routers for unheralded photons with the ideal switching efficiency ($\eta_{\mathrm{SW}} = 1$) . For $n = 2$, the optical converter would enable a maximum conversion efficiency of 0.5 [Table 4.1]. The conversion efficiency of our optical converter is 0.533, which exceeds the maximum achievable efficiency for serial–parallel conversion using unheralded photons, and is double the efficiency (0.25) for that using beamsplitters.

The experimental losses and measured/compensated conversion efficiency are written in Table 4.2. The average transmittance (t) of the converter was 0.731 in the actual experimental setup. The corrected conversion efficiency is estimated to be 0.996 ± 0.006 when the optical loss in the converter (between a single mode fiber (Optical delay 1)

Table 4.2: Experimental losses and measured/compensated conversion efficiency in this work.

Description	Symbol	Value in this work
Observed conversion efficiency	$S(2)$	0.533 ± 0.003
Average transmittance of the converter	t	0.731 ± 0.003
Transmittance-compensated conversion efficiency	$S(2)/t^2$	0.996 ± 0.006

and the output) is compensated. The corrected conversion efficiency of 0.996 is in good agreement with ideal value $S(2)$ =1 for active router with heralding signals [Table.4.1]. This result also confirms the success of our serial–parallel conversion for a series of two heralding signals.

To verify the successful operation of our router, we further measured the routing efficiency η_1 or η_2 which is defined as the probability of routing photon 1 or 2 into output 1 or 2, respectively, whereas the probability of routing photon 1 or 2 into output 2 or 1, respectively, is $1 - \eta_1$ or $1 - \eta_2$, as shown in Fig. 4.5(a). Figure 4.5(b) and 4.5(c) show the theoretical routing efficiencies using (b) a passive router ($\eta_1 = \eta_2 = 0.5$) and (c) an active router ($\eta_1 = \eta_2 = 1$). In our experiment, the routing efficiency is estimated using coincidence events between the series of two heralding signals and the detection signal from detector D1 or D2, and found to be $\eta_1 = 0.99 \pm 0.01$ and $\eta_2 = 0.98 \pm 0.01$, shown in Fig.4.5(d). Note that the routing efficiency is corrected based on the optics components and detection efficiency. This measured value is in good agreement with the predicted value in Fig. 4.5(c). Thus, it can be said that our router can properly guide photons into the appropriate spatial modes. Note that, for our experimental setup, the switching efficiency $\eta_{\mathrm{SW}} = t \times (\eta_1 + \eta_2)/2 = 0.72$.

We note that our serial–parallel converter can be easily expanded for n photon streams by adding EOMs and PBSs. For n photons, $n - 1$ EOMs will be required. The next challenge will be to generate a state of multiple photons in parallel. For such experiments, improving the heralded source with higher $P_{\mathrm{h}}(1)$ and suppressing excess photon emission is important. Recently, a $P_{\mathrm{h}}(1)$ of about 0.7 has been reported [141] using type-II beamlike conditions [121, 141, 142]. Furthermore, the suppression of multi-photon component has been reported using various schemes [116, 117, 120, 122].

4.6 Summary

In conclusion, we realized a serial–parallel conversion for two photons with heralding signals. We theoretically compared the conversion efficiency for n heralded photons with that for n unheralded photons and found that a serial–parallel conversion using heralding signals could be more efficient. With the realization of the two-photon serial–parallel converter, we confirmed the success of serial–parallel conversion for the case of two heralding signals. As a result, we achieved a conversion efficiency of 0.533 ± 0.003, which exceeds the maximum achievable efficiency of 0.5 for serial–parallel conversion using unheralded photons, and is double the efficiency (0.25) possible using beamsplitters. The efficiency of current setup can be increased up to 0.996 ± 0.006 when the losses in the optical converter are corrected for.

Chapter 5

Efficient generation of multi-photon parallel state from multiple HSPSs by active spatial networking

5.1 Introduction

Efficient preparation of the multi-photon parallel state while suppressing the undesired multi-photon components is essential for further scaling up the multi-photon multi-port interference experiments. To do this, we worked for a multiplexed heralded single photon source with cascaded on–off detectors, and serial–parallel conversion for a stream of single photons with heralding signals, as shown in the previous sections. As the next step, it is expected to combine the two methods.

Compared with our two independent works, recently, the attractive method called relative time multiplexing is proposed and demonstrated [132, 133, 143]. This method is focused on the enhancement of heralding probability of the multi-photon parallel state directly by use of active time loop switches. The scheme uses quantum memories consisting of an active router and an optical delay for synchronizing the output timing of heralded photons from different single photon sources. The most interesting advantage is that the number of controlling heralded single photons can be decreased. In other words, we can reduce the number of passes photons through lossy active routers for producing the multi-photon parallel state. Reducing the loss from the router is crucial for efficient generation of multi-photon parallel state. To date, compared with the relative time multiplexing, no method has been proposed to convert photons randomly generated from multiple HSPSs directly to the multi-photon parallel state using active spatial routers. We believe that these two methods are complementary to each other.

In this section, we propose and demonstrate the alternative method to efficiently generate the multi-photon parallel state by an active spatial networking (ASN) when compared to a naive method using N single photon sources. ASN may be more achievable

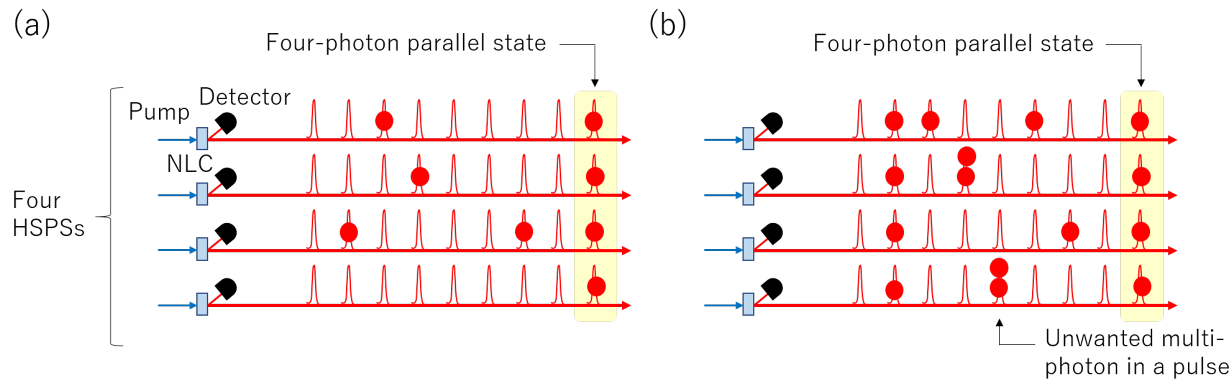

Figure 5.1: (a)Conventional way to generate multi-photon parallel state from multiple heralded single photon sources. For this case, four-photon parallel state of Fock state is produced only when all sources emit single photons simultaneously. (b)This is the case where the power of pump laser is increased.

with emerging integrated optics platforms. Firstly, we also consider how the proposed method allows us to increase the efficiency to prepare N-photon parallel state exponentially when compared with the naive method of N HSPSs. Secondly, we present proof of principle demonstration of ASN using two HSPSs for generating two-photon parallel state. With the realization of an active spatial 2×2 network and a fixed delay, we achieve enhancement factor of 1.59 ± 0.14, compared with the naive source using two HSPSs. When the losses in the setup are corrected for, the enhancement factor of current setup can be increased up to 3.99 ± 0.49. That compensated value is in good agreement with the theoretical prediction.

5.2 Generation of multi-photon parallel state

5.2.1 Previous method: Use of multiple heralded single photon sources

The conventional optical system consisting of only N HSPSs generates the heralding signals of N-photon parallel state with the probability p^N [Fig. 5.1(a)], given the probability to generate heralding signals (heralding probability) p. Furthermore, as the practical way, some groups including us proposed serial-parallel conversion of a stream of single photons from only one source [106, 140, 144]. However, the heralding probability of parametric sources p is limited due to the thermal distribution of the output photon number statistics and the requirement to suppress the multiple-pair generation negligibly low. As increasing the intensity of the pump power to enhance p, the probability to generate unwanted multi-photon state is also increased rapidly [Fig. 5.1(b)]. Even if an ideal photon number resolving detector is available, a maximum heralding probability p is 25% [145]. For quan-

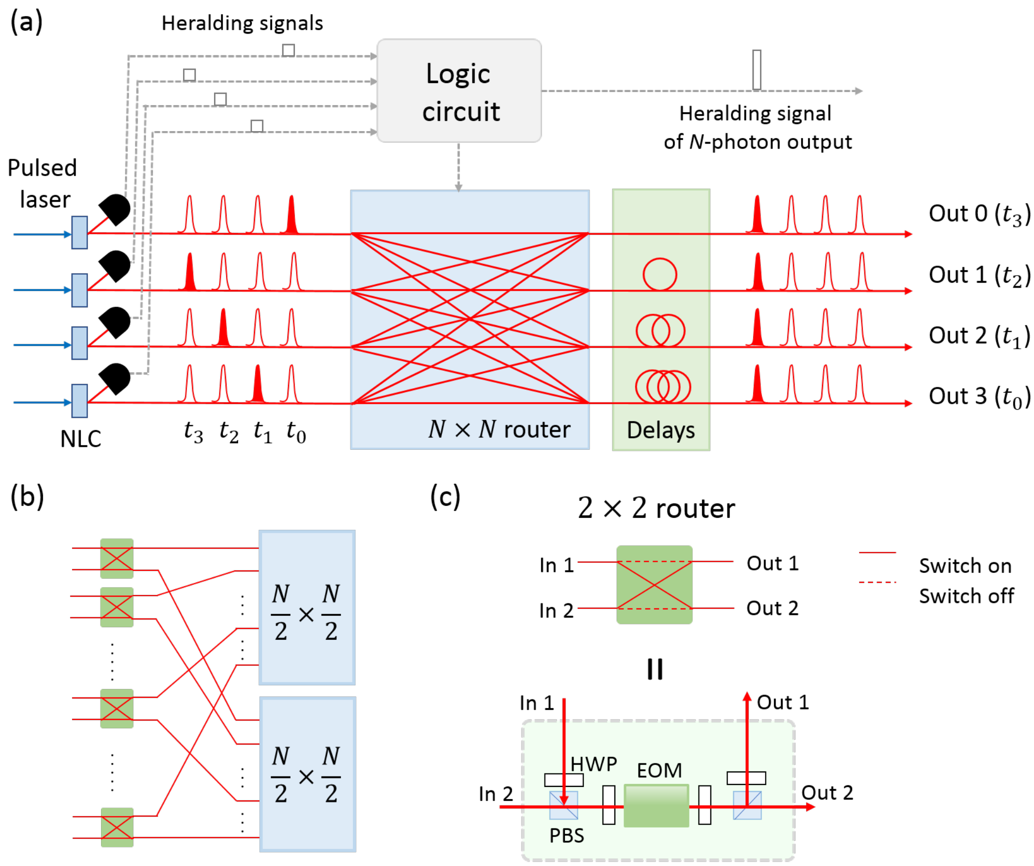

Figure 5.2: Scheme of the setup for generating N single photons simultaneously into different spatial modes (N=4). (b)Our proposed nested active network consisted of 2×2 routers. A $N \times N$ network includes two $N/2 \times N/2$ networks. (c)A 2×2 router. EOM: Electro optics modulator. HWP: Half wave plate. PBS: Polarizing beam splitter.

tum circuits requiring more single photons, the probability of emitting N single photons simultaneously using N HSPSs decreases with increasing N.

5.2.2 Proposed method: Active spatial routing of multiple heralded single photons

Figure 5.2(a) shows a schematic setup of ASN using N HSPSs to efficiently generate N-photon parallel state by a $N \times N$ network and fixed delays. The N nonlinear crystals are pumped by pulse lasers and generate photon pairs. When one of the pairs from each HSPS is detected, a heralding signal is generated with the probability of p. Using the heralding signals from N HSPSs, the logic circuit identifies the spatial and temporal mode of the heralded photons and control a $N \times N$ network which is used to relocate a single photon from an input mode to a desired output mode. When a stream of N heralding signals from N HSPSs is generated (at least one heralding signals is existed at time $t_k (k = 0 \sim N-1)$),

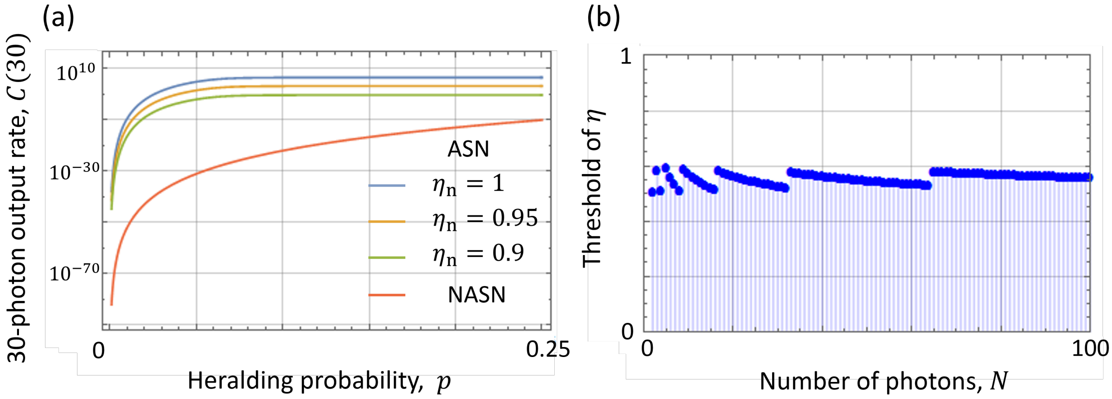

Figure 5.3: (a)The output rate of 30-photon parallel state. Blue, orange, and green lines correspond to the rate for ASN of $\eta = 1$, 0.95, and 0.9. Red line corresponds to the rate for NASN. (b) Minimum threshold of the loss including a 2×2 router η to achieve $R(N) > 1$.

a heralding signal of N-photon output are generated. Note that time-bins are labeled as t_k, where t_0 is the time for the first signal of the stream of heralding signals.

When a heralding signal of N-photon output is generated, N photons emitted from N HSPSs are converted into the desired N photon parallel state, as shown in Fig. 5.2(a). There are two steps. By use of a $N \times N$ network, the photon located at time t_k from one of the HSPSs is routed into the output mode k. After passing through the $N \times N$ network, a photon in the output mode k propagates into fixed delays with the matched length kr, where r is the length between pulses from a pump laser. Finally, N photons are emitted into different spatial modes simultaneously. As shown in Fig.5.2(b), a $N \times N$ network consists of two $N/2 \times N/2$ networks. The minimum unit of the network is a 2×2 active switch, as shown in Fig. 5.2(c). The 2×2 switch can be implemented using one controllable electro-optics modulator, two half wave plates, and two polarizing beam splitters. Note that total number of 2×2 active switches is $N\lceil \log_2 N \rceil/2$, and the depth of $N \times N$ network is $\lceil \log_2 N \rceil$. Although this architecture is similar with that of the combined active switching of a serial-parallel convertor [110, 140, 144] and a spatial multiplexed HSPS[116, 146], the depth of our proposed network is reduced to half.

Firstly, to express the enhancement of generation rate of the N-photon parallel state by use of ASN, the approximate N photon output rate is calculated. Here we assume that the single photon in a pulse from each HSPS is existed with probability $P_{\mathrm{h}}(1)$ of 1 when a heralding signal is generated. The network loss for each photon is given by $\eta_{\mathrm{n}} = \eta^{\lceil \log_2 N \rceil}\eta_{\mathrm{f}}$, where η is the transmittance of a 2×2 switch and η_{f} is the average transmission of delay lines. For the case of ASN using N HSPSs, the approximate N photon output rate is given by,

$$C_{\mathrm{m}}(N) = \frac{R_{\mathrm{rep}}\eta_{\mathrm{n}}^{N}\{1-(1-p)^{N}\}^{N}}{1+(N-1)\{1-(1-p)^{N}\}^{N}}, \tag{5.1}$$

where R_{rep} is the repetition rate of pulsed laser, and the generation rate of photons from each HSPS is $R_{\mathrm{rep}}p$ $(= R_{\mathrm{rep}}pP_{\mathrm{h}}(1))$. Note that the approximate N-fold coincidence count rate is $R_{\mathrm{rep}}N^{N}p^{N}\eta_{\mathrm{n}}^{N}$, assuming $Np \ll 1$.

Figure 5.3(a) shows one example of the 30-photon output rate $C_{\mathrm{m}}(N)$ versus the probability of emitting photons from a HSPS p , for the case of ASN or no use of ASN (NASN). NASN corresponds to a naive method of 30 HSPSs. p is limited up to 25% due to the probabilistic sources. The repetition rate is assumed $R_{\mathrm{rep}} = 8.2 \times 10^{7}$ Hz, which is the same with our pulsed laser (Tsunami, Spectra Physics). Blue line indicates the 30-photon output rates for an ideal system for $\eta = 1$ and $\eta_{\mathrm{f}} = 1$. These lines increase exponentially with increasing p, and saturate up to R_{rep}/n. Orange and green lines indicate the rate for the case with practical routers to have losses $\eta = 0.95$ and 0.9. These results also show that this ASN system can enhance the rate generating the multi-photon parallel state dramatically even though each HSPS cannot generate photons efficiently. This saturation is occurred when $1-(1-p)^{N} \approx 1$. This result means that even if the number of output photons is increased, the number of HSPSs is enough for N when $1-(1-p)^{N} \approx 1$. In comparison, for the case of NASN, the 30-photon output rate increases slowly as increasing p (Red line). As the conventional HSPS limits p, this NASN method is not practical for large N. Thus, we found that this method of ASN has scalability to increase the number of photons for realizing a large-scale photonic quantum processing, even if p is limited for suppressing the multi-pairs generation from photon pair sources.

Secondly, we consider the generation rate of N-photon parallel state when $P_{\mathrm{h}}(1)$ is not 1. The generation rate of N-photon parallel state is $C_{\mathrm{m}}(N)P_{\mathrm{h}}(1)^{N}$. The rate is degraded as $P_{\mathrm{h}}(1)$ is decreased. However, $P_{\mathrm{h}}(1)$ can be improved with current technologies. Experimentally, $P_{\mathrm{h}}(1)$ is the product of detection efficiency of the detector, collection efficiency to couple photons into a fiber, and transmittance of optical components. As the recent development, detection efficiency and collection efficiency can overcome 90%, respectively [65, 111]. Obviously, it is easy to achieve the ideal transmittance of optical components. Thus, the enhancement of heralding probability for the multi-photon parallel state by use of ASN may becomes the final key for realizing large-scale photonic quantum circuits.

Finally, to confirm the enhancement of generation rate of the multi-photon parallel state, the enhancement factor $R(N)$ is defined as the ratio between the generation rate of ASN and a conventional way, given as,

$$R(N) = \frac{C_{\mathrm{m}}(N)}{R_{\mathrm{rep}}p^{N}}, \tag{5.2}$$

where the generation rate of N-photon parallel state from a naive method using N single photon sources is $R_{\mathrm{rep}} p^N P_{\mathrm{h}}(1)^N$. Figure 5.3(b) shows the minimum threshold of η for achieving enhancement, $R(N) > 1$, where we assume $p = 0.01$. When the transmittance of a 2×2 router is higher than the blue dots, the rate generating N-photon parallel state can be enhanced when compared to the method of NASN. For example, for the case that the number of photons is four, the minimum threshold of η is 0.5. Note that the enhancement factor is written as $N^N \eta_{\mathrm{n}}^N$ when assuming $Np \ll 1$.

5.3 Theory of ASN method

Here, we show theoretical description of ASN system using N heralded single photon sources for generating N single photons in different output modes in parallel. We first define the photon number distribution of lth HSPS,

$$P_{\mathrm{th}}(n) = \frac{\bar{N}^n}{(1+\bar{N})^{n+1}}, \tag{5.3}$$

$$P_{\mathrm{h}}^{(l)} = \sum_{m=1}^{\infty} P_{\mathrm{th}}(m)\{1-(1-\eta_{\mathrm{h}})^m\}. \tag{5.4}$$

$$P_{\mathrm{C}}^{(l)}(n) = \sum_{m=n}^{\infty} P_{\mathrm{th}}(m)\{1-(1-\eta_{\mathrm{h}})^m\}(t\eta_{\mathrm{n}})^n(1-t\eta_{\mathrm{n}})^{m-n}, \tag{5.5}$$

where n is the number of photon in a pulse, $P_{\mathrm{th}}(n)$ is the output probability that a photon pair source generates n photon pairs. $\bar{N}$ is the mean number of photon pairs from SPDC. For single mode SPDC, it follows a thermal distribution. $P_{\mathrm{h}}^{(l)}$ is the probability that a heralding signal is produced. η_{h} is the trigger-mode system detection efficiency including the detection efficiency of a detector, coupling efficiency of photons into a fiber, and losses of optical components. $P_{\mathrm{C}}^{(l)}(n)$ is the probability that n photons are generated from the $N \times N$ router when the heralding signal is obtained. t is the transmittance between the SPDC source and the output of the HSPS, and η_{n} is the transmittance of the active network. For our scheme, the value is given by the transmittance of the router including the fibers. Using these equations, the heralding probability $P_{\mathrm{herald}}(N)$ for N-photon parallel state is,

$$P_{\mathrm{herald}}(N) = \frac{\{1-\prod_{l=1}^{N}(1-P_{\mathrm{h}}^{(l)})\}^N}{1+(N-1)\{1-\prod_{l=1}^{N}(1-P_{\mathrm{h}}^{(l)})\}^N}. \tag{5.6}$$

In this experiments, the mean number of photon pairs μ is negligibly low. Therefore, the $P_{\mathrm{herald}}(N)$ and the N-photon output probability $P_{\mathrm{T}}(N)$ are given as,

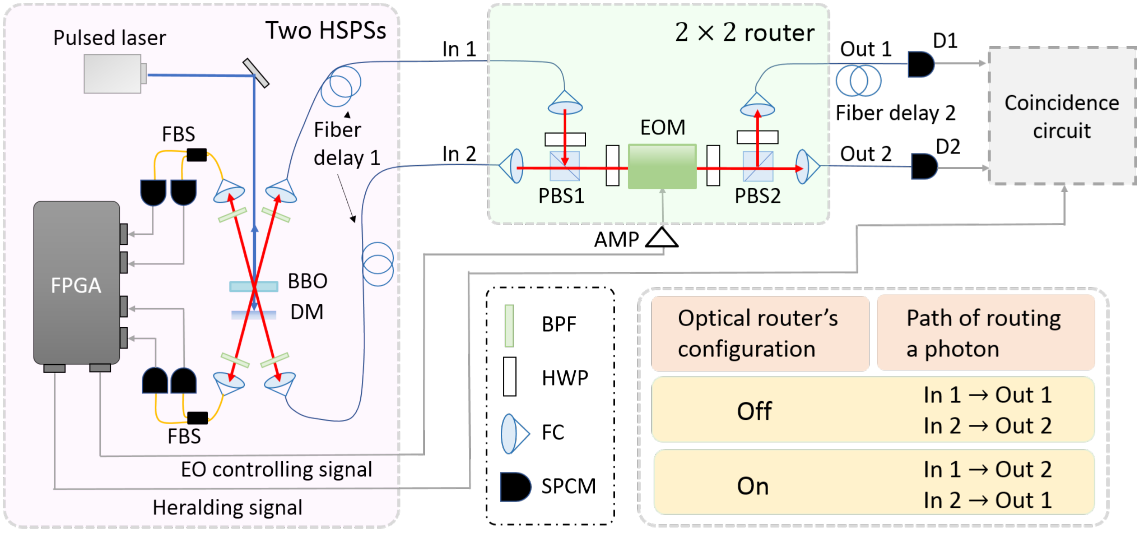

Figure 5.4: Experimental setup of ASN using two heralded single photon sources for efficiently generating two-photon parallel state. FPGA: field programmable gate array. FBS: fiber beam splitter. DM: dichroic mirror. BBO: beta barium borate. PBS: polarizing beam splitter. BPF: band pass filter (2nm). EOM: electro optics modulator. HWP: half wave plate. FC: fiber coupler. SPCM: single photon counting module. AMP: high voltage pulsed amplifier.

$$P_{\text{herald}}(N) = \{1 - \prod_{l=1}^{N}(1 - P_{\text{h}}^{(l)})\}^N, \tag{5.7}$$

$$P_{\text{T}}(N) = \prod_{k=1}^{N} P_{\text{C}}^{(k)}(1), \tag{5.8}$$

$$P_{\text{C}}(n) = (P_{\text{C}}^{(1)}(n) + (1 - P_{\text{h}}^{(1)})(P_{\text{C}}^{(2)}(n) + (1 - P_{\text{h}}^{(2)})(P_{\text{C}}^{(3)}(n) + \cdots)). \tag{5.9}$$

$P_{\text{C}}(n)$ is the output probability of having n photons at the output port k of the ASN system. The coincidence rate for N-photon parallel state is $R_{\text{rep}}P_{\text{T}}(N)\eta_{\text{D}}^{N}$.

In our experiment for $N = 2$, we extended the equation to calculate the rate generating of undesired two-photon parallel state from our ASN system. The probability of having two photons at one output and zero photon at another output is given by,

$$P_{\text{multi}} = P_{\text{C}}^{1}(2)P_{\text{C}}^{2}(0) + P_{\text{C}}^{1}(0)P_{\text{C}}^{2}(2) \tag{5.10}$$

5.4 Experimental setup of optical system for two-photon parallel state

We implemented the source using ASN for N=2. A femtosecond pulse laser (Tsunami with second harmonic generation, Spectra Physics, repetition rate of 82 MHz and central wavelength of 390 nm) is used to pump a nonlinear crystal (beta barium borate, Type - I, thickness of 1.5mm). The pump laser generates photon pairs in the forward direction (SPDC -A). After passing through the BBO crystal, the laser is reflected by a dichroic mirror (DM) and generates photon pairs in the backward direction (SPDC-B). For each photon pair source, one of the photon pairs are detected by a cascaded detector consisting two single photon detectors (SPCM-AQR, Excelitas Technologies) and a fiber beam splitter, because deadtime (40ns) of the detector is larger than the interval (12.2ns) between the pump pulse. The time-bin information of heralding signals from four detectors is recognized by the field programmable gate array (FPGA, National Instruments). The FPGA generates EO controlling signals and two-photon heralding signals when the target photons to be controlled are generated from two sources. For this experiment, the target photons are composed of the four patterns that at least one detection signal appears at each time t_0 and t_1 ($t_1 - t_0 = 24.4$ns). The details are written in Appendix A.

The heralded photons from two HSPSs are sent to the two input port (In1 and In2) of the 2×2 router consisting of an electro-optics modulator (EOM), polarizing beam splitters (PBS), and half wave plates (HWP). Long polarization maintaining fibers (85m, Fiber delay 1) are used for compensating the delay caused by the electric signal processing. The active 2×2 router is driven by the EO controlling signals from FPGA when the heralding signals of the target photons are generated. After passing through a fiber delay line (5m, Fiber delay 2), the target photons to be controlled are routed into the desired two photon parallel state, which two single photons are emitted in parallel from different output ports (Out1 and Out2). Finally, the two photons are detected by two detectors (D1, D2) . The 4-fold coincidence counts are measured among the detection signals from two SPCMs and the two-photon heralding signals from the FPGA.

5.5 Experimental results and discussion

5.5.1 The output photon number distribution

To check the performance to experimentally enhance the generation rate of two-photon parallel state by use of the method of ASN, we implement a four-fold coincidence measurement and compare the four-fold coincidence rates between the method of ASN and NASN. In Fig. 5.5(a), we summarized the observed or estimated coincidence rates between the heralding signals of two-photon output and the two detection signals at the output, which corresponds to the generation rate of the heralded two photon parallel state.

Firstly, we evaluate the performance of two HSPSs (HSPS-A and HSPS-B). HSPS-A and HSPS-B correspond to the source using SPDC-A and SPDC-B, respectively. We estimate the heralding probability and the probability to generate one photon when the heralding signal is produced from the experimental parameters $P_{\mathrm{h}}(1)$. The heralding signal

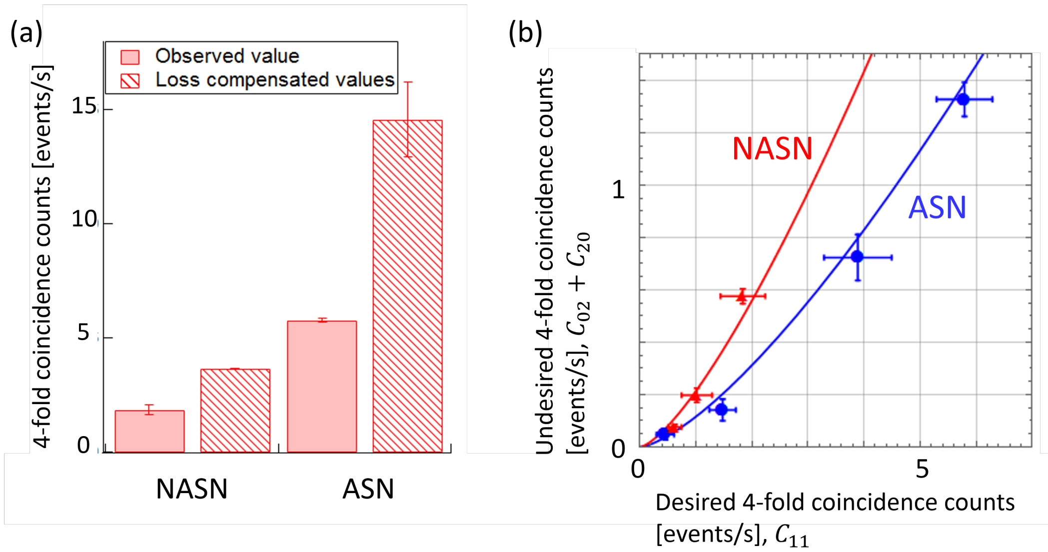

Figure 5.5: (a) Measured 4-fold coincidence counts per a second for the cases of ASN and NASN (Filled red bars). Meshed red bars corresponds to the estimated value of measured values when losses of routers are corrected for. (b) Undesired 4-fold coincidence count rate $C_{02}+C_{20}$ versus desired 4-fold coincidence count rate C_{11}. Red and blue dots show the case of NSAN and SAN. Red and blue lines show the theoretical predictions.

of HSPS-A and HSPS-B p is $(3.62 \pm 0.01) \times 10^{-3}$ and $(4.63 \pm 0.01) \times 10^{-3}$, respectively. The two-fold coincidence rate from SPDC-A and SPDC-B is $(1.44 \pm 0.02) \times 10^4$ and $(2.07 \pm 0.03) \times 10^4$ cps. Therefore, $P_{\mathrm{h}}(1)\eta_{\mathrm{D}}$ of HSPS-A and HSPS-B are $(4.87 \pm 0.01) \times 10^{-2}$ and $(5.46 \pm 0.01) \times 10^{-2}$, where η_{D} is the detection efficiency of the detector and we assume η_{D}=0.6.

In our experiments, the measured four-fold coincidence events between heralding signals and the detection signals from detectors D1 and D2 is 5.79 ± 0.09 cps, shown in red bars in Fig. 5.5(a). This result indicates that the two photons are sent to the different output ports simultaneously with this rate. The coincidence counts is 1.84 ± 0.22 cps when EOM is not operated, indicating that only one of the four target photons (Pattern B) is emitted. Thus, we confirm that our source enhance the generation rate of the two-photon parallel state.

To evaluate the enhancement of the generation rate of the two-photon parallel state, we estimate the enhancement factor $R(2)$ of Eq.5.2. The four-fold coincidence events per a second can be estimated 3.65 ± 0.08 cps from two kinds of the two-fold coincidence rate from SPDC-A and SPDC-B, $(1.44 \pm 0.02) \times 10^4$ and $(2.07 \pm 0.03) \times 10^4$ cps (the red mashed bar of NASN in Fig. 5.5(a)). The enhancement factor is found to be 1.59 ± 0.14, which exceeds 1. The results indicates that the generation rate of two-photon parallel state is enhanced by use of the method of ASN. The red meshed bar of ASN indicates the loss compensated four-fold coincidence count rate 14.57 ± 1.64 cps. Then, we consider two kinds of losses; the transmittance of 2×2 router written in Table 5.1 and the success probability of detecting a stream of two single photons by a cascade detector consisting of two bucket detectors and a beam splitter of 50% [146]. When these losses are compensated, the ratio between the red meshed bar of ASN and NASN is found to be 3.99 ± 0.49. The loss-compensated enhancement factor is in good agreement with ideal value $4(= N^2)$ for the case of $N = 2$.

The source to generate the multi-photon parallel state, consisting of multiple HSPSs, emits occasionally the undesired multi-photon state with the same number of photons due to the thermal distribution of the output photon number statistics of SPDC. In the case of N=2, the undesired two-photon state corresponds to the case where two photons are existed at either output, no photons are existed at another output. To confirm the generation rate of the undesired two photon state, we further measure the 4-fold coincidence events ($C_{2,0} + C_{0,2}$). $C_{a,b}$ indicates that a detector at Out 1 detects a photons and a detector at Out 2 detects b photons. Figure 5.5(b) shows $C_{2,0} + C_{0,2}$ at the output of the ASN and NASN systems versus the desired state $C_{1,1}$. Here, we assumed that $C_{2,1}$ and $C_{3,0}$ are ignored because the mean number of photon pairs from photon pair sources are small. The rate of generating undesired state using the method of ASN (blue dots) is suppressed by about half when comparing to the method of NASN (red dots). The observed results show that we can confirm the suppression of the undesired state by use of active spatial routing using multiple heralded single photon sources. This is because the generation rate of the two-photon parallel state is increased by not increasing the intensity of the pump laser. The obtained experimental results are in good agreements with the theoretical predictions (blue and red curves). The results are predicted from the observed experimental parameters summarized in Table 5.1.

For the realization of the practical source to emit the multi-photon parallel state, it is necessary to improve the performance of each HSPS, like as $P_{\mathrm{h}}(1) = 1$. In additional, if a controllable active network which relocate single photons in the arbitrary spatial and temporal modes into the arbitrary modes can be achievable, the generation rate of N single photons is expected to be enhanced up to p. This ideal and deterministic source is the key to the realization of large-scale photonic quantum computation, communication, and metrology.

5.5.2 Test of the two-photon interference experiments

Figure 5.6 shows the Hong-Ou-Mandel (HOM) dip signals between the two photons from the two outputs from the ASN system. The result in Fig. 5.6(a) indicates measured four-fold coincidence events of HOM dip (Pattern A and Pattern B). The result in Fig. 5.6(b) indicates measured four-fold coincidence events of HOM dip (only Pattern B). The

Table 5.1: Observed parameters. Each small alphabet of A and B corresponds to HSPS-A and HSPS-B.

Description	Symbol	Value in this work
Mean photon number per pulse (HSPS-A)	$\bar{N}$	0.063
Mean photon number per pulse (HSPS-B)	$\bar{N}$	0.116
Trigger-mode system detection efficiency of HSPS-A	η_{h}	0.058(1)
Trigger-mode system detection efficiency of HSPS-B	η_{h}	0.040(1)
Optical transmittance of HSPS-A	t	0.081(1)
Optical transmittance of HSPS-B	t	0.091(1)
Assumed detector efficiency	η_{D}	0.60
Transmittance of 2×2 router (In1 - Out1)	η_{n}	0.683(1)
Transmittance of 2×2 router (In1 - Out2)	η_{n}	0.726(2)
Transmittance of 2×2 router (In2 - Out1)	η_{n}	0.743(2)
Transmittance of 2×2 router (In2 - Out 2)	η_{n}	0.699(2)

visibility of obtained HOM dip is defined as,

$$V = \frac{N_{\max} - N_{\min}}{N_{\max}}, \tag{5.11}$$

where $N_{\max}$ and $N_{\min}$ is the maximum and minimum parameters of the fitted Gaussian functions (red curves). The visibilities of the two dips are 72 % and 74%, subtracting multi-photon pairs. We achieved quantum interference signals which is exceeding the classical limit (50%). However, the visibility is not ideal. Here, we discuss the reason why the visibility of HOM dip is decreased. The main reasons which we focus on is the effect of group velocity mismatch and group velocity dispersion of a single mode fiber.

The effect of group velocity mismatch (GVM) is written in [68]. GVM is due to the group velocity dispersion in the nonlinear crystal. The HOM dip function by accounting for the effect of timing jitters between the two photons is,

$$F(\tau) = \int_0^{L\Delta u} \int_0^{L\Delta u} g(x) g(x') \left(1 - e^{-\left(\frac{\tau - x - x' - L\Delta u}{\tau_C}\right)^2}\right) dx dx', \tag{5.12}$$

$$\Delta u = \frac{1}{\nu_{ge}(\lambda/2)} - \frac{1}{\nu_{go}(\lambda)}, \tag{5.13}$$

$$g(x) = \begin{cases} \tau & (0 \leq x \leq L) \\ 0 & (\text{otherwise}) \end{cases} \tag{5.14}$$

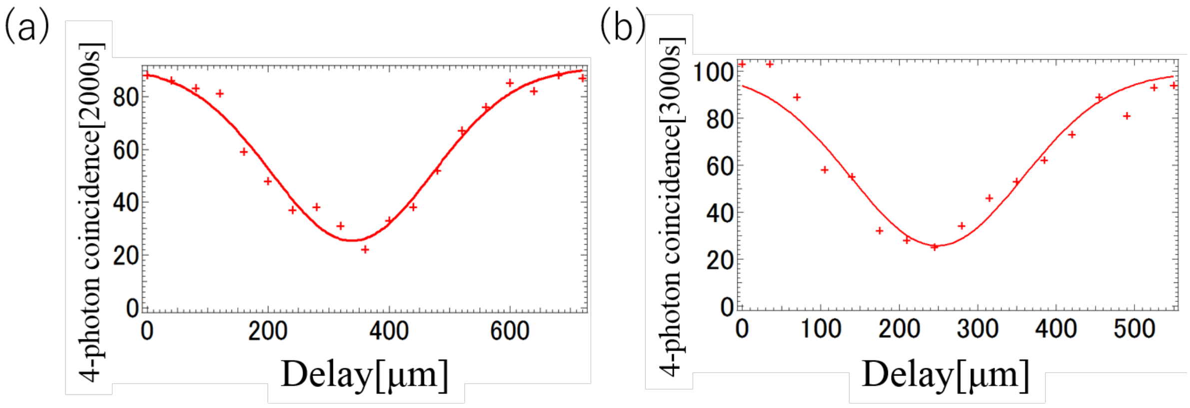

Figure 5.6: (a) Measured four-fold coincidence events of HOM dip (Pattern A and Pattern B).(b) Measured four-fold coincidence events of HOM dip (Pattern B).

In this experiments, the crystal length of BBO is 1.5μm, and the bandwidth of heralded photons is 2 nm. $\nu_{ge}(\lambda)$ and $\nu_{go}(\lambda)$ are the group velocity of the extraordinary and ordinary rays for the wavelength λ, which is the down converted photons. $g(x)$ is the photon pair creation rate in the crystal. τ_C is the coherence time of the input photon. As the results, the estimated visibility from the paper [68] V_{GVM} is 0.929.

The four-fold coincidence events of HOM dip function by accounting for the effect of group velocity dispersion of single mode fibers between the two photons (see Apendix B) is,

$$P_{4\text{C}}(\tau) = \frac{1}{4} - \frac{1}{4\sqrt{1+\sigma^4\Gamma^2}}\exp\left[\frac{-\sigma^2(\tau+2\Gamma\omega_0)^2 + 4\sigma^2\Gamma\omega_0(\tau+\Gamma\omega_0)}{4(1+\sigma^4\Gamma^2)}\right]. \tag{5.15}$$

where $\Gamma_{12} = k^{(2)}(L_1 - L_2)/2$ is the effect of group velocity dispersion of a fiber (In this experiment, $L_1 - L_2 = 2.5$m). The experimental effect of GVD in the PMF fiber is 225 fs^2/mm. ω_0 is the central wavelength of heralded photons 780nm. As the results, the calculated visibility V_{GVD} is 0.770.

The approximately estimated visibility of the observed HOM dip is,

$$V \approx V_{\text{GVM}} V_{\text{GVD}} = 0.715. \tag{5.16}$$

This predicted value is almost agreement with the experimental observed values. The slight differences are due to the mode mismatch between input photons and a non-zero pump pulse duration [68]. V_{GVM} can be improved by referring [68, 65]. V_{GVD} can be improved by compensated the unbalanced GVD or use of photons with narrower bandwidth. We think the indistinguishabliity of photons from the QD with micropiller keeps high even after serial-parallel conversion because of the very narrow bandwidth of generated photons [110].

5.6 Summary

In this section, as the way to increase the heralding probability of the multi-photon parallel state, we propose the method to efficiently generate N-photon parallel state, by an active spatial networking (ASN) using a $N \times N$ network and optical delay lines. We show that the proposed method allows us to prepare N-photon parallel state with an efficiency exponentially greater than N HSPSs with no active routers. We also show an experimental demonstration of ASN using two HSPSs for generating two-photon parallel state with the realization of an active spatial 2×2 network and a fixed delay. We achieve enhancement factor of 1.59 ± 0.14, compared with the naive source using two HSPSs. When the losses in the setup are compensated, the enhancement factor of current setup increases up to 3.99 ± 0.49, which is in good agreement with the theoretical prediction.

Chapter 6

Evaluation of bipartite entanglement between two optical multi-mode systems using mode discrete fourier transform circuits

6.1 Introduction

As we mentioned in the introduction of this thesis, the multi-photon interferometer with linear optical circuit has been applied for quantum computation [23], quantum communication [30, 31, 32], quantum sensing [25, 26]. Then, one of the most important fundamental phenomena is entanglement. Until now, various kinds of experiments with entanglement between two-mode and two-photon systems are reported [88]. As the next step, it is well known that high dimensional entanglement between two multi-mode multi-photon local systems can be useful for various quantum applications, such as quantum repeater [21, 147, 148] or remote state preparation [149].

Photons become a promising platform to encode high-dimensional entanglement in various degree of freedom, such as polarization mode [141], frequency mode [150, 99], orbital angular momentum mode [151, 152, 153], temporal mode [154], path mode [155], the combination of two modes called hyper entanglement [156]. High-dimensional entanglement with photons have been demonstrated recently in various degree of freedom as not only fundamental interest but also available state. However, the evaluation of the high-dimensional entangled state by use of quantum full state tomography (FST) [157, 158] is a crucial challenge since it is difficult to characterize its non-classical features that scale up exponentially the dimension of its Hilbert space as the number of photons and modes increases. FST quickly becomes impractical in higher dimensional entanglement. Thus, it is desirable to develop more specific theories that make use of convenience to quantify the observed entanglement.

Recently, the easy and scalable way to verify entanglement has been proposed for photons, from Wu and Hofmann [47]. Their new proposal is that we can efficiently evaluate the characteristic signatures of the bipartite entanglement between two multi-mode systems that is generated by propagating multiple single photons through beam splitters, one of the high dimensional entanglement. According to their method, we can verify generated entanglement experimentally just by achieving the photon number statistics before and after passing through their proposed discrete mode fourier transform circuits. This results in the exponential decrease in the measurement setups for verifying entanglement. Note that this method is attractive attention since it can expand to verify other various kinds of entanglement.

Here, we report the first demonstration for verifying the generated bipartite entanglement between two local multimode-multiphoton modes. As the smallest non-trivial case, we evaluated the entanglement that is generated by propagating three single photons through three beam splitters. The verification of entanglement is realized using two super stable 3-mode DFT circuit which are made of linear optics. Then, we use two key technical approaches; a displaced-Sagnac architecture [25, 34, 159] and a hybrid polarizing beam splitter [34]. As the results, we successfully achieved the correlations of the photon number statistics between the two systems with and without DFT circuits, and the sum of the fidelities $F_{\boldsymbol{n}} + F_K = 1.555 \pm 0.018$, which exceed the lower bound 4/3 for verifying the generation of entanglement with 12.3 standard deviation. Compared with the previous method to efficiently obtain the multi-photon tomography [160, 161, 162], our method is more practical since it can directly verify the generation of entanglement.

6.2 Method to verify the generation of bipartite entanglement

To verify the experimentally generated bipartite entanglement between two optical systems ρ_{exp}, it is necessary to confirm correlation between two complementary optical systems A and B. Our collaborators, Wu and Hofmann, proposed the novel method to verify the generation of entanglement just by two measurements instead of Full state tomography. They have reported that the entanglement can be verified from two sets of output photon number correlation results between two optical systems by use of discrete fourier transform (DFT) circuits. In this section, firstly we introduce the state of entanglement and the method proposed by Wu and Hofmann [47]. Secondly, we explain the case of verifying three-photon entanglement between two three-mode systems.

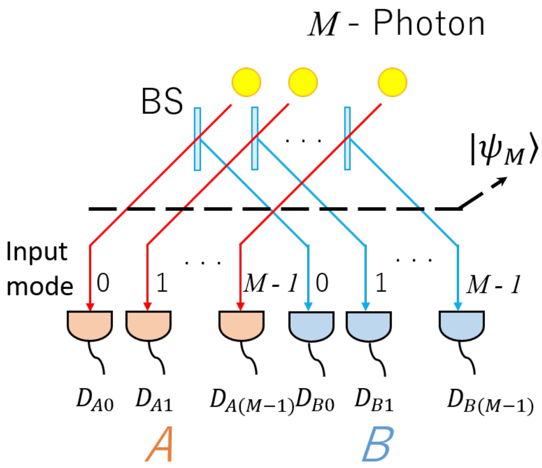

Figure 6.1: Schematic illustration of setup to generate the bipartite entanglement between two optical systems A and B. The total number of photons is M. M detectors in mode A detect N photons, and M detectors in mode B detect $M - N$ photons.

6.2.1 Bipartite entanglement between two optical multi-mode systems

Here, we discuss the generation of entanglement between two local mode A and B. As shown in Fig. 6.1, M photons in M input modes is split by M beam splitters (BSs) and divided into two local separate modes A and B. Then, the photon number state $|\psi_M\rangle = \left((|1\rangle_{\rm A}|0\rangle_{\rm B} + |0\rangle_{\rm A}|1\rangle_{\rm B})/\sqrt{2}\right)^{\otimes M}$ is obtained. However, the Hilbert space existed in $|\psi_M\rangle$, between mode A and mode B, includes many different photon number distributions. For accessing the entanglement subspaces of each local mode A and B, it is useful to postselect the total numbers in the local modes by detecting the distribution of N photons in mode A, and $M - N$ photons in mode B within each local system. Then, the entanglement state $|\phi_{N,M-N}\rangle$ is given by,

$$|\phi_{N,M-N}\rangle = \frac{1}{\sqrt{\begin{pmatrix} M \\ N \end{pmatrix}}} \sum_{|n|=N} |\boldsymbol{n}\rangle_A |\overline{\boldsymbol{n}}\rangle_B\,, \tag{6.1}$$

where $\boldsymbol{n}$ are the M-dimensional vectors describing the photon number distribution of the local M modes, and $|\boldsymbol{n}\rangle_A|\overline{\boldsymbol{n}}\rangle_B$ satisfies $\boldsymbol{n} + \overline{\boldsymbol{n}} = (1, 1, \ldots, 1)$.

6.2.2 Verification of generating entanglement

First, the photon number statistics of generated entanglement $\rho_{\rm exp}$ is measured. The schematic setup is shown in Fig. 6.1. Then, we just get the correlation when N photons are detected in the system A and $M - N$ photons are detected in the system B.

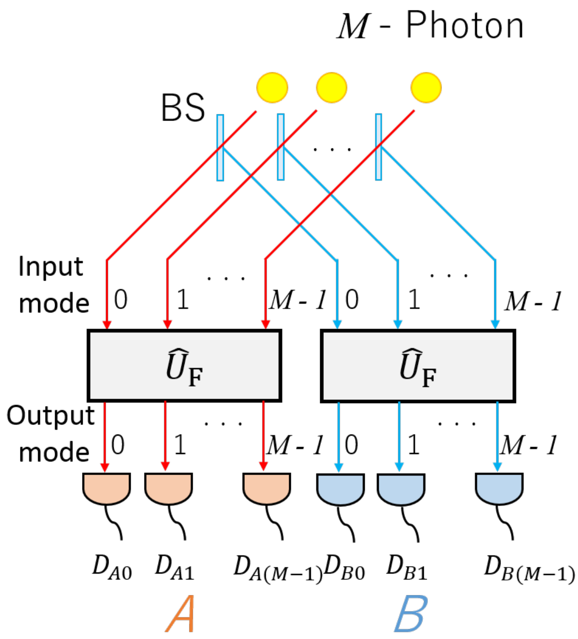

Figure 6.2: Schematic illustration of setup to achieve the photon number distribution between the output modes of DFTs.

Secondly, it is important to obtain the parameters of coherence in the generated entanglement ρ_{exp}. The coherence of the generated state have to be achieved to verify the state as the quantum state. Although it is necessary to identify the quantum coherence of the generated entanglement between the mode A and B, the detected photon number distribution in Fig. 6.1 does not include the information. To solve this problem, as shown in Fig. 6.2, it is useful to use the application of discrete fourier transforms (DFTs) to relate two sets of modes to each other, which is proposed in Wu's paper [47]. The DFT $\hat{U}_{\text{F}}$ consisting of the matrix elements that connect the output photon number distribution in output modes k to the input photon number distributions in input modes m is given by,

$$\hat{U}_{\text{F}}^{\dagger}\hat{b}_k^{\dagger}\hat{U}_{\text{F}} = \sum_{m=0}^{M-1} \frac{1}{\sqrt{M}} \text{e}^{-\text{i}\frac{2\pi}{M}km} \hat{a}_m^{\dagger}. \tag{6.2}$$

According to DFT, the state of entanglement $\hat{\rho}_{\text{exp.}}$ is transformed to,

$$\hat{\rho}_{\text{exp.}} \to \hat{U}_{\text{F}} \otimes \hat{U}_{\text{F}} \hat{\rho}_{\text{exp.}} \hat{U}_{\text{F}}^{\dagger} \otimes \hat{U}_{\text{F}}^{\dagger}. \tag{6.3}$$

This state has the information of coherence in the real part. Thus, the second step for verification is to achieve the photon number distribution between the output modes of DFTs. Note that this measurement is also postselection for N photons in mode A and $M - N$ photons in mode B.

As the next step, the fidelity are calculated from the observed two photon number distributions. The observed correlation in the poseselected photon number distribution between input modes without DFT can be evaluated by the fidelity F_n. F_n is given by the probability of the observed distribution, and summing over the probability of all correctly correlated combinations of photon number distributions $(\boldsymbol{n}, \overline{\boldsymbol{n}})$ (the bases of Eq. 6.1) between mode A and B,

$$F_n = \sum \langle \boldsymbol{n}\overline{\boldsymbol{n}} | \hat{\rho}_{\mathrm{exp.}} | \boldsymbol{n}\overline{\boldsymbol{n}} \rangle \,, \tag{6.4}$$

where $\hat{\rho}_{\mathrm{exp.}}$ is the density operator of the experimentally generated state. Similarly, the observed correlation in the postselected distribution between the output modes of DFTs can be quantified by the fidelity F_K. F_K is given by the probability of the observed photon number distribution, and summing over the probability of all correctly correlated combinations of photon number distribution $(\boldsymbol{n}_A, \boldsymbol{n}_B)$ between mode A and B,

$$F_K = \sum \langle \boldsymbol{n}_{\mathrm{A}}\boldsymbol{n}_{\mathrm{B}} | \hat{U}_{\mathrm{F}} \otimes \hat{U}_{\mathrm{F}} \hat{\rho}_{\mathrm{exp.}} \hat{U}_{\mathrm{F}}^{\dagger} \otimes \hat{U}_{\mathrm{F}}^{\dagger} | \boldsymbol{n}_{\mathrm{A}}\boldsymbol{n}_{\mathrm{B}} \rangle \,. \tag{6.5}$$

Based on the relation between photon number distributions before and after the DFTs, we can verify the observed entanglement between two multi-mode systems. When the generated state is at least entangled, the lower bound of $F_{\boldsymbol{n}} + F_K$ is given by,

$$F_{\boldsymbol{n}} + F_K \geq 1 + \frac{1}{\min_{\boldsymbol{p}} d_{\boldsymbol{p}}}, \tag{6.6}$$

where $0 \leq F_{\boldsymbol{n}} \leq 1$, $0 \leq F_K \leq 1$. The detail discussion of the value is given in [47]. Any state that exceeds this bound is entangled. We can verify the M-photon entanglement between the two-mode local system by evaluating the the correlations between the postselected photon number distributions in the input modes and the output modes of DFTs. If the experimental state $\hat{\rho}_{\mathrm{exp.}}$ exceed the lower bound, the generation of entanglement is verified. Note that if the generated state is not entangled (separable state or mixed state), $F_{\boldsymbol{n}} + F_K$ can not overcome the bound, max $F_{\boldsymbol{n}} = 1$, max $F_K = 1/\min_{\boldsymbol{p}} d_{\boldsymbol{p}}$.

6.2.3 k-value

Here, we introduce the k-value, and the correlation of k-value between two system. But the detail definition of k-value can not be written here because it is so complicated. Therefore, please see ref [47].

The operation of DFT is based on the cyclic ordering of the modes between input and output. This cyclic operation can be used to define the cyclic mode shift operator $\hat{S}^{\dagger}$. The cyclic mode shift operation that transforms the creation operator of the nth mode into the operator of the $(n{+}1)$th mode,

$$\hat{S}\hat{a}_n\hat{S}^{\dagger} = \hat{a}_{n+1}, \tag{6.7}$$

where $\hat{a}_{M-1}$ is transformed into $\hat{a}_0$. For example, $\hat{S}|110\rangle = |011\rangle$. This shift operator applies to the output state after DFT. The effect of the output mode shift operation is given by,

$$\hat{S}\hat{U}_{\mathrm{F}}^{\dagger}|\boldsymbol{n}\rangle = \mathrm{e}^{\mathrm{i}\frac{2\pi}{M}K(\boldsymbol{n})}\hat{U}_{\mathrm{F}}^{\dagger}|\boldsymbol{n}\rangle. \tag{6.8}$$

k-value $K(\boldsymbol{n})$ is the value of the total mode index of the photon number state $|\boldsymbol{n}\rangle$ is given by,

$$K(\boldsymbol{n}) = \sum_{k=0}^{M-1} n_k k \quad (\mathrm{mod} M). \tag{6.9}$$

For the case of $|1100\rangle$, K is 1 (=$0 \times 1 + 1 \times 1 + 2 \times 0 + 3 \times 0$).

According to the k-value correlation between two systems A and B, we can estimate the output photon number distribution of DFT. If the input state is ideally entangled, the bunching effect of the output photon number distribution of DFT is appeared when $K_A + K_B$=0. For our experiments of $M = 3$, the bunching effects are appeared when $K_A = K_B = 0$, $K_A = 1$ and $K_B = 2$, or $K_A = 2$ and $K_B = 1$.

6.2.4 Specific case for three-photon entanglement between two three-mode systems

As the non-trivial case, we performed the experiment for the three photons, and verified the generated three-photon entanglement between two three-mode systems. Then, the ideal entangled state between two optical systems A and B is,

$$|\phi_{2,1}\rangle = \frac{1}{\sqrt{3}}(|110\rangle_A|001\rangle_B + |101\rangle_A|010\rangle_B + |011\rangle_A|100\rangle_B). \tag{6.10}$$

This state $|\phi_{2,1}\rangle$ indicates entanglement with the eighteen dimensional Hilbert space between the six dimensional Hilbert space of two photons in the three modes of A $\{|110\rangle_A, |101\rangle_A, |011\rangle_A, |200\rangle_A, |020\rangle_A, |002\rangle_A\}$, and the three dimensional Hilbert space of the single photon in the three modes of B $\{|100\rangle_B, |010\rangle_B, |001\rangle_B\}$. In the experiments, there is a possibility that two photons in the system A are detected in the same mode due to the unwanted multi-photon pair generation from the sources. According to the equation 6.4, F_n consists of three of eighteen possible outcomes for the case of $|\phi_{2,1}\rangle$,

$$F_{\boldsymbol{n}} = P_{\mathrm{exp.}}(110, 001) + P_{\mathrm{exp.}}(101, 010) + P_{\mathrm{exp.}}(011, 100), \tag{6.11}$$

where $P_{\mathrm{exp.}}(p_A, p_B)$ (ex. $P_{\mathrm{exp.}}(110, 001) = \langle 110001|\hat{\rho}_{\mathrm{exp.}}|110001\rangle$) is the pattern probability represented by the photon number distribution in A and B. When DFTs are applied to $|\phi_{2,1}\rangle$, the the ideal state between the output of DFTs is,

$$\begin{aligned}\hat{U}_{\mathrm{F}}\hat{U}_{\mathrm{F}}|\phi_{2,1}\rangle = &\frac{\sqrt{2}}{3}(|002\rangle_A|001\rangle_B + |020\rangle_A|010\rangle_B + |200\rangle_A|100\rangle_B)\\ &+\frac{1}{3}(|110\rangle_A|001\rangle_B + |101\rangle_A|010\rangle_B + |110\rangle_A|001\rangle_B).\end{aligned} \tag{6.12}$$

Then, the six outcomes are related to the correlation of the two k-value K_A and K_B in A and B. In other words, the outcomes of Eq.6.12 is appeared in $K_A + K_B = 0$. According to the equation 6.5, F_K consists of six of eighteen possible outcomes,

$$\begin{aligned} F_K &= P_{\text{exp.}}(110,001) + P_{\text{exp.}}(101,010) + P_{\text{exp.}}(011,100) \\ &+ P_{\text{exp.}}(200,100) + P_{\text{exp.}}(020,010) + P_{\text{exp.}}(002,001). \end{aligned} \tag{6.13}$$

For the case of three photons, $d_{\boldsymbol{p}}$ is 3. Therefore, generation of entanglement can be verified if,

$$F_{\boldsymbol{n}} + F_K > \frac{4}{3}. \tag{6.14}$$

Note that the maximum of $F_{\boldsymbol{n}} + F_K$ is 4/3 when the generated state is separable state.

6.3 Experimental setup

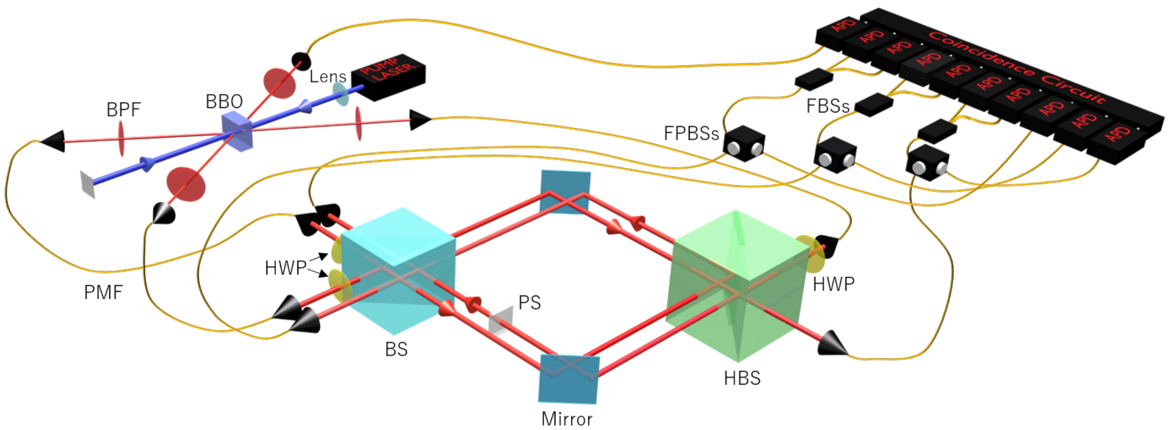

Figure 6.3: The experimental optical setup of generating and evaluating entanglement. Input three photons are generated from a heralded single photon source and a photon pair source. A heralded photon and a pair of photons is input into a polarization independent mode DFT. After 3 photons enters a polarization independent mode DFT, the output photons are detected with a heralding signal.

Figure 6.3 shows the experimental setup to verify entanglement. This consists of the three photon source, a super stable polarization independent discrete fourier transform circuit, and the measurement system. In this section, we explain them on detail.

6.3.1 Construction of a three-photon source

Figure 6.4 (a)/(b) shows the schematic setup of a 3-photon generating source and the optical implementation of the source. For the 3 photons required for the entanglement

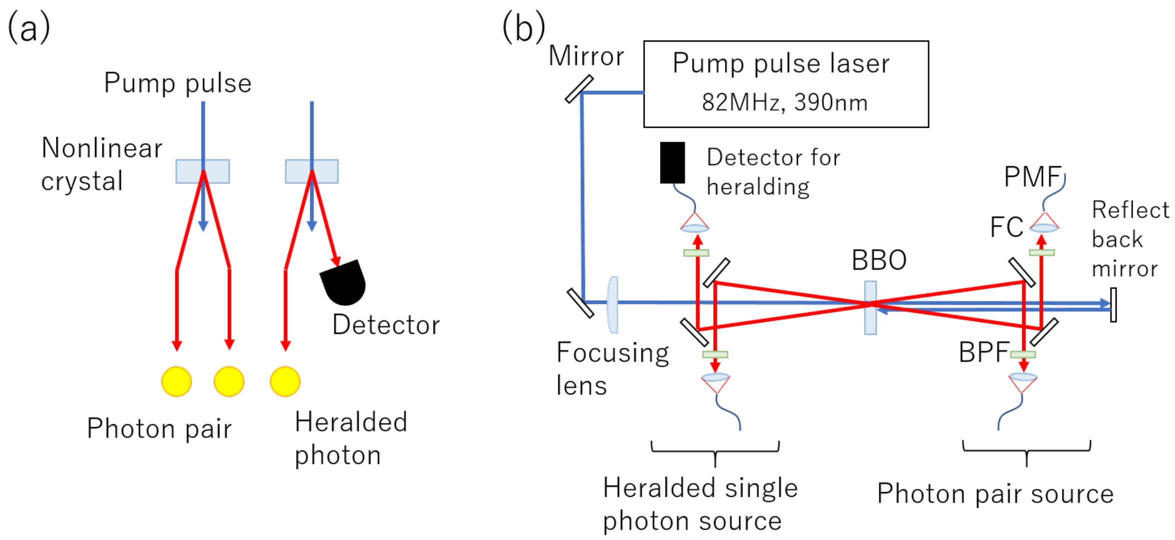

Figure 6.4: (a)The schematic setup of a 3-photon generating source consisting a heralded single photon source and a photon pair source. When two independent sources fire simultaneously, the three-photon parallel state is generated. (b) Optical implementation of a photon pair source and a heralded single photon source. BPF : Band pass filter ($\Delta\lambda$ =2nm), FC : Fiber coupler, PMF : Polarization maintaining fiber.

generation, we constructed a heralded single photon source and a photon pair source. A femtosecond pulsed laser (Tsunami with second harmonic generation, Spectra Physics, repetition rate of 82 MHz and central wavelength of 390 nm) is used to pump a beta barium borate (BBO) crystal (Type - I, thickness of 1.6 mm). The injected pump laser pulses generate photon pairs via the process of spontaneous parametric down conversion, in the forward direction. After passing through the BBO crystal, the pump laser is reflected by a mirror and generates photon pairs in the backward direction. The generated photons are coupled into the polarization maintaining fibers, after removing the scattered pump light by using an interference filter (center wavelength of 780 nm, full width at half maximum of 2 nm). One of the photon pair is used for a heralded single photon source, and another is used for a photon pair source. Then, the heralded photons and the pairs of photons were delivered to the input of the DFT circuit or directly to the measurement system.

6.3.2 Super stable polarization independent discrete fourier transform circuit

As referred to ref [84], we designed and constructed the 3-mode discrete fourier transform circuit. Figure 2(a) shows our designed 3-mode DFT, consisting of some kinds of linear optics; balanced beam splitters (R=1/2), a unbalanced beam splitter (R=1/3), and phase

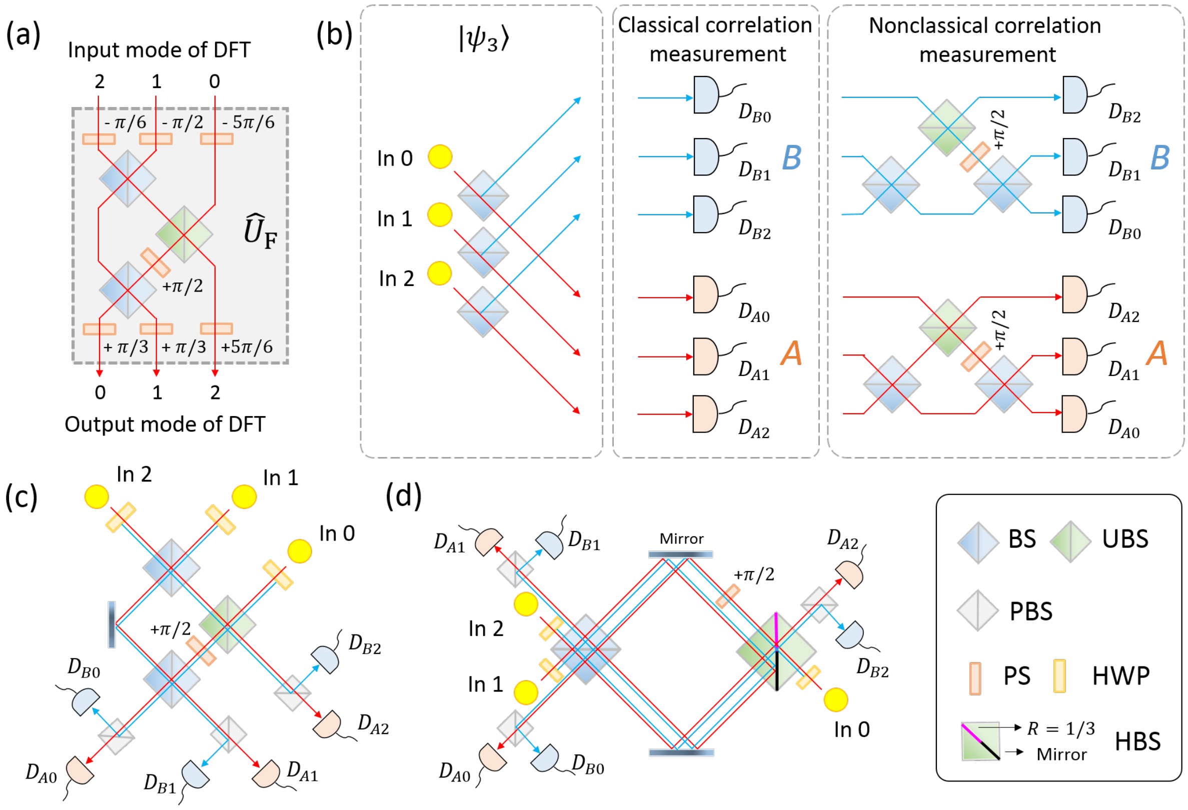

Figure 6.5: Optical quantum circuit for evaluating entanglement. (a) Design of optical 3-mode discrete fourier transform. which are consisted of linear optics. BS : Beam splitter. UBS : Unbalanced beam splitter (Reflectance of 1/3). PS : Phase shifter. (b)Photonic scheme using two DFTs Red arrow corresponds to mode A (T : Transmittance mode of BS, and H : Horizontal mode of polarization of photon). Blue arrow corresponds to mode B (R : Reflectance mode of BS, and V : Vertical mode of polarization of photon).(c) A semi-simplified circuit of Fig.6.5(a), made by polarization independent DFT circuit. PBS : Polarizing beam splitter. HWP : Half wave plate. (d)A final simplified circuit of Fig.6.5(a). This system includes one super stable optical interferometer realized by using displaced Sagnac architecture. A hybrid beam splitter (HBS) includes two planes, the reflectance of them is 1/3 and 1 (mirror).

shifters. The matrix of 3-mode DFT $\hat{U}_{\mathrm{F}}$ is given as,

$$\hat{U}_{\mathrm{F}} = \frac{1}{\sqrt{3}} \begin{pmatrix} 1 & 1 & 1 \\ 1 & \mathrm{e}^{\mathrm{i}\frac{2}{3}\pi} & \mathrm{e}^{\mathrm{i}\frac{4}{3}\pi} \\ 1 & \mathrm{e}^{\mathrm{i}\frac{4}{3}\pi} & \mathrm{e}^{\mathrm{i}\frac{2}{3}\pi} \end{pmatrix}. \tag{6.15}$$

Figure 6.5(b) shows a schematic of the optical quantum circuit for generating and evaluating the bipartite entanglement between two local modes. Input 3 photons are split by 3 beam splitters (BSs), and are divided into two local systems A (transmittance side) and B (reflectance side). The generated state passes our two designed 3-mode DFT circuits which is consisted of linear optics. Finally, for accessing the entanglement subspace, we measured the postselected events by detecting the distribution of 2 photons in mode A, and 1 photon in mode B within each local system. Note that three phase sifters on the input side are removed because of over all phase for the bipartite entanglement, and three phase shifters on the output side are also removed because of no interference between modes after them.

To realize the optical circuit of Fig.6.5(b), it is necessary to stabilize the drafts and vibrations of the optics between the two 3-mode DFTs. Then, we designed a stabilized quantum circuit, using a polarization independent optical DFT circuit. By replacing BSs with half wave plates (HWPs), it is possible to realize the system of Fig. 6.5(c) with only one polarization independent DFT circuit (Fig.6.5(c)). Furthermore, in order to stabilize the path difference inside the interferometer, we realized a highly stable photonic quantum circuit for the simplified 3-mode DFT for evaluating the bipartite 3-photon entanglement between the horizontal(A) and vertical(B) modes (Fig.6.5(d)), by using the technologies of polarization independent displaced-Sagnac architecture [25, 159, 34] and a hybrid beam splitter (HBS) [34] which contains an unbalanced BS (R=1/3) and a mirror. In this setup, all the input 3-photon pass though the same optical components inside the interferometer so that all the modes are super-robust against any drafts and vibrations of the optical components.

6.3.3 Measurement of photon number distribution

Here, we measured the photon number distribution of the generated entanglement and the output state of DFTs. As the measurement system in Fig. 6.3, we used 3 fiber polarizing beam splitters (FPBS), 3 fiber beam splitters (FBS), and 10 detectors. A FPBS is used for separating the each output mode to horizontal and vertical modes. A FBS is used for counting 2-photon in one mode events at the mode A arm. Using the system, the distribution was measured with postselected detection using the 4-fold coincidence counts among 2 photons in mode A (Horizontal mode), 1 photon in mode B (Vertical mode), and the heralding signal from a heralded single photon source. Then, we can obtain the 18 possible combinations of four-photon coincidence events by use of Multi channel photon counter (DPC-230, Becker & Hickl GmbH).

6.4 Details of our DFT circuit

6.4.1 Hong-Ou-Mandel interference at each beam splitters

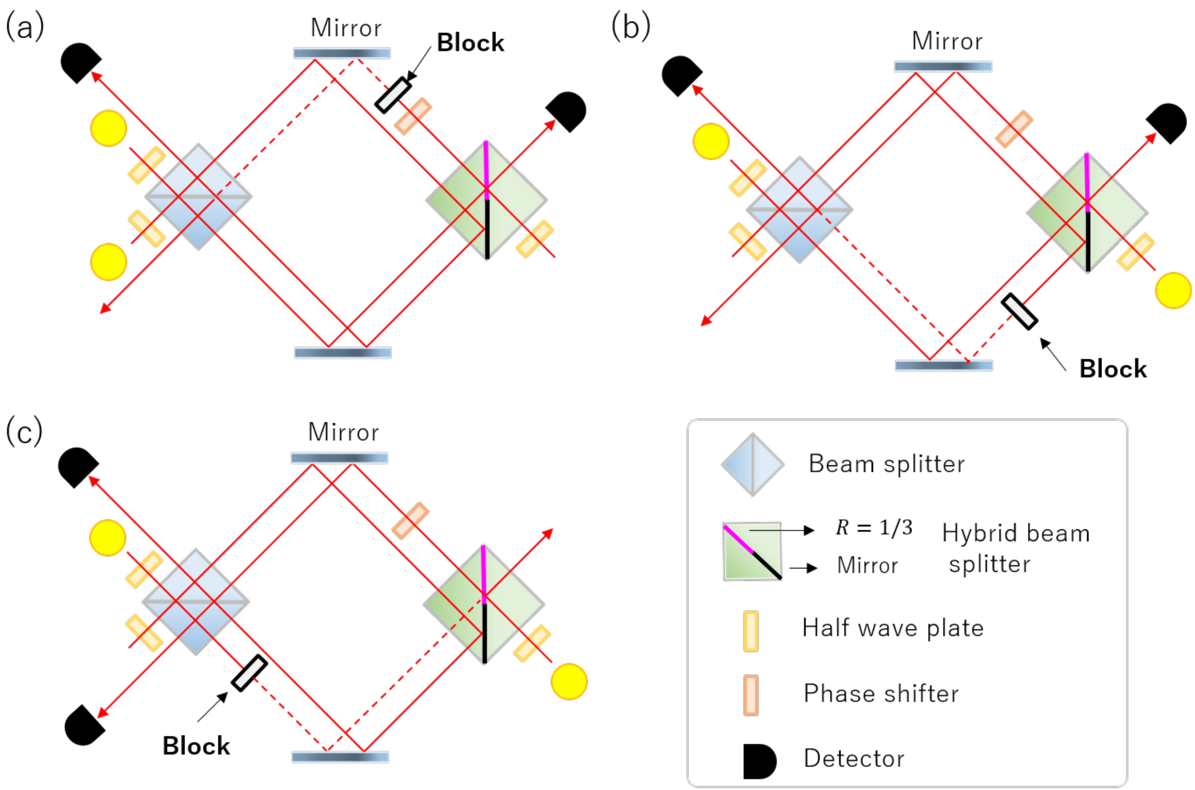

Figure 6.6: Schematic illustration of Hong-Ou-Mandel (HOM) interferometer using horizontal (H) or vertical (V) two photons at one of the beam splitters consisting of discrete mode fourier transform (DFT) circuit. Then, the unwanted optical path is blocked. In the DFT circuit, HOM interference using two photons have been occurred three times. (a)HOM interference using photon pairs from a photon pair source at the balanced BS. (b) HOM interference using two photons from independent two heralded single photon sources (HSPS) at the HBS. (c) HOM interference using two photons from independent two heralded single photon sources (HSPS) at the BS.

Figure 6.6 shows a schematic illustration of Hong-Ou-Mandel (HOM) interferometer using horizontal (H) or vertical (V) two photons at one of the beam splitters consisting of discrete mode fourier transform (DFT) circuit. At the first BS, we measured the two-fold coincidence counts using two photons from a photon pair source, as shown in Fig. 6.6(a). At the second HBS and BS, we measured the four-fold coincidence counts using

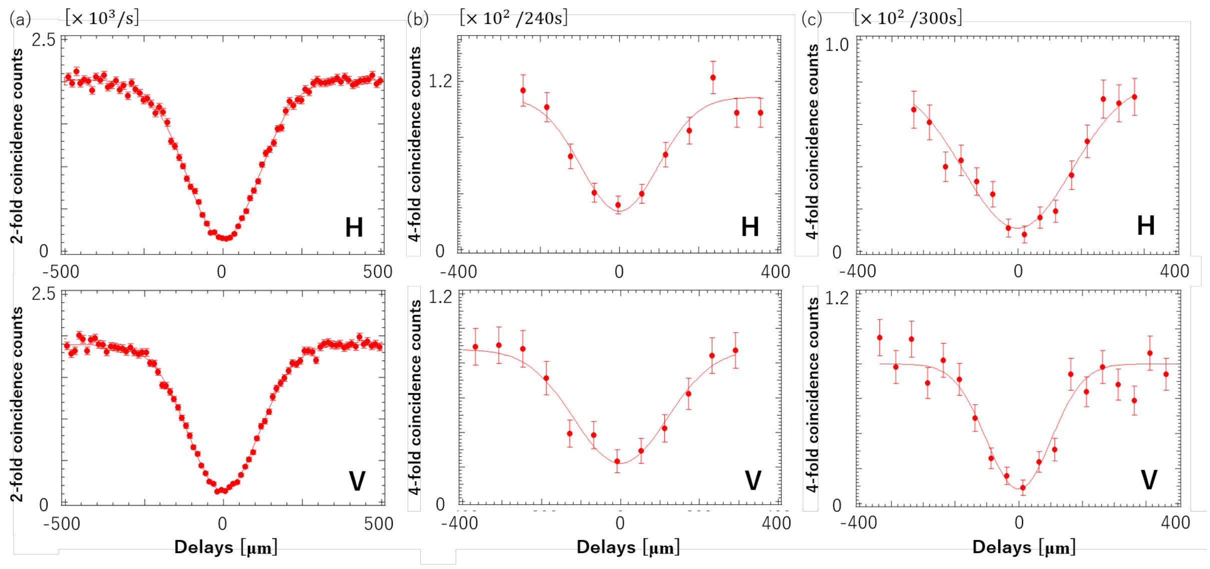

Figure 6.7: (a)Two-fold coincidence counts at the BS using photon pairs. The upper figure shows the signal using two horizontal (H) photons, and the lower figure shows the signal using two vertical (V) photons. (b)Four-fold coincidence counts at the HBS using heralded photons. (c)Four-fold coincidence counts at the BS using heralded photons.

two heralded photons from different heralded single photon sources, as shown in Figs. 6.6 (b)/(c).

Figure 6.7 shows the observed dip signal of HOM interference. Then, we evaluated these visibilities on the basis of H and V. As the results, the visibilities are 0.928 ± 0.008 and 0.930 ± 0.008 at the first BS on H and V polarization (Fig. 6.7(a)), 0.869 ± 0.095, 0.871 ± 0.066 at the second HBS on H and V polarization (Fig. 6.7(b)) (this value is compensated using the ideal visibility 0.866), 0.864 ± 0.016, 0.895 ± 0.095 at the third BS on H and V polarization (Fig. 6.7(c)). Note that they are subscribed the multi-photon generation.

6.4.2 Experimental behavior of the custom hybrid optic elements

We measured each reflectance of a BS and a HBS, assuming the same reflectance on the basis of H and V. It is found that the reflectance of the first BS is 0.52, that of the second HBS is 0.36., and that of the third BS is 0.46.

6.4.3 Stability of optical DFT circuit

To confirm the stability of our constructed optical DFT circuit, we measured the detection signals from the Mach–Zehnder interferometer (MZI) with changing the phase of one path

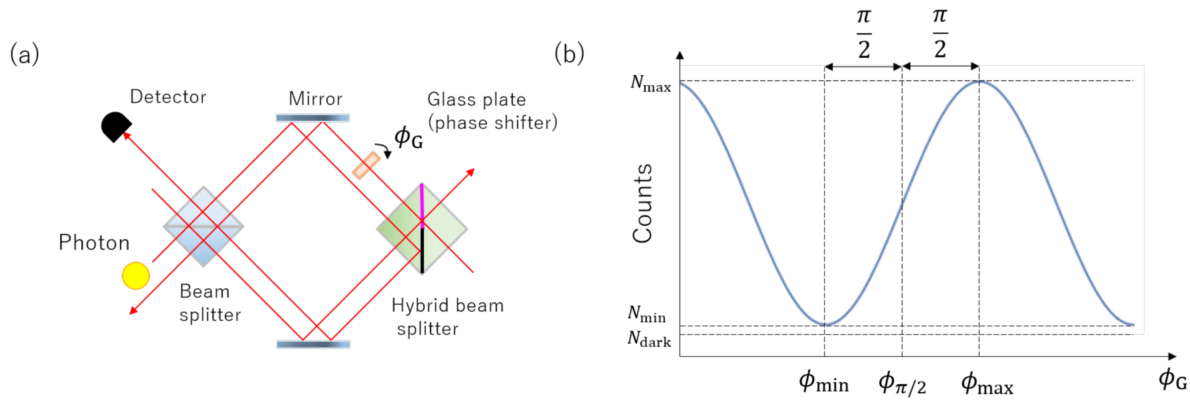

Figure 6.8: (a)Optical setup to confirm the stability of our DFT circuit. (b)Schematic detection signals of MZI.

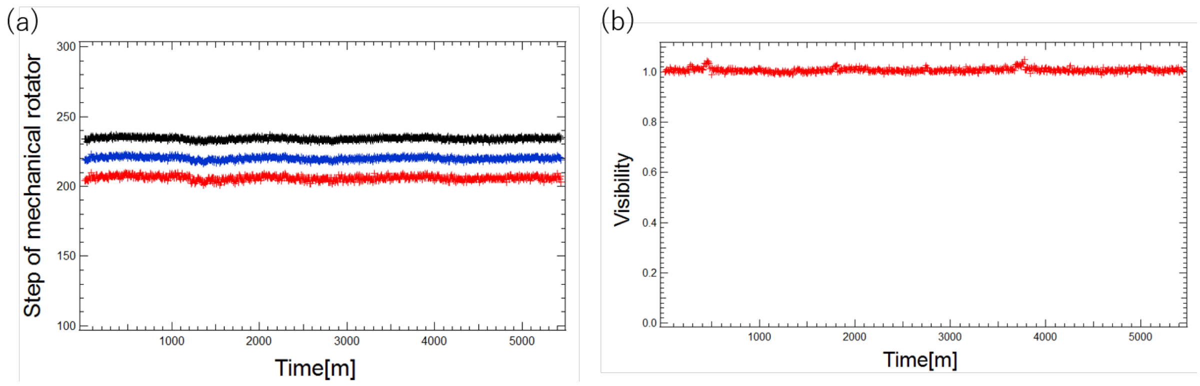

Figure 6.9: (a)The location of the step number of the mechanical moter for the glass plate. Black dots corresponds to the case of $\phi_{\max}$. Blue dots corresponds to the case of $\phi_{\pi/2}$. Red dots corresponds to the case of $\phi_{\min}$. (b)The visibility of MZI.

for a few days. Figure 6.8(a) shows the schematic setup of MZI of our DFT. Single photons at 780nm are inserted into one input mode, and the output photons are detected by a single photon detector. As changing the phase ϕ_{G} cyclically, we measure the detection fringe signals for over 5000 minutes [Fig. 6.8(b)]. Once a eight minutes, we check the visibility of MZI V_{MZI} given as,

$$V_{\mathrm{MZI}} = \frac{N_{\max} - N_{\min}}{N_{\max} + N_{\min} - 2N_{\mathrm{dark}}}, \tag{6.16}$$

where $N_{\max}, N_{\min}, N_{\mathrm{dark}}$ is the counts for the maximum, minimum, and dark counts of the detector. N_{dark} is 518 counts per a second. In our experiments, we rotate the grass plate as the phase shifter with the mechanical system. The angle of the grass plate is changed with 0.000125 degree per one step. Figure 6.9(a) shows the step number of the mechanical moter for the glass plate for the patameters $\phi_{\max}, \phi_{\min}, \phi_{\pi/2}$. Black, red, and blue dots correspond to $\phi_{\max}, \phi_{\min}, \phi_{\pi/2}$. $\phi_{\pi/2}$ is setted to the average step of $\phi_{\max}$ and

$\phi_{\min}$. This results means that the step number of the mechanical moter for $\phi_{\mathrm{G}} = \pi/2$ is stabilized for over 5000 minutes. Figure 6.9(b) shows the obtained visibility V_{MZI} for over three days. As the results, we could confirm the stability of our optical DFT circuit for over 5000 minutes. The average V_{MZI} is 1.008 ± 0.007.

6.5 Experimental results and discussion

6.5.1 Experimental verification of generating entanglement

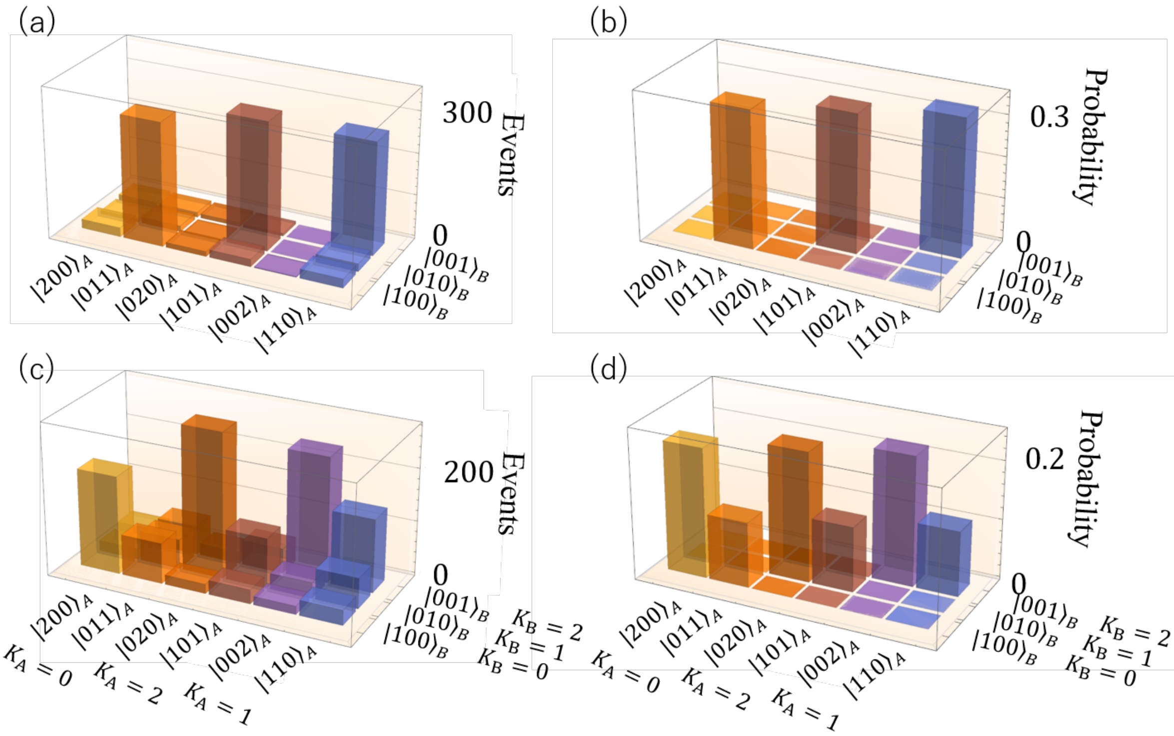

Figure 6.10: (a)Experimental photon number distribution of the entanglement $|\phi_{2,1}\rangle$. (b)Ideal photon number distribution of the entanglement $|\phi_{2,1}\rangle$. (c)Experimental photon number distribution of the output modes in a DFT. (d)Ideal photon number distribution of the output modes in a DFT.

Figure 6.10 shows (a)/(b) the experimental/ideal photon number distribution of photon number detection events for the state $|\phi_{2,1}\rangle$, and (c)/(d) the experimental/ideal photon number distribution of photon number detection events for the output state of a DFT. K_A and K_B are k-value in the system A and B. For the case before DFTs in Fig.4(a), 3 bunching effects were appeared almost equally on the basis $\{|011\rangle_A|100\rangle_B$, $|101\rangle_A|010\rangle_B$, $|110\rangle_A|001\rangle_B\}$. For the case after DFTs in Fig.6.10(c), 6 bunching effects were appeared biaselly on the basis $\{|200\rangle_A|100\rangle_B$, $|020\rangle_A|010\rangle_B$, $|002\rangle_A|001\rangle_B$ $|011\rangle_A|100\rangle_B$, $|101\rangle_A|010\rangle_B$, $|110\rangle_A|001\rangle_B\}$. Each raw data is tables 6.1-6.3. Both results in Fig.

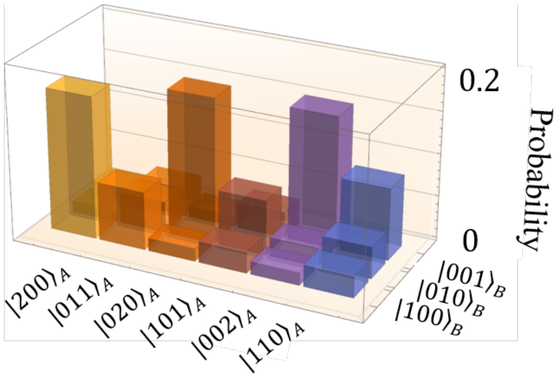

Figure 6.11: Loss-compensated photon number distribution of Fig. 6.10(c).

6.10(a)(c) agree well with theory in Fig. 6.10(b)(d). From these measurement, we calculate the fidelities $F_{\boldsymbol{n}}$ and F_K to the ideal target state $|\phi_{2,1}\rangle$ of Fig.6.10(b) and $\hat{U}_{\mathrm{F}}\hat{U}_{\mathrm{F}}|\phi_{2,1}\rangle$ of Fig.6.10(d). As a result, we found $F_{\boldsymbol{n}} = 0.843 \pm 0.011$ and $F_K = 0.712 \pm 0.014$, respectively. The sum of them is $F_{\boldsymbol{n}} + F_K = 1.555 \pm 0.018$. The value exceeds the lower bound 4/3 with 12.3 standard deviation. We hence can verify that the generated state is entangled in this way. Note that the asymmetry in the counts is due to a slight misalignment in the experiment. Errors in the fidelity are calculated by using statistical Poissonian errors in count rates. With this method, it is possible to judge whether the generated state is entangled, using two kinds of measurement, nonscalably.

Figure 6.11 shows the loss-compensated output photon number distribution. Here, we estimate the distribution before coupling into fibers (FPBSs and FBSs). As the total losses of the measurement system including fiber couplers are unbiased, the amplitude of the bunching of Fig. 6.10(c) is slightly unbiased.

Table 6.1: The experimentally observed raw data of a set of the 18 combinations of four-photon coincidence events after 3-mode DFTs.

	$\|200\rangle_A$	$\|011\rangle_A$	$\|020\rangle_A$	$\|101\rangle_A$	$\|002\rangle_A$	$\|110\rangle_A$
$\|100\rangle_B$	186	77	18	27	16	29
$\|010\rangle_B$	20	56	276	95	30	58
$\|001\rangle_B$	30	54	22	47	238	139

6.5.2 Photon number distribution for the case that k-value is not correlated

To confirm the photon number distribution and the fidelity when the k-value is not correlated, we measured the output photon number distribution when the timing of inputting

Table 6.2: The experimentally observed raw data of a set of the 18 combinations of four-photon coincidence events before 3-mode DFTs.

	$\|200\rangle_A$	$\|011\rangle_A$	$\|020\rangle_A$	$\|101\rangle_A$	$\|002\rangle_A$	$\|110\rangle_A$
$\|100\rangle_B$	22	296	12	18	2	22
$\|010\rangle_B$	8	14	2	307	0	19
$\|001\rangle_B$	14	12	10	7	0	270

Table 6.3: The experimentally observed raw data of a set of the 18 combinations of four-photon coincidence events after DFTs in the case of mode mismatch.

	$\|200\rangle_A$	$\|011\rangle_A$	$\|020\rangle_A$	$\|101\rangle_A$	$\|002\rangle_A$	$\|110\rangle_A$
$\|100\rangle_B$	20	64	22	46	20	73
$\|010\rangle_B$	38	95	40	112	48	129
$\|001\rangle_B$	42	112	48	87	38	124

three photons to the circuit is completely shifted. When the k-value is not correlated, the output state is given by,

$$\begin{aligned}\hat{U}_{\mathrm{F}}\hat{U}_{\mathrm{F}}|\phi_{2,1}\rangle = & \frac{1}{3\sqrt{3}}(|002\rangle_A|001\rangle_B + |002\rangle_A|010\rangle_B \\ & + |002\rangle_A|100\rangle_B + |020\rangle_A|001\rangle_B \\ & + |020\rangle_A|010\rangle_B + |020\rangle_A|100\rangle_B \\ & + |200\rangle_A|001\rangle_B + |200\rangle_A|010\rangle_B \\ & + |200\rangle_A|100\rangle_B) + \\ & \frac{\sqrt{2}}{3\sqrt{3}}(|110\rangle_A|001\rangle_B + |110\rangle_A|010\rangle_B \\ & + |110\rangle_A|100\rangle_B + |101\rangle_A|001\rangle_B \\ & + |101\rangle_A|010\rangle_B + |101\rangle_A|100\rangle_B \\ & + |011\rangle_A|001\rangle_B + |011\rangle_A|010\rangle_B \\ & + |011\rangle_A|100\rangle_B).\end{aligned} \tag{6.17}$$

Figure 6.12(a)/(b) shows the observed/ideal correlation of the output state for the case of three mode mismatch. We found $F_K = 0.344 \pm 0.014$. $F_K + F_{\boldsymbol{n}} = 1.187 \pm 0.018$ is smaller than the bound of 4/3 with 8.1 standard deviation. We emphasize that the entanglement emerges only as a result of photon bunching. This bunching effect can also be seen in the high probabilities for two photons in the same mode. Without this effect of multi-photon interference, the correlation of k-value disappears and the probability of finding the photons in separate modes increases to twice that of finding the photons in the same mode. Note that when losses of the measurement system are corrected, the unbiased bunching effect of Fig. 6.12 is almost changed.

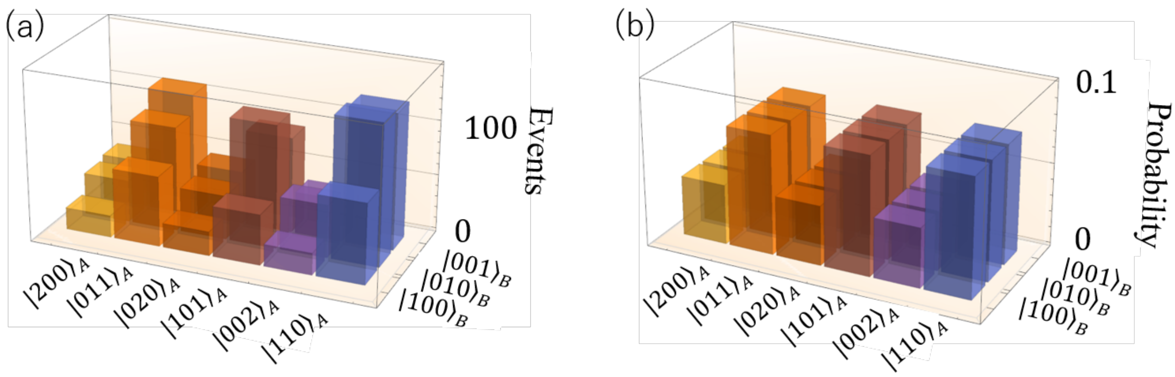

Figure 6.12: (a)Experimental photon number distribution of the output modes in a DFT for the case of three mode mismatch.(b)Ideal photon number distribution of the output modes in a DFT for the case of three mode mismatch.

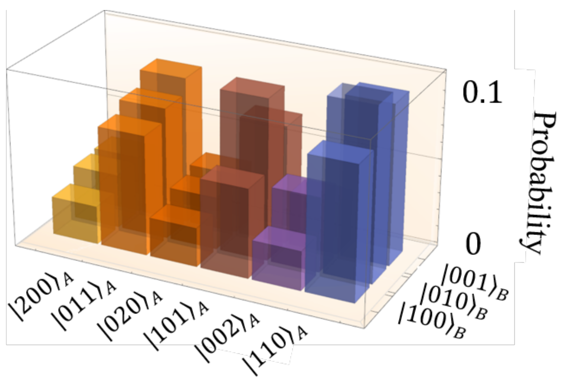

Figure 6.13: Loss-compensated photon number distribution of Fig. 6.12(a).

6.5.3 Estimated photon number distribution

Here, we estimate the effect of possible error sources on the performance of the circuit, and the reason of the non-unity fidelities $F_{\boldsymbol{n}}$ and F_K. The degradation in the observed visibility of the two photon interference is due to the spatio-temporal mode mismatch of the photons. Based on the analysis similar to ref. [163], we found the fidelities before and after the 3-mode DFT ($F_{\boldsymbol{n}}$=0.867 and F_K=0.729), where the multi-pair emission events from two photon pair sources and the actual reflectivity of the BSs are taken into account. The sum of them is 1.596. These three values are good agreement with the measured fidelities. Figure 6.14 shows the calculated output photon number distribution ,which is relatively similar to the observed distribution in Fig 6.11.

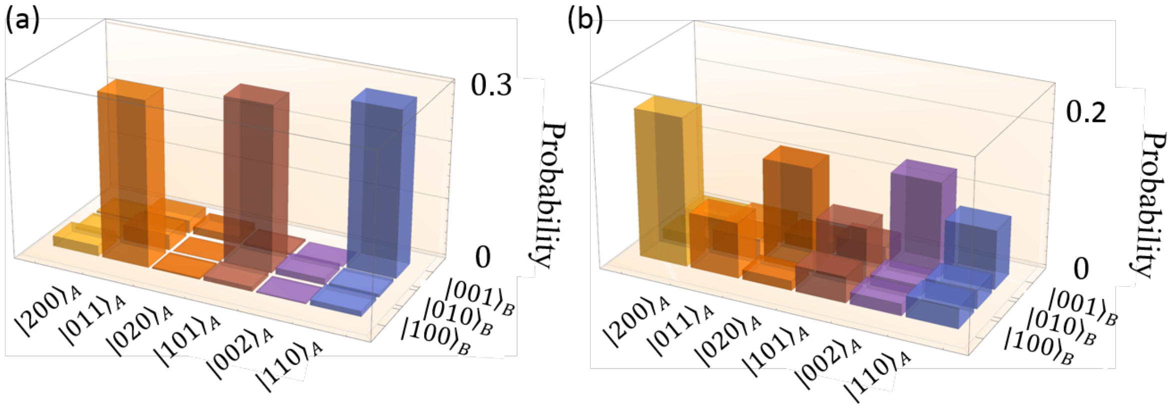

Figure 6.14: Estimated photon number distribution between two three-mode systems with and without DFTs.

6.5.4 Tighter bounds of quantum state fidelity

Here we evaluated the robustness of the state $|\phi_{2,1}\rangle$ in terms of the quantum state fidelity F_{state} to potential error sources [47].

The qunatum state fidelity gives a lower bound for both fidelities.

$$\min(F_n + F_K) = 2F_{\text{state}}. \tag{6.18}$$

If we apply the entanglement criterion of eq.6.14, the lower bound for separable states is,

$$\min(F_n + F_K) = 4/3. \tag{6.19}$$

We find that this limit is always exceeded for $F_{\text{state}} > 2/3$. A quantum state fidelity of more than 2/3 guarantees entanglement verification using the criterion of eq. 6.14. Note that the sufficiency of 2/3 fidelity for the generated entanglement is derived from the worst case for M=3.

6.6 Summary

In this section, we first demonstrated the novel method to verify the generation of bipartite entanglement between two optical multi-photon and multi-mode systems by use of mode fourier transform circuits. The experiment for verifying entanglement was realized using two super stable 3-mode DFT circuit which are made of linear optics. Here, we used two key technical approaches; a displaced-Sagnac architecture [25, 34, 159] and a hybrid polarizing beam splitter [34]. As the results, we successfully achieved the correlations of the photon number statistics between the two systems with and without DFT circuits, and the sum of the fidelities $F_{\boldsymbol{n}}+F_K = 1.555 \pm 0.018$, which exceed the lower bound 4/3 for verifying the generation of entanglement with 12.3 standard deviation. Our experimental results pave the novel way to understand the entanglement with high dimensional degree of freedom by use of a few resources for evaluating the quantum state.

Chapter 7

Summary of this study

In this thesis, the author studied about two research for quantum technologies using multi-photon interference. The first topic is the efficient generation of the multi-photon parallel state as the input state of the quantum circuit (Chapter 3–5). The second topic is the first demonstration of the novel method to evaluate high-dimensional entanglement between multi-photon and multi-mode systems (Chapter 6).

In Chapter 3, we reported the realization of a multiplexed heralded single photon sources using photon number resolving detectors, for suppressing the probability of generating more than two photons in a pulse. As below, we summarize the results.

- We developed the theory of the photon number distribution of multiplexed HSPSs using cascaded on–off detectors. According to our numerical analysis, we found that even a small number of detector cascade is very effective in reducing excess photon emission.
- We realized the multiplexed HSPS using cascaded on–off detectors. Compared to the conventional HSPS, the two-photon probability was reduced to $44.2\pm$ 0.7 %.

In Chapter 4, we reported the serial–parallel conversion for single photons with heralding signals. The convertor can route a stream of single photons from only one source into different spatial mode, and emit the multi-photon parallel state. As below, we summarize the results.

- We theoretically compared the conversion efficiency for multiple heralded photons with that for unheralded photons, and found that a serial–parallel conversion using heralding signals could be more efficient.
- With the realization of the two-photon serial–parallel converter, we confirmed the success of serial–parallel conversion for the case of two heralding signals. As a result, we achieved a conversion efficiency of 0.533 ± 0.003, which exceeds the maximum

achievable efficiency of 0.5 for serial–parallel conversion using unheralded photons, and is double the efficiency (0.25) possible using beamsplitters.

In Chapter 5, we reported the generation of multi-photon parallel state using actively spatial routing network. We proposed and demonstrated the alternative method to efficiently generate the multi-photon parallel state by use of an active $N \times N$ network. As below, we summarize the results.

- We found that the proposed method allows us to increase the efficiency to prepare N-photon parallel state exponentially when compared with the naive method of N HSPSs.
- With the realization of an active spatial 2×2 network and a fixed delay, we achieved enhancement factor of 1.59 ± 0.14, compared with the naive source using two HSPSs. We confirmed the performance of our proposed method.

In Chapter 6, we reported the evaluation of bipartite entanglement between two optical multi-mode systems using mode discrete fourier transform circuits. This method was proposed by our collaborators. The method decreases exponentially the resources for verification of generated entanglement. As below, we summarize the results.

- The verification of entanglement was realized using two super stable 3-mode DFT circuit which are made of linear optics. Then, we used two key technical approaches; a displaced-Sagnac architecture and a hybrid polarizing beam splitter.
- We successfully achieved the correlations of the photon number statistics between the two systems with and without DFT circuits, and the sum of the fidelities $F_{\boldsymbol{n}} + F_K = 1.555 \pm 0.018$, which exceed the lower bound $4/3$ for verifying the generation of entanglement with 12.3 standard deviation.

Recently, Kaneda and Kwiat reported the high efficient single photon generation via active time multiplexing on active time multiplexing [164]. Remarkably, their source emits single photons with the probability of 67% when heralding signals are generated. This is the most efficient source of the world, including single emitters. In their paper, they also mentioned the possible improvement about suppression of unwanted multi-photon generation and the way to do multi-photon interference experiment using their single photon source. These problems can be solved by our research written in Chapter 3 and Chapter 4. These recent results indicate that the active routing of single photons with heralding signals has the possibility to realize the deterministic single photon source and the deterministic source to generate the multi-photon parallel state in the near future.

Appendix A

Detail on 2×2 router

Routing the two photons from two HSPSs

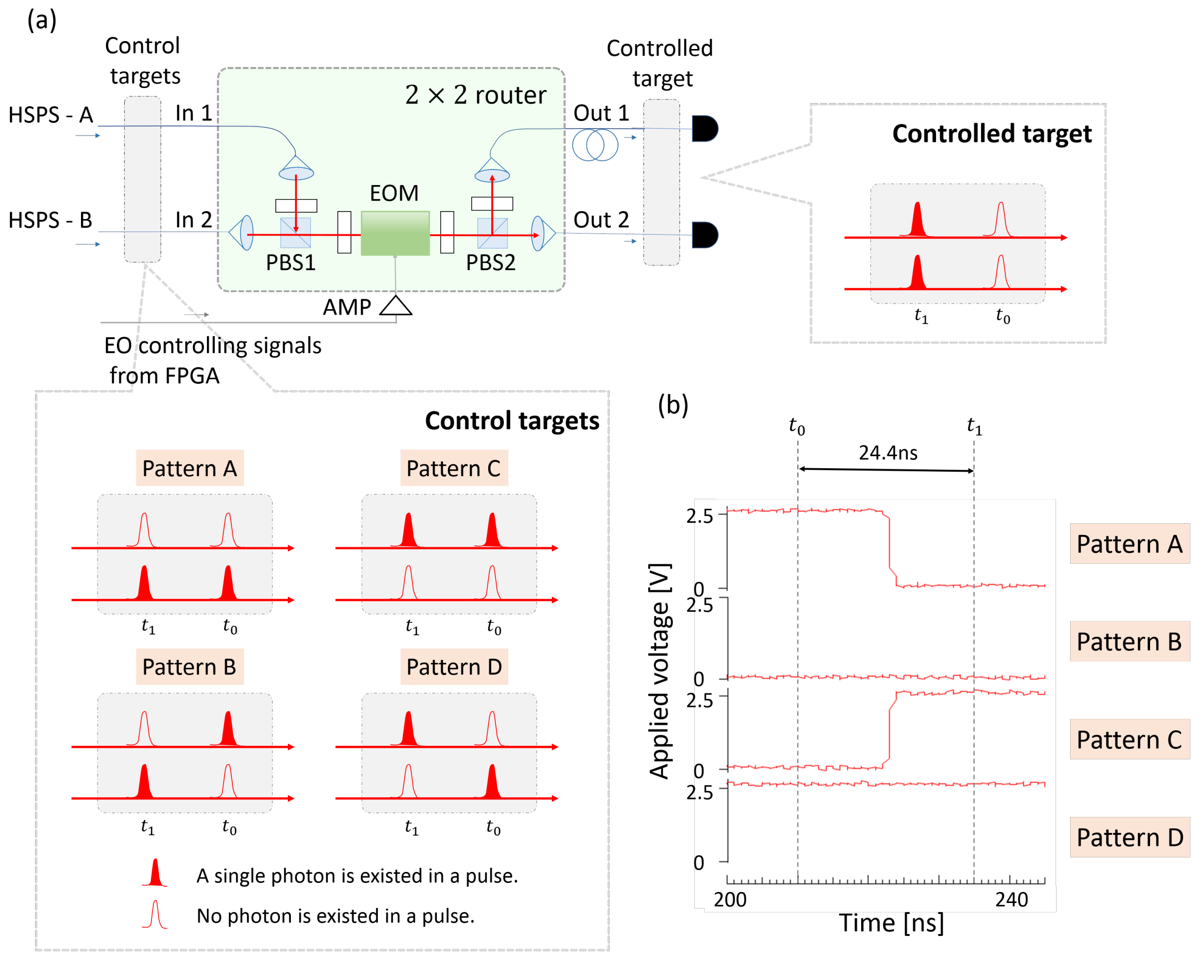

Figure A.1: (a)Schematic illustration of our 2×2 router. There are four patterns (A,B,C,D) as control targets, and one output pattern as controlled target. (b)Electrical pulse sequences from FPGA as EO controlling signals. These sequences are obtained by an oscilloscope.

In this appendix, we show the performance of our 2×2 router about the details of the control targets which are converted to two-photon parallel state and the electrical pulse sequences from the FPGA.

Figure A.1(a) shows the schematic illustration of the 2×2 router that we made. In the main text, the generated photons from a HSPS in the forward direction (HSPS-A) and a HSPS in the backforward direction (HSPS-B) are emitted into the inputs (In1, In2) of the 2×2 router. Then, there are four patterns as control targets calling Pattern A,B,C,D. Patten A is the case where HSPS-B generates a stream of two single photons. Pattern B is the case where HSPS-A generates a photon at time t_0 and HSPS-B generates a photon at time t_1. Pattern C is the case where HSPS-A generates a stream of two single photons. Pattern D is the case where HSPS-B generates a photon at time t_0 and HSPS-A generates a photon at time t_1. After the routing, all the patterns are converted to the desired two-photon parallel state, which two single photons are generated in different spatial modes (Out1, Out2) in parallel. Note that the illustration of filled pulse means the existence of a single photon in a pulse, and the illustration of unfilled pulse means the no existence of any photons in a pulse.

Figure A.1(b) shows the electrical pulse sequences from the FPGA as EO controlling signals. These sequences are obtained by an oscilloscope. The horizontal axis indicated the time from the detection signal of the first photon from a SPDC. According to the four patterns (A,B,C,D) as shown in Fig A.1(a), the number of the patterns of EO controlling signals is also four. When a HSPS-A (-B) direction generates a stream of two single photons, FPGA emits an EO controlling signal of ON (OFF) at t_0 and OFF (ON) at t_1. When a HSPS-A (-B) direction generates a photon at t_0 and a HSPS -B (-A) direction generates a photon at t_1, FPGA emits the signal of ON (OFF) at t_0 and ON (OFF) at t_1. Each EO controlling signal corresponds to the pattern of control targets.

Testing FPGA controlled switching scheme

To confirm the operation of the FPGA program which we made, we measure the two output signals; heralding signals and EO controlling signals when two TTL signals from a digital pulse generator (DG645) are input. Figure A.2 shows the schematic setup to test the FPGA controlled switching scheme. The pulse width o signal A and signal B is 40 ns, and the relative time between the rising edge of the two signals are changed. The two TTL signals, Signal A and Signal B, are converted to LVDS signals, and are connected to the FPGA system. The two output signals from the FPGA are converted to TTL signals again, and are measured by an oscilloscope (OCS). In DG645, the two input signals are copied, and input to OCS. In the main experiment, the heralding signals of HSPS-A are input into the ports (input 1 and input 2), and the signals of HSPS-B are input into the ports (input 3 and input 4).

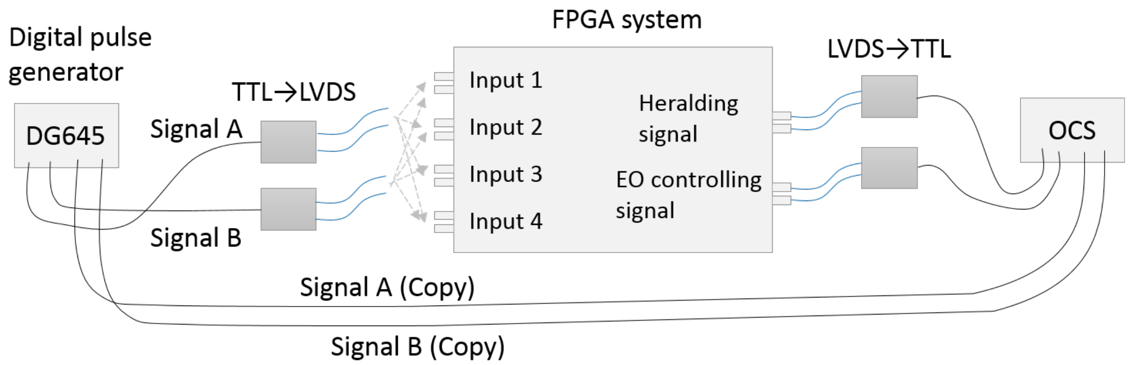

Figure A.2: Schematic setup for testing FPGA controlled switching method. The two input signals are emitted from a digital pulse generator (DG645). LVDS : Low voltage differential signaling.

Figure A.3 shows the obtained signals from OCS. The signals in Fig. A.3(a)/(b) indicates the case where signal A and signal B input to input 1 and input 2, respectively. This corresponds to Pattern A. The signals in Fig. A.3(c)/(d) indicates the case where signal A and signal B input to input 3 and input 4, respectively. This corresponds to Pattern C. The signals in Fig. A.3(e)/(f) indicates the case where signal A and signal B input to input 1 and input 3, respectively. This corresponds to Pattern B and Pattern D. Note that if the delay is applied to signal A, the heralding signals are disappeared.

Finally, I comment about the configuration of the FPGA program. First, the additional fluctuation of the rising time of $1/R_{\mathrm{FPGA}}$ is occurred, where R_{FPGA} is the sampling rate of the FPGA. This is because the FPGA read the input analog signal in the digital signal. Therefore, in the experiments of FPGA, the rising time of the active switch includes $1/R_{\mathrm{FPGA}}$. Note that reading the time of only the rising edge of the input signal is better for stable behavior than reading the time of both the rising and falling of the signal. Secondly, the sampling rate of the FPGA has to overcome the repetition rate of the pump pulsed laser with the difference of two times. Thirdly, I used basically the method of pipeline as the structure of the program which I made.

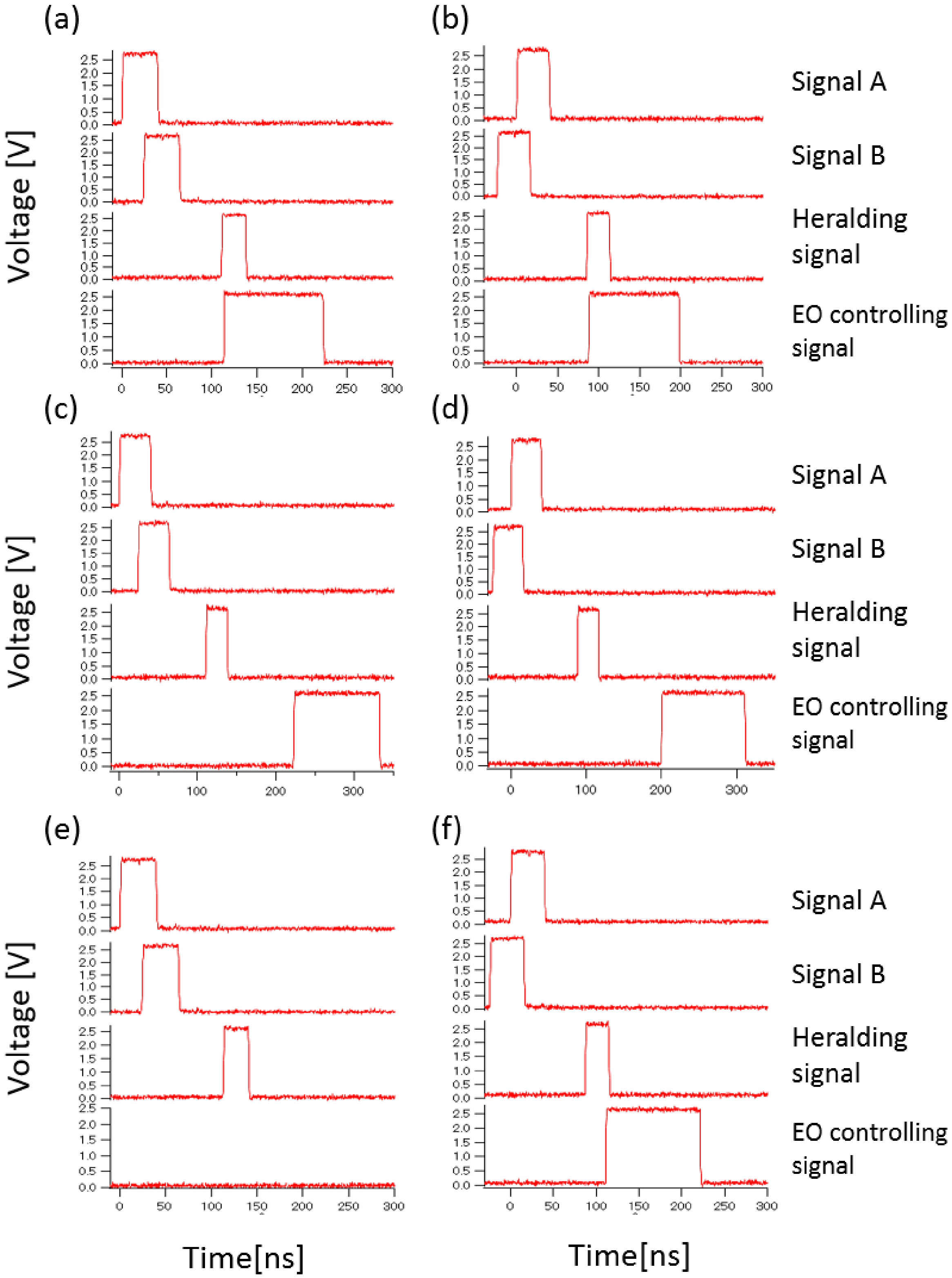

Figure A.3: Two kinds of TTL signals (A,B) from DG645, and heralding signals and EO controlling signals from the FPGA, obtained by an oscilloscope (OSC). (a)(b) The signals are obtained for input 1 and 2. (c)(d) The signals are obtained for input 3 and 4. (e)(f) The signals are obtained for input 1 and 3.

Appendix B

Theory of two photon interference between photons with the effect of group velocity dispersion

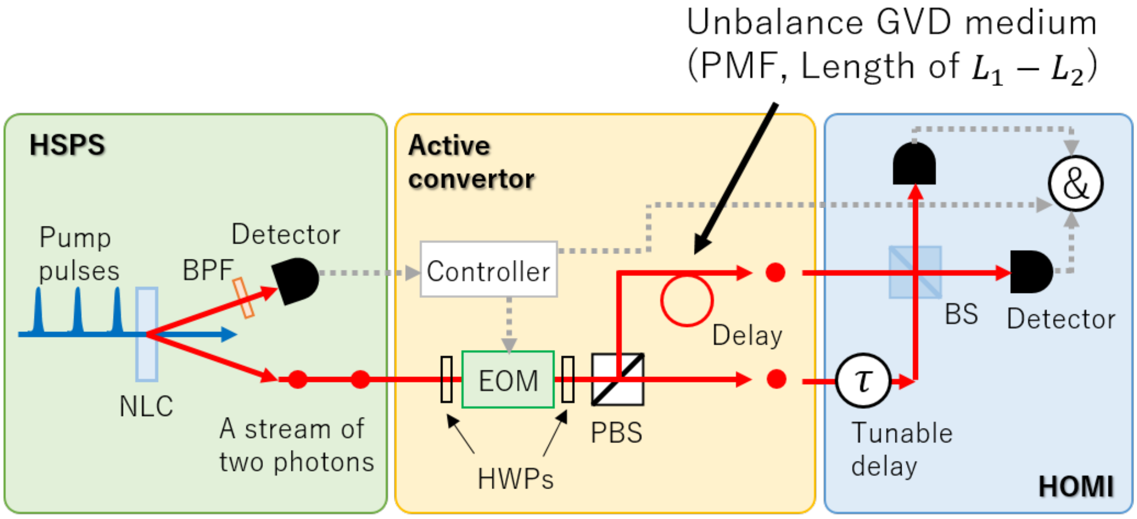

Figure B.1: Schematic illustration of two-photon interference experiment between two photons from a serial-parallel convertor. Unbalanced GVD medium causes the degradation of the visibility of HOM interference.

Here, we calculate the theory of two-photon interference between independent heralded single photons with the unbalanced effect of group velocity dispersion. This equation is developed with reference to the papers [165, 166, 167] and the advice of Prof. Okamoto. In our experiments, the multi-photon parallel state consists of multiple photons which pass through various optical path. Especially, each photon propagates into fibers with different length. In our calculation, we assume that the delay fiber has group velocity dispersion which we can not ignore. Note that we use the model of serial-parallel conversion as non-trivial case.

Figure B.1 shows the schematic setup of Hong-Ou-Mandel (HOM) interferometer by use of a two-photon serial-parallel convertor. The initial four photon state $|\Psi_4\rangle$ is the product of two independent heralded single photons,

$$|\Psi_4\rangle = \iiiint d\omega_{\mathrm{i1}} d\omega_{\mathrm{i2}} d\omega_{\mathrm{s1}} d\omega_{\mathrm{s2}} f_1(\omega_{\mathrm{i1}}, \omega_{\mathrm{s1}}) f_2(\omega_{\mathrm{i2}}, \omega_{\mathrm{s2}}) \hat{a}^\dagger_{\mathrm{i1}}(\omega_{\mathrm{i1}}) \hat{a}^\dagger_{\mathrm{i2}}(\omega_{\mathrm{i2}}) \hat{a}^\dagger_{\mathrm{s1}}(\omega_{\mathrm{s1}}) \hat{a}^\dagger_{\mathrm{s2}}(\omega_{\mathrm{s2}})|0\rangle \tag{B.1}$$

where the label of operators and joint spectral amplitude and frequency indicates the first(1) or second(2) photons of a stream of two photons at the arm of signal(s) or idler(i) photons. Here, we assume that the signal photons are used as heralding photons.

To estimate the dip of HOMI between output two photons from a serial-parallel convertor, we calculate the four fold coincidence probability with the relative time delay τ. Then, the heralding photons are labeled $\mathrm{h1}, \mathrm{h2}$ and the heralded photons are labeled $\mathrm{d1}, \mathrm{d2}$. The detection operator that four photons are detected at the times $t_{\mathrm{h1}}, t_{\mathrm{h2}}, t_{\mathrm{d1}}, t_{\mathrm{d2}}$ respectively is,

$$\hat{\Pi}_{\mathrm{4C}}(t_{\mathrm{h1}}, t_{\mathrm{h2}}, t_{\mathrm{d1}}, t_{\mathrm{d2}}) = \hat{E}^{(-)}_{\mathrm{d2}}(t_{\mathrm{d2}}) \hat{E}^{(-)}_{\mathrm{d1}}(t_{\mathrm{d1}}) \hat{E}^{(-)}_{\mathrm{h2}}(t_{\mathrm{h2}}) \hat{E}^{(-)}_{\mathrm{h1}}(t_{\mathrm{h1}})|0\rangle \langle 0|\hat{E}^{(+)}_{\mathrm{h1}}(t_{\mathrm{h1}}) \hat{E}^{(+)}_{\mathrm{h2}}(t_{\mathrm{h2}}) \hat{E}^{(+)}_{\mathrm{d1}}(t_{\mathrm{d1}}) \hat{E}^{(+)}_{\mathrm{d2}}(t_{\mathrm{d2}}) \tag{B.2}$$

The relation between the input and output positive field operators of the beam splitter(BS) can be described as,

$$\hat{E}^{(+)}_{\mathrm{h1}}(t_{\mathrm{h1}}) = \int_0^\infty d\omega_{\mathrm{h1}} F_{\mathrm{s1}}(\omega_{\mathrm{h1}}) \hat{a}_{\mathrm{s1}}(\omega_{\mathrm{h1}}) \mathrm{e}^{-i\omega_{\mathrm{h1}} t_{\mathrm{h1}}} \tag{B.3}$$

$$\hat{E}^{(+)}_{\mathrm{h2}}(t_{\mathrm{h2}}) = \int_0^\infty d\omega_{\mathrm{h2}} F_{\mathrm{s2}}(\omega_{\mathrm{h2}}) \hat{a}_{\mathrm{s2}}(\omega_{\mathrm{h2}}) \mathrm{e}^{-i\omega_{\mathrm{h2}} t_{\mathrm{h2}}} \tag{B.4}$$

$$\hat{E}^{(+)}_{\mathrm{d1}}(t_{\mathrm{d1}}) = \frac{1}{\sqrt{2}} \int_0^\infty d\omega_{\mathrm{d1}} [\sqrt{T} \theta_{\mathrm{i1}}(\omega_{\mathrm{d1}}) \hat{a}_{\mathrm{i1}}(\omega_{\mathrm{d1}}) \mathrm{e}^{-i\omega_{\mathrm{d1}}\tau} + i\sqrt{R} \theta_{\mathrm{i2}}(\omega_{\mathrm{d1}}) \hat{a}_{\mathrm{i2}}(\omega_{\mathrm{d1}})] \mathrm{e}^{-i\omega_{\mathrm{d1}} t_{\mathrm{d1}}} \tag{B.5}$$

$$\hat{E}^{(+)}_{\mathrm{d2}}(t_{\mathrm{d2}}) = \frac{1}{\sqrt{2}} \int_0^\infty d\omega_{\mathrm{d2}} [i\sqrt{R} \theta_{\mathrm{i1}}(\omega_{\mathrm{d2}}) \hat{a}_{\mathrm{i1}}(\omega_{\mathrm{d2}}) \mathrm{e}^{-i\omega_{\mathrm{d2}}\tau} + \sqrt{T} \theta_{\mathrm{i2}}(\omega_{\mathrm{d2}}) \hat{a}_{\mathrm{i2}}(\omega_{\mathrm{d2}})] \mathrm{e}^{-i\omega_{\mathrm{d2}} t_{\mathrm{d2}}} \tag{B.6}$$

$$F_{\mathrm{s}j}(\omega) = \exp\left(-\frac{(\omega - \omega_{\mathrm{s0}})^2}{\sigma_{\mathrm{s}j}}\right) \tag{B.7}$$

$$\theta_{\mathrm{i}j}(\omega) = \exp\left(-\frac{ik^{(2)}_{\mathrm{i}j} L_j (\omega - \omega_{\mathrm{i}j0})^2}{2}\right) \tag{B.8}$$

where $F_{\mathrm{s}j}(\omega) (j = 1, 2)$ is the function of a band pass filter (BPF) with the bandwidth of $\sigma_{\mathrm{s}j}$ at the signal (heralding) arm, and $\theta_{\mathrm{i}j}(\omega) (j = 1, 2)$ is the term of group velocity dispersion of the first(1) or second(2) photons. $L_j (j = 1, 2)$ is the length of the medium with the dispersion. The four-fold coincidence probability $P_{4C}(t_{h1}, t_{h2}, t_{d1}, t_{d2})$ can be found as,

$$P_{4C}(t_{h1}, t_{h2}, t_{d1}, t_{d2}) = \langle \Psi_4 | \hat{\Pi}_{4C} | \Psi_4 \rangle \tag{B.9}$$

where the detection speed is assumed to be slower than the pulse width. From Exp.2.20, the spectra of high pure heralded photons with negligible group velocity mismatch is Gaussian frequency distribution,

$$f_j(\omega) = \frac{1}{\sqrt{2\pi}\sigma_j} \exp\left(\frac{-(\omega - \omega_{j0})^2}{2\sigma_j^2} \right), (j = 1, 2). \tag{B.10}$$

where $\omega_{j0} (j = 1, 2)$ is the mean frequency of heralded photons (1 or 2), and σ_j is the bandwidth of the spectra. From the above equations, we can calculate the four fold coincidence probability as varying the time delay τ,

$$\begin{aligned} P_{4C}(\tau) = \iint & d\omega_{d1} d\omega_{d2} \\ & \left| T\xi_1(\omega_{d1})\xi_2(\omega_{d2}) - R\xi_1(\omega_{d2})\xi_2(\omega_{d1}) \mathrm{e}^{-i(\omega_{d2}-\omega_{d1})\tau} \right|^2 \end{aligned} \tag{B.11}$$

$$\xi_j(\omega) = f_j(\omega)\theta_{ij}(\omega), (j = 1, 2). \tag{B.12}$$

If the beamsplitter is balanced ($T = R = 1/2$) and the spectra of two heralded photons are the same ($f(\omega) = f_1(\omega) = f_2(\omega)$ and $\omega_0 = \omega_{10} = \omega_{20}$), $P_{4C}(\tau)$ is given as,

$$\begin{aligned} P_{4C}(\tau) &= \frac{1}{2} \iint |g_1(\omega_1) g_2(\omega_2)|^2 d\omega_1 d\omega_2 - \frac{1}{2} \left| \int \xi_1(\omega)\xi_2^*(\omega) \mathrm{e}^{i\omega\tau} d\omega \right|^2 \\ &= \frac{1}{4} - \frac{1}{2} \left| \int |g(\omega)|^2 \mathrm{e}^{i(\omega\tau + \Gamma_{12}(\omega-\omega_c)^2)} d\omega \right|^2 \end{aligned} \tag{B.13}$$

where $\Gamma_{12} = k_{i1}^{(2)} L_1/2 - k_{i2}^{(2)} L_2/2$, and ω_c is the central frequency of heralded photons. The function of four-fold coincidence counts is,

$$P_{4C}(\tau) = \frac{1}{4} - \frac{1}{4\sqrt{1 + \sigma^4\Gamma^2}} \exp\left[\frac{-\sigma^2(\tau + 2\Gamma\omega_0)^2 + 4\sigma^2\Gamma\omega_0(\tau + \Gamma\omega_0)}{4(1 + \sigma^4\Gamma^2)} \right] \tag{B.14}$$

where ω_C is assumed to be ω_0.

References

[1] T. D. Ladd, F. Jelezko, R. Laflamme, Y. Nakamura, C. Monroe, J. L. O'Brien, Quantum computers, Nature 464 (7285) (2010) 45–53.

[2] C. L. Degen, F. Reinhard, P. Cappellaro, Quantum sensing, Reviews of Modern Physics 89 (3) (2017) 35002.

[3] N. Gisin, G. Ribordy, W. Tittel, H. Zbinden, Quantum cryptography, Reviews of Modern Physics 74 (1) (2002) 145–195.

[4] I. Buluta, F. Nori, Quantum Simulators, Science 326 (5949) (2009) 108 LP – 111.

[5] I. M. Georgescu, S. Ashhab, F. Nori, Quantum simulation, Reviews of Modern Physics 86 (1) (2014) 153–185.

[6] V. Giovannetti, S. Lloyd, L. Maccone, Advances in quantum metrology, Nature Photonics 5 (4) (2011) 222–229.

[7] P.-A. Moreau, E. Toninelli, T. Gregory, M. J. Padgett, Imaging with quantum states of light, Nature Reviews Physics 1 (6) (2019) 367–380.

[8] P. W. Shor, Algorithms for quantum computation: discrete logarithms and factoring, in: Proceedings 35th Annual Symposium on Foundations of Computer Science, 1994, pp. 124–134.

[9] Quantum search algorithms, in: I. L. Chuang, M. A. Nielsen (Eds.), Quantum Computation and Quantum Information: 10th Anniversary Edition, Cambridge University Press, Cambridge, 2010, pp. 248–276.

[10] B. P. Lanyon, J. D. Whitfield, G. G. Gillett, M. E. Goggin, M. P. Almeida, I. Kassal, J. D. Biamonte, M. Mohseni, B. J. Powell, M. Barbieri, A. Aspuru-Guzik, A. G. White, Towards quantum chemistry on a quantum computer, Nature Chemistry 2 (2) (2010) 106–111.

[11] W. S. Bakr, J. I. Gillen, A. Peng, S. Fölling, M. Greiner, A quantum gas microscope for detecting single atoms in a Hubbard-regime optical lattice, Nature 462 (7269) (2009) 74–77.

[12] C. Weitenberg, M. Endres, J. F. Sherson, M. Cheneau, P. Schauß, T. Fukuhara, I. Bloch, S. Kuhr, Single-spin addressing in an atomic Mott insulator, Nature 471 (7338) (2011) 319–324.

[13] A. Friedenauer, H. Schmitz, J. T. Glueckert, D. Porras, T. Schaetz, Simulating a quantum magnet with trappedions, Nature Physics 4 (10) (2008) 757–761.

[14] R. Islam, E. E. Edwards, K. Kim, S. Korenblit, C. Noh, H. Carmichael, G. D. Lin, L. M. Duan, C. C. Joseph Wang, J. K. Freericks, C. Monroe, Onset of a quantum phase transition with a trapped ion quantum simulator, Nature Communications 2 (1) (2011) 376–377.

[15] X. Peng, J. Zhang, J. Du, D. Suter, Quantum simulation of a system with competing two- and three-body interactions., Physical review letters 103 (14) (2009) 140501.

[16] M. Neeley, M. Ansmann, R. C. Bialczak, M. Hofheinz, E. Lucero, A. D. O'Connell, D. Sank, H. Wang, J. Wenner, A. N. Cleland, M. R. Geller, J. M. Martinis, A. A. Houck, H. E. Türeci, J. Koch, X. Peng, J. Zhang, J. Du, D. Suter, N. Xu, X. Peng, P. Wang, S. Wu, D. Lu, R. Islam, E. E. Edwards, K. Kim, S. Korenblit, C. Noh, H. Carmichael, G. D. Lin, L. M. Duan, C. C. Joseph Wang, J. K. Freericks, C. Monroe, A. Friedenauer, H. Schmitz, J. T. Glueckert, D. Porras, T. Schaetz, J. Grembecka, S. He, A. Shi, T. Purohit, A. G. Muntean, R. J. Sorenson, H. D. Showalter, M. J. Murai, A. M. Belcher, T. Hartley, J. L. Hess, T. Cierpicki, On-chip quantum simulation with superconducting circuits, Nature Physics 8 (3) (2009) 292–299.

[17] J. L. O'Brien, A. Furusawa, J. Vu**v**ckolić, Photonic quantum technologies, Nature Photonics 3 (12) (2009) 687–695.

[18] V. Scarani, H. Bechmann-Pasquinucci, N. J. Cerf, M. Du**v**sek, N. Lütkenhaus, M. Peev, The security of practical quantum key distribution, Reviews of Modern Physics 81 (3) (2009) 1301–1350.

[19] Y. Liu, T.-Y. Chen, L.-J. Wang, H. Liang, G.-L. Shentu, J. Wang, K. Cui, H.-L. Yin, N.-L. Liu, L. Li, X. Ma, J. S. Pelc, M. M. Fejer, C.-Z. Peng, Q. Zhang, J.-W. Pan, Experimental Measurement-Device-Independent Quantum Key Distribution, Physical Review Letters 111 (13) (2013) 130502.

[20] H.-K. Lo, M. Curty, K. Tamaki, Secure quantum key distribution, Nature Photonics 8 (2014) 595.

[21] K. Azuma, K. Tamaki, W. J. Munro, All-photonic intercity quantum key distribution, Nature Communications 6 (2015) 10171.

[22] S.-K. Liao, W.-Q. Cai, W.-Y. Liu, L. Zhang, Y. Li, J.-G. Ren, J. Yin, Q. Shen, Y. Cao, Z.-P. Li, F.-Z. Li, X.-W. Chen, L.-H. Sun, J.-J. Jia, J.-C. Wu, X.-J. Jiang, J.-F. Wang, Y.-M. Huang, Q. Wang, Y.-L. Zhou, L. Deng, T. Xi, L. Ma, T. Hu, Q. Zhang, Y.-A. Chen, N.-L. Liu, X.-B. Wang, Z.-C. Zhu, C.-Y. Lu, R. Shu, C.-Z. Peng, J.-Y. Wang, J.-W. Pan, Satellite-to-ground quantum key distribution, Nature 549 (2017) 43.

[23] E. Knill, R. Laflamme, G. J. Milburn, A scheme for efficient quantum computation with linear optics, Nature 409 (6816) (2001) 46–52.

[24] S.-H. Tan, P. P. Rohde, The resurgence of the linear optics quantum interferometer — recent advances & applications, Reviews in Physics 4 (2019) 100030.

[25] T. Nagata, R. Okamoto, J. L. O'Brien, K. Sasaki, S. Takeuchi, Beating the Standard Quantum Limit with Four-Entangled Photons, Science 316 (5825) (2007) 726 LP – 729.

[26] T. Ono, R. Okamoto, S. Takeuchi, An entanglement-enhanced microscope, Nature Communications 4 (2013) 2426.

[27] J. C. F. Matthews, X.-Q. Zhou, H. Cable, P. J. Shadbolt, D. J. Saunders, G. A. Durkin, G. J. Pryde, J. L. O'Brien, Towards practical quantum metrology with photon counting, Npj Quantum Information 2 (2016) 16023.

[28] K. E. Dorfman, F. Schlawin, S. Mukamel, Nonlinear optical signals and spectroscopy with quantum light, Reviews of Modern Physics 88 (4) (2016) 45008.

[29] Z.-E. Su, Y. Li, P. P. Rohde, H.-L. Huang, X.-L. Wang, L. Li, N.-L. Liu, J. P. Dowling, C.-Y. Lu, J.-W. Pan, Multiphoton Interference in Quantum Fourier Transform Circuits and Applications to Quantum Metrology, Physical Review Letters 119 (8) (2017) 80502.

[30] N. Gisin, R. Thew, Quantum communication, Nature Photonics 1 (2007) 165.

[31] H. J. Kimble, The quantum internet, Nature 453 (7198) (2008) 1023–1030.

[32] S. Wengerowsky, S. K. Joshi, F. Steinlechner, H. Hübel, R. Ursin, An entanglement-based wavelength-multiplexed quantum communication network, Nature 564 (7735) (2018) 225–228.

[33] R. Okamoto, J. L. O'Brien, H. F. Hofmann, S. Takeuchi, Realization of a Knill-Laflamme-Milburn controlled-NOT photonic quantum circuit combining effective optical nonlinearities, Proceedings of the National Academy of Sciences 108 (25) (2011) 10067 LP – 10071.

[34] T. Ono, R. Okamoto, M. Tanida, H. F. Hofmann, S. Takeuchi, Implementation of a quantum controlled-SWAP gate with photonic circuits, Scientific Reports 7 (2017) 45353.

[35] M. Krenn, M. Huber, R. Fickler, R. Lapkiewicz, S. Ramelow, A. Zeilinger, Generation and confirmation of a (100 × 100)-dimensional entangled quantum system, Proceedings of the National Academy of Sciences 111 (17) (2014) 6243 LP – 6247.

[36] S. Aaronson, A. Arkhipov, The Computational Complexity of Linear Optics, Vol. 9, 2010.

[37] A. Neville, C. Sparrow, R. Clifford, E. Johnston, P. M. Birchall, A. Montanaro, A. Laing, Classical boson sampling algorithms with superior performance to near-term experiments, Nature Physics 13 (2017) 1153.

[38] J. Carolan, C. Harrold, C. Sparrow, E. Martín-López, N. J. Russell, J. W. Silverstone, P. J. Shadbolt, N. Matsuda, M. Oguma, M. Itoh, G. D. Marshall, M. G. Thompson, J. C. F. Matthews, T. Hashimoto, J. L. O'Brien, A. Laing, Universal linear optics, Science 349 (6249) (2015) 711 LP – 716.

[39] F. Flamini, L. Magrini, A. S. Rab, N. Spagnolo, V. D'Ambrosio, P. Mataloni, F. Sciarrino, T. Zandrini, A. Crespi, R. Ramponi, R. Osellame, Thermally reconfigurable quantum photonic circuits at telecom wavelength by femtosecond laser micromachining, Light: Science &Amp; Applications 4 (2015) e354.

[40] T. Rudolph, Why I am optimistic about the silicon-photonic route to quantum computing, APL Photonics 2 (3) (2017) 30901.

[41] I. Holzman, Y. Ivry, Superconducting Nanowires for Single-Photon Detection: Progress, Challenges, and Opportunities, Advanced Quantum Technologies 2 (3-4) (2019) 1800058.

[42] D. Bouwmeester, J.-W. Pan, K. Mattle, M. Eibl, H. Weinfurter, A. Zeilinger, Experimental quantum teleportation, Nature 390 (6660) (1997) 575–579.

[43] S. K. Özdemir, A. Miranowicz, M. Koashi, N. Imoto, Quantum-scissors device for optical state truncation: A proposal for practical realization, Physical Review A 64 (6) (2001) 63818.

[44] A. Peruzzo, P. Shadbolt, N. Brunner, S. Popescu, J. L. O'Brien, A Quantum Delayed-Choice Experiment, Science 338 (6107) (2012) 634 LP – 637.

[45] B. G. Christensen, K. T. McCusker, J. B. Altepeter, B. Calkins, T. Gerrits, A. E. Lita, A. Miller, L. K. Shalm, Y. Zhang, S. W. Nam, N. Brunner, C. C. W. Lim, N. Gisin, P. G. Kwiat, Detection-Loophole-Free Test of Quantum Nonlocality, and Applications, Physical Review Letters 111 (13) (2013) 130406.

[46] J.-S. Tang, Y.-T. Wang, S. Yu, D.-Y. He, J.-S. Xu, B.-H. Liu, G. Chen, Y.-N. Sun, K. Sun, Y.-J. Han, C.-F. Li, G.-C. Guo, Experimental investigation of the no-signalling principle in parity-time symmetric theory using an open quantum system, Nature Photonics 10 (2016) 642.

[47] J. Y. Wu, H. F. Hofmann, Evaluation of bipartite entanglement between two optical multi-mode systems using mode translation symmetry, New Journal of Physics 19 (10).

[48] C. Kurtsiefer, S. Mayer, P. Zarda, H. Weinfurter, Stable solid-state source of single photons, Physical Review Letters 85 (2) (2000) 290–293.

[49] H. Langenberg, Climate & water, Nature 419 (6903) (2002) 187.

[50] M. Pelton, C. Santori, J. Vucković, B. Zhang, G. S. Solomon, J. Plant, Y. Yamamoto, Efficient Source of Single Photons: A Single Quantum Dot in a Micropost Microcavity, Physical Review Letters 89 (23) (2002) 233602.

[51] H. G. Barros, A. Stute, T. E. Northup, C. Russo, P. O. Schmidt, R. Blatt, Deterministic single-photon source from a single ion, New Journal of Physics 11 (10) (2009) 103004.

[52] W. E. Moerner, Single-photon sources based on single molecules in solids, New Journal of Physics 6 (2004) 88.

[53] K. H. Madsen, S. Ates, J. Liu, A. Javadi, S. M. Albrecht, I. Yeo, S. Stobbe, P. Lodahl, Efficient out-coupling of high-purity single photons from a coherent quantum dot in a photonic-crystal cavity, Physical Review B 90 (15) (2014) 155303.

[54] O. Gazzano, S. Michaelis de Vasconcellos, C. Arnold, A. Nowak, E. Galopin, I. Sagnes, L. Lanco, A. Lemaître, P. Senellart, Bright solid-state sources of indistinguishable single photons, Nature Communications 4 (2013) 1425.

[55] H. Wang, Y.-M. He, T.-H. Chung, H. Hu, Y. Yu, S. Chen, X. Ding, M.-C. Chen, J. Qin, X. Yang, R.-Z. Liu, Z.-C. Duan, J.-P. Li, S. Gerhardt, K. Winkler, J. Jurkat, L.-J. Wang, N. Gregersen, Y.-H. Huo, Q. Dai, S. Yu, S. Höfling, C.-Y. Lu, J.-W. Pan, Towards optimal single-photon sources from polarized microcavities, Nature Photonics 13 (11) (2019) 770–775.

[56] A. W. Schell, H. Takashima, S. Kamioka, Y. Oe, M. Fujiwara, O. Benson, S. Takeuchi, Highly Efficient Coupling of Nanolight Emitters to a Ultra-Wide Tunable Nanofibre Cavity, Scientific Reports 5 (2015) 9619.

[57] N. Somaschi, V. Giesz, L. De Santis, J. C. Loredo, M. P. Almeida, G. Hornecker, S. L. Portalupi, T. Grange, C. Antón, J. Demory, C. Gómez, I. Sagnes, N. D. Lanzillotti-Kimura, A. Lemaítre, A. Auffeves, A. G. White, L. Lanco, P. Senellart, Near-optimal single-photon sources in the solid state, Nature Photonics 10 (5) (2016) 340–345.

[58] M. Fujiwara, K. Yoshida, T. Noda, H. Takashima, A. W. Schell, N. Mizuochi, S. Takeuchi, Manipulation of single nanodiamonds to ultrathin fiber-taper nanofibers and control of NV-spin states toward fiber-integratedλ-systems, Nanotechnology 27 (45) (2016) 455202.

[59] S. Saijo, Y. Matsuzaki, S. Saito, T. Yamaguchi, I. Hanano, H. Watanabe, N. Mizuochi, J. Ishi-Hayase, AC magnetic field sensing using continuous-wave optically detected magnetic resonance of nitrogen-vacancy centers in diamond, Applied Physics Letters 113 (8) (2018) 82405.

[60] T. Müller, C. Hepp, B. Pingault, E. Neu, S. Gsell, M. Schreck, H. Sternschulte, D. Steinmüller-Nethl, C. Becher, M. Atatüre, Optical signatures of silicon-vacancy spins in diamond, Nature Communications 5 (1) (2014) 3328.

[61] A. Soujaeff, T. Nishioka, T. Hasegawa, S. Takeuchi, T. Tsurumaru, K. Sasaki, M. Matsui, Quantum key distribution at 1550 nm using a pulse heralded single photon source, Optics Express 15 (2) (2007) 726.

[62] M. D. Eisaman, J. Fan, A. Migdall, S. V. Polyakov, Invited Review Article: Single-photon sources and detectors, Review of Scientific Instruments 82 (7) (2011) 071101.

[63] J. E. Sharping, K. F. Lee, M. A. Foster, A. C. Turner, B. S. Schmidt, M. Lipson, A. L. Gaeta, P. Kumar, Generation of correlated photons in nanoscale silicon waveguides, Optics Express 14 (25) (2006) 12388.

[64] S. Clemmen, K. P. Huy, W. Bogaerts, R. G. Baets, P. Emplit, S. Massar, Continuous wave photon pair generation in silicon-on-insulator waveguides and ring resonators, Optics Express 17 (19) (2009) 16558.

[65] F. Kaneda, K. Garay-Palmett, A. B. U'Ren, P. G. Kwiat, Heralded single-photon source utilizing highly nondegenerate, spectrally factorable spontaneous parametric downconversion 24 (10) (2016) 10733–10747.

[66] C. Greganti, P. Schiansky, I. A. Calafell, L. M. Procopio, L. A. Rozema, P. Walther, Tuning single-photon sources for telecom multi-photon experiments, Optics Express 26 (3) (2018) 3286–3302.

[67] A. Tanaka, R. Okamoto, H. H. Lim, S. Subashchandran, M. Okano, L. Zhang, L. Kang, J. Chen, P. Wu, T. Hirohata, S. Kurimura, S. Takeuchi, Noncollinear parametric fluorescence by chirped quasi-phase matching for monocycle temporal entanglement, Optics Express 20 (23) (2012) 25228.

[68] M. Tanida, R. Okamoto, S. Takeuchi, Highly indistinguishable heralded single-photon sources using parametric down conversion, Optics Express 20 (14) (2012) 15275.

[69] T. Jennewein, R. Ursin, M. Aspelmeyer, A. Zeilinger, Performing high-quality multi-photon experiments with parametric down-conversion, Journal of Physics B: Atomic, Molecular and Optical Physics 42 (11) (2009) 114008.

[70] J. W. Silverstone, D. Bonneau, K. Ohira, N. Suzuki, H. Yoshida, N. Iizuka, M. Ezaki, C. M. Natarajan, M. G. Tanner, R. H. Hadfield, V. Zwiller, G. D. Marshall, J. G. Rarity, J. L. O'Brien, M. G. Thompson, On-chip quantum interference between silicon photon-pair sources, Nature Photonics 8 (2013) 104.

[71] Quantum information in photons and atoms, in: B. W. Lovett, P. Kok (Eds.), Introduction to Optical Quantum Information Processing, Cambridge University Press, Cambridge, 2010, pp. 111–112.

[72] Quantum computation, in: I. L. Chuang, M. A. Nielsen (Eds.), Quantum Computation and Quantum Information: 10th Anniversary Edition, Cambridge University Press, Cambridge, 2010.

[73] R. Loudon, The quantum theory of light, Oxford University Press, 2000.

[74] A. Ling, A. Lamas-Linares, C. Kurtsiefer, Absolute rates of spontaneous parametric down conversion into a single transverse Gaussian mode, Conference on Quantum Electronics and Laser Science (QELS) - Technical Digest Series (2008) 1–7.

[75] S. Y. Baek, Y. H. Kim, Spectral properties of entangled photons generated via type-I frequency-nondegenerate spontaneous parametric down-conversion, Physical Review A - Atomic, Molecular, and Optical Physics 80 (3) (2009) 1–7.

[76] P. R. Tapster, J. G. Rarity, Photon statistics of pulsed parametric light, Journal of Modern Optics 45 (3) (1998) 595–604.

[77] S. Castelletto, I. P. Degiovanni, A. Migdall, M. Ware, On the measurement of two-photon single-mode coupling efficiency in parametric down-conversion photon sources, New Journal of Physics 6 (2004) 87.

[78] P. Kolenderski, W. Wasilewski, K. Banaszek, Modeling and optimization of photon pair sources based on spontaneous parametric down-conversion, Physical Review A 80 (1) (2009) 13811.

[79] L. E. Vicent, A. B. U'Ren, R. Rangarajan, C. I. Osorio, J. P. Torres, L. Zhang, I. A. Walmsley, Design of bright, fiber-coupled and fully factorable photon pair sources, New Journal of Physics 12 (9) (2010) 93027.

[80] B. Septriani, J. A. Grieve, K. Durak, A. Ling, Thick-crystal regime in photon pair sources, Optica 3 (3) (2016) 347–350.

[81] A. Anwar, C. P, S. G. Reddy, N. Lal, R. P. Singh, Selecting the pre-detection characteristics for fiber coupling of parametric down-converted biphoton modes, Optics Communications 382 (2017) 219–224.

[82] C. K. Hong, Z. Y. Ou, L. Mandel, Measurement of subpicosecond time intervals between two photons by interference, Physical Review Letters 59 (18) (1987) 2044–2046.

[83] M. Tillmann, S.-H. Tan, S. E. Stoeckl, B. C. Sanders, H. de Guise, R. Heilmann, S. Nolte, A. Szameit, P. Walther, Generalized Multiphoton Quantum Interference, Physical Review X 5 (4) (2015) 41015.

[84] M. Reck, A. Zeilinger, H. J. Bernstein, P. Bertani, Experimental realization of any discrete unitary operator, Physical Review Letters 73 (1) (1994) 58–61.

[85] S. Rahimi-Keshari, M. A. Broome, R. Fickler, A. Fedrizzi, T. C. Ralph, A. G. White, Direct characterization of linear-optical networks, Optics Express 21 (11) (2013) 13450–13458.

[86] W. R. Clements, P. C. Humphreys, B. J. Metcalf, W. S. Kolthammer, I. A. Walmsley, Optimal design for universal multiport interferometers, Optica 3 (12) (2016) 1460–1465.

[87] M. Tillmann, C. Schmidt, P. Walther, On unitary reconstruction of linear optical networks, Journal of Optics 18 (11) (2016) 114002.

[88] J.-W. Pan, Z.-B. Chen, C.-Y. Lu, H. Weinfurter, A. Zeilinger, M. Żukowski, Multiphoton entanglement and interferometry, Reviews of Modern Physics 84 (2) (2012) 777–838.

[89] A. ***v***Cernoch, J. Soubusta, L. Bart***v***sková, M. Du***v***sek, J. Fiurá***v***sek, Experimental Realization of Linear-Optical Partial swap Gates, Physical Review Letters 100 (18) (2008) 180501.

[90] A. Politi, J. C. F. Matthews, J. L. O'Brien, Shor's Quantum Factoring Algorithm on a Photonic Chip, Science 325 (5945) (2009) 1221 LP – 1221.

[91] K. Chen, C.-M. Li, Q. Zhang, Y.-A. Chen, A. Goebel, S. Chen, A. Mair, J.-W. Pan, Experimental Realization of One-Way Quantum Computing with Two-Photon Four-Qubit Cluster States, Physical Review Letters 99 (12) (2007) 120503.

[92] Y. C. Jeong, C. Di Franco, H. T. Lim, M. S. Kim, Y. H. Kim, Experimental realization of a delayed-choice quantum walk, Nature Communications 4 (2013) 1–7.

[93] S. Takeuchi, Experimental demonstration of a three-qubit quantum computation algorithm using a single photon and linear optics, Physical Review A 62 (3) (2000) 32301.

[94] A. Peruzzo, A. Laing, A. Politi, T. Rudolph, J. L. O'Brien, Multimode quantum interference of photons in multiport integrated devices, Nature Communications 2 (2011) 224.

[95] J. Wang, F. Sciarrino, A. Laing, M. G. Thompson, Integrated photonic quantum technologies, Nature Photonics.

[96] B. Fang, M. Menotti, M. Liscidini, J. E. Sipe, V. O. Lorenz, Three-Photon Discrete-Energy-Entangled W State in an Optical Fiber, Physical Review Letters 123 (7) (2019) 70508.

[97] J.-W. Pan, D. Bouwmeester, M. Daniell, H. Weinfurter, A. Zeilinger, Experimental test of quantum nonlocality in three-photon GreenbergerHorneZeilinger entanglement, Nature 403 (6769) (2000) 515–519.

[98] J. C. Adcock, C. Vigliar, R. Santagati, J. W. Silverstone, M. G. Thompson, Programmable four-photon graph states on a silicon chip, Nature Communications 10 (1) (2019) 3528.

[99] M. Kues, C. Reimer, P. Roztocki, L. R. Cortés, S. Sciara, B. Wetzel, Y. Zhang, A. Cino, S. T. Chu, B. E. Little, D. J. Moss, L. Caspani, J. Azaña, R. Morandotti, On-chip generation of high-dimensional entangled quantum states and their coherent control, Nature 546 (2017) 622.

[100] A. Aspuru-guzik, P. Walther, Photonic quantum simulators, Nature Physics 8 (4) (2012) 285–291.

[101] C. Sparrow, E. Martín-López, N. Maraviglia, A. Neville, C. Harrold, J. Carolan, Y. N. Joglekar, T. Hashimoto, N. Matsuda, J. L. O'Brien, D. P. Tew, A. Laing, Simulating the vibrational quantum dynamics of molecules using photonics, Nature 557 (7707) (2018) 660–667.

[102] T. Kobayashi, R. Ikuta, S. Yasui, S. Miki, T. Yamashita, H. Terai, T. Yamamoto, M. Koashi, N. Imoto, Frequency-domain Hong-Ou-Mandel interference, Nature Photonics 10 (2016) 441.

[103] V. S. Shchesnovich, Partial indistinguishability theory for multiphoton experiments in multiport devices, Physical Review A 91 (1) (2015) 13844.

[104] A. J. Menssen, A. E. Jones, B. J. Metcalf, M. C. Tichy, S. Barz, W. S. Kolthammer, I. A. Walmsley, Distinguishability and Many-Particle Interference, Physical Review Letters 118 (15) (2017) 1–6.

[105] S. Laibacher, V. Tamma, Symmetries and entanglement features of inner-mode-resolved correlations of interfering nonidentical photons, Physical Review A 98 (5).

[106] X.-J. Wang, B. Jing, P.-F. Sun, C.-W. Yang, Y. Yu, V. Tamma, X.-H. Bao, J.-W. Pan, Experimental Time-Resolved Interference with Multiple Photons of Different Colors, Physical Review Letters 121 (8) (2018) 80501.

[107] S. Agne, T. Kauten, J. Jin, E. Meyer-Scott, J. Z. Salvail, D. R. Hamel, K. J. Resch, G. Weihs, T. Jennewein, Observation of Genuine Three-Photon Interference, Physical Review Letters 118 (15) (2017) 4–7.

[108] J. B. Spring, B. J. Metcalf, P. C. Humphreys, W. S. Kolthammer, X.-M. Jin, M. Barbieri, A. Datta, N. Thomas-Peter, N. K. Langford, D. Kundys, J. C. Gates, B. J. Smith, P. G. R. Smith, I. A. Walmsley, Boson Sampling on a Photonic Chip, Science 339 (6121) (2013) 798 LP – 801.

[109] N. Spagnolo, C. Vitelli, M. Bentivegna, D. J. Brod, A. Crespi, F. Flamini, S. Giacomini, G. Milani, R. Ramponi, P. Mataloni, R. Osellame, E. F. Galvão, F. Sciarrino, Experimental validation of photonic boson sampling, Nature Photonics 8 (8) (2014) 615–620.

[110] H. Wang, Y. He, Y.-H. Li, Z.-E. Su, B. Li, H.-L. Huang, X. Ding, M.-C. Chen, C. Liu, J. Qin, J.-P. Li, Y.-M. He, C. Schneider, M. Kamp, C.-Z. Peng, S. Höfling, C.-Y. Lu, J.-W. Pan, High-efficiency multiphoton boson sampling, Nature Photonics 11 (6) (2017) 361–365.

[111] H.-S. Zhong, Y. Li, W. Li, L.-C. Peng, Z.-E. Su, Y. Hu, Y.-M. He, X. Ding, W. Zhang, H. Li, L. Zhang, Z. Wang, L. You, X.-L. Wang, X. Jiang, L. Li, Y.-A. Chen, N.-L. Liu, C.-Y. Lu, J.-W. Pan, 12-Photon Entanglement and Scalable

Scattershot Boson Sampling with Optimal Entangled-Photon Pairs from Parametric Down-Conversion, Physical Review Letters 121 (25) (2018) 250505.

[112] D. J. Brod, E. F. Galvão, A. Crespi, R. Osellame, N. Spagnolo, F. Sciarrino, Photonic implementation of boson sampling: a review, Advanced Photonics 1 (3) (2019) 1–14.

[113] T. B. Pittman, B. C. Jacobs, J. D. Franson, Single photons on pseudodemand from stored parametric down-conversion, Physical Review A - Atomic, Molecular, and Optical Physics 66 (4) (2002) 7.

[114] A. L. Migdall, D. Branning, S. Castelletto, Tailoring single-photon and multiphoton probabilities of a single-photon on-demand source, Physical Review A 66 (5) (2002) 053805.

[115] J. H. Shapiro, F. N. Wong, On-demand single-photon generation using a modular array of parametric downconverters with electro-optic polarization controls, Optics Letters 32 (18) (2007) 2698.

[116] X.-s. Ma, S. Zotter, J. Kofler, T. Jennewein, A. Zeilinger, Experimental generation of single photons via active multiplexing, Physical Review A 83 (4) (2011) 043814.

[117] M. J. Collins, C. Xiong, I. H. Rey, T. D. Vo, J. He, S. Shahnia, C. Reardon, T. F. Krauss, M. J. Steel, A. S. Clark, B. J. Eggleton, Integrated spatial multiplexing of heralded single-photon sources, Nature Communications 4 (2013) 2582.

[118] D. Bonneau, G. J. Mendoza, J. L. O'Brien, M. G. Thompson, Effect of loss on multiplexed single-photon sources, New Journal of Physics 17 (4) (2015) 043057.

[119] G. J. Mendoza, R. Santagati, J. Munns, E. Hemsley, M. Piekarek, E. Martín-López, G. D. Marshall, D. Bonneau, M. G. Thompson, J. L. O'Brien, Active temporal and spatial multiplexing of photons, Optica 3 (2) (2016) 127.

[120] F. Kaneda, B. G. Christensen, J. J. Wong, H. S. Park, K. T. McCusker, P. G. Kwiat, Time-multiplexed heralded single-photon source, Optica 2 (12) (2015) 1010.

[121] C. Zhang, Y.-F. Huang, Z. Wang, B.-H. Liu, C.-F. Li, G.-C. Guo, Experimental Greenberger-Horne-Zeilinger-Type Six-Photon Quantum Nonlocality, Physical Review Letters 115 (26) (2015) 260402.

[122] C. Xiong, X. Zhang, Z. Liu, M. J. Collins, A. Mahendra, L. G. Helt, M. J. Steel, D. Y. Choi, C. J. Chae, P. H. W. Leong, B. J. Eggleton, Active temporal multiplexing of indistinguishable heralded single photons, Nature Communications 7 (1) (2016) 10853.

[123] K. Tsujino, S. Takeuchi, K. Sasaki, Detailed analysis of the fidelity of quantum teleportation using photons: Considering real experimental parameters, Physical Review A 66 (4) (2002) 042314.

[124] T. Horikiri, Y. Takeno, A. Yabushita, T. Kobayashi, Photon-number-resolved heralded-photon source for improved quantum key distribution, Physical Review A 76 (1) (2007) 012306.

[125] M. J. Fitch, B. C. Jacobs, T. B. Pittman, J. D. Franson, Photon-number resolution using time-multiplexed single-photon detectors, Physical Review A 68 (4) (2003) 043814.

[126] P. Kok, S. L. Braunstein, Postselected versus nonpostselected quantum teleportation using parametric down-conversion, Physical Review A 61 (4) (2000) 042304.

[127] S. Miki, T. Yamashita, Z. Wang, H. Terai, A 64-pixel NbTiN superconducting nanowire single-photon detector array for spatially resolved photon detection, Optics Express 22 (7) (2014) 7811.

[128] R. J. A. Francis-Jones, R. A. Hoggarth, P. J. Mosley, All-fiber multiplexed source of high-purity single photons, Optica 3 (11) (2016) 1270–1273.

[129] C. Joshi, A. Farsi, S. Clemmen, S. Ramelow, A. L. Gaeta, Frequency multiplexing for quasi-deterministic heralded single-photon sources, Nature Communications 9 (1) (2018) 847.

[130] S.-l. Liu, Q. Zhou, Z.-y. Zhou, S.-k. Liu, Y. Li, Y.-h. Li, C. Yang, Z.-h. Xu, G.-c. Guo, B.-s. Shi, Multiplexing heralded single photons in orbital-angular-momentum space, Physical Review A 100 (1) (2019) 13833.

[131] E. Jakeman, E. R. Pike, The intensity-fluctuation distribution of Gaussian light, Journal of Physics A: General Physics 1 (1) (1968) 318.

[132] F. Kaneda, F. Xu, J. Chapman, P. G. Kwiat, Quantum-memory-assisted multi-photon generation for efficient quantum information processing, Optica 4 (9) (2017) 1034–1037.

[133] X. Zhang, Y. H. Lee, B. A. Bell, P. H. W. Leong, T. Rudolph, B. J. Eggleton, C. Xiong, Indistinguishable heralded single photon generation via relative temporal multiplexing of two sources, Optics Express 25 (21) (2017) 26067–26075.

[134] F. Marsili, V. B. Verma, J. A. Stern, S. Harrington, A. E. Lita, T. Gerrits, I. Vayshenker, B. Baek, M. D. Shaw, R. P. Mirin, S. W. Nam, Detecting single infrared photons with 93% system efficiency, Nature Photonics 7 (3) (2013) 210–214.

[135] X.-L. Niu, Y.-F. Huang, G.-Y. Xiang, G.-C. Guo, Z. Y. Ou, Beamlike high-brightness source of polarization-entangled photon pairs, Optics Letters 33 (9) (2008) 968.

[136] O. Kwon, Y.-W. Cho, Y.-H. Kim, Single-mode coupling efficiencies of type-II spontaneous parametric down-conversion: Collinear, noncollinear, and beamlike phase matching, Physical Review A 78 (5) (2008) 053825.

[137] G. J. Mendoza, R. Santagati, J. Munns, E. Hemsley, M. Piekarek, E. Martin-Lopez, G. D. Marshall, D. Bonneau, M. G. Thompson, J. L. O'Brien, Active Temporal Multiplexing of Photons.

[138] X. Ding, Y. He, Z.-C. Duan, N. Gregersen, M.-C. Chen, S. Unsleber, S. Maier, C. Schneider, M. Kamp, S. Höfling, C.-Y. Lu, J.-W. Pan, On-Demand Single Photons with High Extraction Efficiency and Near-Unity Indistinguishability from a Resonantly Driven Quantum Dot in a Micropillar, Physical Review Letters 116 (2) (2016) 020401.

[139] J. C. Loredo, M. A. Broome, P. Hilaire, O. Gazzano, I. Sagnes, A. Lemaitre, M. P. Almeida, P. Senellart, A. G. White, Boson Sampling with Single-Photon Fock States from a Bright Solid-State Source, Physical Review Letters 118 (13) (2017) 130503.

[140] F. Lenzini, B. Haylock, J. C. Loredo, R. A. Abrahão, N. A. Zakaria, S. Kasture, I. Sagnes, A. Lemaitre, H.-P. Phan, D. V. Dao, P. Senellart, M. P. Almeida, A. G. White, M. Lobino, Active demultiplexing of single photons from a solid-state source, Laser & Photonics Reviews 11 (3) (2017) 1600297.

[141] X.-L. Wang, L.-K. Chen, W. Li, H.-L. Huang, C. Liu, C. Chen, Y.-H. Luo, Z.-E. Su, D. Wu, Z.-D. Li, H. Lu, Y. Hu, X. Jiang, C.-Z. Peng, L. Li, N.-L. Liu, Y.-A. Chen, C.-Y. Lu, J.-W. Pan, Experimental Ten-Photon Entanglement, Physical Review Letters 117 (21) (2016) 210502.

[142] S. Takeuchi, Beamlike twin-photon generation by use of type II parametric down-conversion, Optics Letters 26 (11) (2001) 843.

[143] M. Gimeno-Segovia, H. Cable, G. J. Mendoza, P. Shadbolt, J. W. Silverstone, J. Carolan, M. G. Thompson, J. L. O'Brien, T. Rudolph, Relative multiplexing for minimising switching in linear-optical quantum computing, New Journal of Physics 19 (6) (2017) 63013.

[144] T. Kiyohara, R. Okamoto, S. Takeuchi, Serial-parallel conversion for single photons with heralding signals, Optics Express 25 (26) (2017) 32443.

[145] A. Christ, C. Silberhorn, Limits on the deterministic creation of pure single-photon states using parametric down-conversion, Physical Review A 85 (2) (2012) 23829.

[146] T. Kiyohara, R. Okamoto, S. Takeuchi, Realization of multiplexing of heralded single photon sources using photon number resolving detectors, Optics Express 24 (24) (2016) 27288.

[147] Y. Hasegawa, R. Ikuta, N. Matsuda, K. Tamaki, H.-K. Lo, T. Yamamoto, K. Azuma, N. Imoto, Experimental time-reversed adaptive Bell measurement towards all-photonic quantum repeaters, Nature Communications 10 (1) (2019) 378.

[148] Z.-D. Li, R. Zhang, X.-F. Yin, L.-Z. Liu, Y. Hu, Y.-Q. Fang, Y.-Y. Fei, X. Jiang, J. Zhang, L. Li, N.-L. Liu, F. Xu, Y.-A. Chen, J.-W. Pan, Experimental quantum repeater without quantum memory, Nature Photonics 13 (9) (2019) 644–648.

[149] M. Rådmark, M. Wieśniak, M. Żukowski, M. Bourennane, Experimental multilocation remote state preparation, Physical Review A 88 (3) (2013) 32304.

[150] Z. Xie, T. Zhong, S. Shrestha, X. Xu, J. Liang, Y.-X. Gong, J. C. Bienfang, A. Restelli, J. H. Shapiro, F. N. C. Wong, C. Wei Wong, Harnessing high-dimensional hyperentanglement through a biphoton frequency comb, Nature Photonics 9 (2015) 536.

[151] A. Mair, A. Vaziri, G. Weihs, A. Zeilinger, Entanglement of the orbital angular momentum states of photons, Nature 412 (6844) (2001) 313–316.

[152] D. Kawase, Y. Miyamoto, M. Takeda, K. Sasaki, S. Takeuchi, Observing quantum correlation of photons in laguerre-gauss modes using the gouy phase, Physical Review Letters 101 (5) (2008) 1–4.

[153] M. Malik, M. Erhard, M. Huber, M. Krenn, R. Fickler, A. Zeilinger, Multi-photon entanglement in high dimensions, Nature Photonics 10 (2016) 248.

[154] A. Martin, T. Guerreiro, A. Tiranov, S. Designolle, F. Fröwis, N. Brunner, M. Huber, N. Gisin, Quantifying Photonic High-Dimensional Entanglement, Physical Review Letters 118 (11) (2017) 1–5.

[155] J. Wang, S. Paesani, Y. Ding, R. Santagati, P. Skrzypczyk, A. Salavrakos, J. Tura, R. Augusiak, L. Man$\boldsymbol{v}$cinska, D. Bacco, D. Bonneau, J. W. Silverstone, Q. Gong, A. Acín, K. Rottwitt, L. K. Oxenløwe, J. L. O'Brien, A. Laing, M. G. Thompson, Multidimensional quantum entanglement with large-scale integrated optics, Science 360 (6386) (2018) 285 LP – 291.

[156] J. T. Barreiro, N. K. Langford, N. A. Peters, P. G. Kwiat, Generation of Hyperentangled Photon Pairs, Physical Review Letters 95 (26) (2005) 260501.

[157] D. F. V. James, P. G. Kwiat, W. J. Munro, A. G. White, Measurement of qubits, Physical Review A 64 (5) (2001) 52312.

[158] J. B. Altepeter, E. R. Jeffrey, P. G. Kwiat, Photonic State Tomography, in: P. R. Berman, C. C. B. T. A. I. A. Lin Molecular, and Optical Physics (Eds.), Advances In Atomic, Molecular, and Optical Physic, Vol. 52, Academic Press, 2005, pp. 105–159.

[159] R. Okamoto, J. L. O'Brien, H. F. Hofmann, T. Nagata, K. Sasaki, S. Takeuchi, An Entanglement Filter, Science 323 (5913) (2009) 483 LP – 485.

[160] J. G. Titchener, A. S. Solntsev, A. A. Sukhorukov, Two-photon tomography using on-chip quantum walks, Optics Letters 41 (17) (2016) 4079–4082.

[161] L. Banchi, W. S. Kolthammer, M. S. Kim, Multiphoton Tomography with Linear Optics and Photon Counting, Physical Review Letters 121 (25) (2018) 250402.

[162] J. G. Titchener, M. Gräfe, R. Heilmann, A. S. Solntsev, A. Szameit, A. A. Sukhorukov, Scalable on-chip quantum state tomography, npj Quantum Information 4 (1) (2018) 19.

[163] T. Nagata, R. Okamoto, H. F. Hofmann, S. Takeuchi, Analysis of experimental error sources in a linear-optics quantum gate, New Journal of Physics 12 (4) (2010) 43053.

[164] F. Kaneda, P. G. Kwiat, High-efficiency single-photon generation via large-scale active time multiplexing, Science Advances 5 (10) (2019) eaaw8586.

[165] X. Ma, X. Li, L. Cui, X. Guo, L. Yang, Effect of chromatic-dispersion-induced chirp on the temporal coherence properties of individual beams from spontaneous four-wave mixing, Physical Review A 84 (2) (2011) 23829.

[166] C. I. Osorio, N. Sangouard, R. T. Thew, On the purity and indistinguishability of down-converted photons, Journal of Physics B: Atomic, Molecular and Optical Physics 46 (5) (2013) 55501.

[167] X. Ma, L. Cui, X. Li, Hong-Ou-Mandel interference between independent sources of heralded ultrafast single photons: influence of chirp, Journal of the Optical Society of America B 32 (5) (2015) 946–954.

Publication List

Journal papers

1. T. Kiyohara, R. Okamoto, and S. Takeuchi, "Realization of multiplexing of heralded single photon sources using photon number resolving detectors", Opt. Express, **24**(24), (2016) 27288-27297. (Chapter 3)

2. T. Kiyohara, R. Okamoto, and S. Takeuchi, "Serial-parallel conversion for single photons with heralding signals", Opt. Express, **25**(26), (2017) 32443-32450. (Chapter 4)

3. T. Kiyohara, R. Okamoto, and S. Takeuchi, "Generation of heralded two-photon parallel state using actively spatial routing network", in preparation, (2020). (Chapter 5)

4. T. Kiyohara, N. Yamashiro, R. Okamoto, H. Araki, J.-Y. Wu, H. F. Hofmann, and S. Takeuchi, "Direct verification of entanglement between two multimode - multiphoton systems", in preparation, (2020). (Chapter 6)

International Conference

1. T. Kiyohara, R. Okamoto, and S. Takeuchi, "A robust multiplexed single photon source with excess-photon suppression", *The 4th International Workshop on Microcavities and Their Applications*, Hokkaido, Japan, 2015.[Poster]

2. T. Kiyohara, R. Okamoto, and S. Takeuchi, "An excess-photon suppressed heralded single photon source combining multiple down-converters and cascaded detectors", *SPIE Optics + Photonics*, San Diego, United States, 2016.[Oral]

3. T. Kiyohara, R. Okamoto, and S. Takeuchi, "Realization of multiplexing of heralded single photon sources using cascaded on-off detectors", *CLEO/Europe-EQEC 2017 the Conference on Lasers and Electro-Optics/Europe and the European Quantum Electronics Conference*, Munich, Germany, 2017.[Oral]

4. T. Kiyohara, R. Okamoto, and S. Takeuchi, "Serial-parallel conversion for single photons with heralding signals", *The 24th Congress of the International Commission for Optics*, Tokyo, Japan, 2017.[Oral]

5. T. Kiyohara, R. Okamoto, and S. Takeuchi, “Realization of a multiplexed heralded single photon source combining with photon number discrimination, and a serial-parallel convertor”, *Okinawa School in Physics: Coherent Quantum Dynamics*, Okinawa, Japan, 2017.[Poster]

6. T. Kiyohara, R. Okamoto, and S. Takeuchi, “Serial-parallel conversion for a heralded single photon source”, *SPIE Optics + Photonics*, San Diego, United States, 2018.[Poster]

7. T. Kiyohara, R. Okamoto, and S. Takeuchi, “Serial-parallel conversion for a heralded single photon source”, *US-Japan QELS-13, the 13th Japan-US Joint Seminar on Quantum Electronics and Laser Spectroscopy*, Ishikawa, Japan, 2018.[Poster]

8. T. Kiyohara, R. Okamoto, and S. Takeuchi, “Serial-parallel conversion for a stream of single photons using heralding signals”, *Quantum 2019*, Torino, Italy, 2019.[Poster]

Domestic Conference

1. 清原孝行, 岡本亮, 竹内繁樹, “多重化伝令付き単一光子源を用いた 2 光子量子干渉実験”, 第 *30* 回量子情報技術研究会, 17, 大阪大学 豊中キャンパス (大阪), 2015 年 5 月.[Poster]

2. 清原孝行, 岡本亮, 竹内繁樹, “多重化伝令付き単一光子源による光子数分布制御と 2 光子量子干渉実験”, 日本物理学会, 第 *71* 回年次秋季大会, 17pAC-1，関西大学 千里山キャンパス (大阪), 2015 年 9 月.[Oral]

3. 清原孝行, 岡本亮, 竹内繁樹, “光子対数識別と多重化を組み合わせた伝令付き単一光子源”, 第 *63* 回応用物理学会春季学術講演会, 20p-W541-2, 東京工業大学 大岡山キャンパス (東京), 2016 年 3 月.[Oral]

4. 清原孝行, 岡本亮, 竹内繁樹, “光子対数識別と多重化を用いた伝令付き単一光子源の出力光子数分布の評価”, 第 *30* 回量子情報技術研究会, 32, 高知工科大学 永国寺キャンパス (高知), 2016 年 5 月.[Poster]

5. 山城直毅, 清原孝行, 岡本亮, ホフマンホルガ, 竹内繁樹, “多光子多モードもつれ状態のコヒーレンスに関する研究”, 第 *32* 回量子情報技術研究会, 33, 高知工科大学 永国寺キャンパス (高知), 2016 年 5 月.[Poster]

6. 山城直毅, 清原孝行, 岡本亮, Jun-Yi Wu, ホフマンホルガ, 竹内繁樹, “多光子多モードもつれ状態のコヒーレンスに関する研究 2”, 第 *33* 回量子情報技術研究会, 42, 高エネルギー加速器研究機構 小林ホール (茨城), 2016 年 11 月.[Poster]

7. 山城直毅, 清原孝行, 岡本亮, Jun-Yi Wu, ホフマンホルガ, 竹内繁樹, “2 つの多光子システム間もつれ状態の検討実験 1”, 日本物理学会，第 *72* 回年次春季大会, 18pB22-4，大阪大学 豊中キャンパス (大阪), 2017 年 3 月.[Oral]

8. 山城直毅, 荒木裕貴, 清原孝行, 岡本亮, Jun-Yi Wu, ホフマンホルガ, 竹内繁樹, "2 つの多光子システム間もつれ状態の検討実験 2", 日本物理学会，第 *73* 回年次春季大会, 22aK203-6，東京理科大学 野田キャンパス (東京), 2018 年 3 月.[Oral]

9. 清原孝行, 岡本亮, 竹内繁樹, "伝令信号を用いた光子列のシリアルパラレル変換", 第 *38* 回量子情報技術研究会, 38, 広島国際会議場 (広島), 2018 年 6 月.[Poster]

10. 清原孝行, 岡本亮, 竹内繁樹, "伝令信号による複数光子の効率的な動的ルーティング法", 日本物理学会, 第 *73* 回年次秋季大会, 9pA316-7，同志社大学 京田辺キャンパス (大阪), 2018 年 9 月.[Oral]

11. 松本一勢, 清原孝行, 岡本亮, ホフマンホルガ, 竹内繁樹, "2 組の多光子多モードシステム間もつれ状態を用いたノンフォック状態の生成", 第 *39* 回量子情報技術研究会 , 33, 東京大学 駒場リサーチキャンパス 先端科学技術研究センター (東京), 2018 年 11 月.[Poster]

12. 清原孝行, 岡本亮, 竹内繁樹, "[第 3 回フォトニクス奨励賞受賞記念講演] 伝令信号を用いた単一光子列のシリアルパラレル変換", 第 *66* 回応用物理学会春季学術講演会, 10p-S422-9, 東京工業大学 大岡山キャンパス (東京), 2019 年 3 月.[Oral]

13. 亀井祐希, 曹博, 清原孝行, 岡本亮, 竹内繁樹, "同一空間モードに生成したもつれ光子対の空間的分離に関する研究", 第 *40* 回量子情報技術研究会, 42, 九州大学 筑紫キャンパス (福岡), 2019 年 5 月.[Poster]

14. 松本一勢, 清原孝行, 岡本亮, ホフマンホルガ, 竹内繁樹, "多光子多モードシステム間もつれ状態を用いたノンフォック状態生成に向けて", 第 *80* 回応用物理学会春季学術講演会, 21a-E207-5, 北海道大学，札幌キャンパス (北海道), 2019 年 9 月.[Oral]

Acknowledgements

I am deeply grateful to my supervisor, Prof. S. Takeuchi at Kyoto University, for giving me the opportunity to do a lots of interesting research. In this six years, he has supported not only my all research subjects but also my research life. I am confident that his kind comments and advises enhanced my ability as a researcher.

I really thank Assoc. Prof. R. Okamoto for his kind discussions, ideas, and advises to help my experiments. The discussion with him was very meaningful, and led to many breakthroughs in my research. Without his support, the fruitful experimental results shown in this thesis have never obtained.

I greatly appreciate Prof. M. Shiraishi at Kyoto University for his helpful suggestions and advises to proceed my research, and for reviewing this thesis. I also deeply appreciate Assoc. Prof. T. Asano at Kyoto University for our fruitful discussions and interesting comments, and for reviewing this thesis.

I would like to express our collaborators, Assoc. Prof. H. F. Hofmann and Dr. Jun-Yi Wu from Hiroshima University. Our fruitful collaborative research has produced very meaningful results, as shown in section 6. Their unique ideas always gave delight to us.

I greatly thank Prof. O. Sakai (current affiliation: the University of Shiga Prefecture), Assis. Prof. H. Takashima, Dr. M. Okano (current affiliation: santec), Dr. T. Ono (current affiliation: NICT), Dr. T. Tashima, Dr. B. Cao, Dr. Y. Mukai at Kyoto University, and Assis. Prof. K. Tsujino at Tokyo Woman's Medical University for their great suggestions, advises, and supports to my study.

I deeply appreciate the secretaries of our laboratory, Ms. R. Ito, Ms. R. Okamoto, and Ms. R. Nakanishi. Their careful supports help my research. I also wish to thank all the students of Prof. Takeuchi's group. Especially, I am glad to work with Mr. N. Yamashiro and Mr. H. Araki for the experiment in Chapter 6. Without their hard works, the research has not been succeeded.

I gratefully appreciate the financial support of Japan Society for the Promotion of Science (JSPS) for accepting me as JSPS Research Fellow.

I am grateful to my family. They supports me during my research life. Without their warm help, I can not graduate Kyoto University.

The research presented in this dissertation was supported by JSPS-KAKENHI (No. 26220712, 26610052, 25707034), JST-CREST (JPMJCR1674), MEXT Q-Leap, JSPS-FIRST, the Project for Developing Innovation Systems of MEXT, the Research Foundation for Opto-Science and Technology, the Research Fellow of Japan Society for the Promotion of Science (No. 17J06932).